ABSTRACT

Title of dissertation: WAVE IMPEDANCE SELECTION FOR
PASSIVITY-BASED BILATERAL
TELEOPERATION

Nicholas John D'Amore,
Doctor of Philosophy, 2016

Dissertation directed by: Professor David L. Akin
Department of Aerospace Engineering

When a task must be executed in a remote or dangerous environment, teleoperation systems may be employed to extend the influence of the human operator. In the case of manipulation tasks, haptic feedback of the forces experienced by the remote (slave) system is often highly useful in improving an operator's ability to perform effectively. In many of these cases (especially teleoperation over the internet and ground-to-space teleoperation), substantial communication latency exists in the control loop and has the strong tendency to cause instability of the system. The first viable solution to this problem in the literature was based on a scattering/wave transformation from transmission line theory. This wave transformation requires the designer to select a wave impedance parameter appropriate to the teleoperation system. It is widely recognized that a small value of wave impedance is well suited to free motion and a large value is preferable for contact tasks. Beyond this basic observation, however, very little guidance exists in the literature regarding the selection of an appropriate value. Moreover, prior research on impedance selection

generally fails to account for the fact that in any realistic contact task there will simultaneously exist contact considerations (perpendicular to the surface of contact) and quasi-free-motion considerations (parallel to the surface of contact). The primary contribution of the present work is to introduce an approximate linearized optimum for the choice of wave impedance and to apply this quasi-optimal choice to the Cartesian reality of such a contact task, in which it cannot be expected that a given joint will be either perfectly normal to or perfectly parallel to the motion constraint.

The proposed scheme selects a wave impedance matrix that is appropriate to the conditions encountered by the manipulator. This choice may be implemented as a static wave impedance value or as a time-varying choice updated according to the instantaneous conditions encountered. A Lyapunov-like analysis is presented demonstrating that time variation in wave impedance will not violate the passivity of the system. Experimental trials, both in simulation and on a haptic feedback device, are presented validating the technique. Consideration is also given to the case of an uncertain environment, in which an a priori impedance choice may not be possible.

WAVE IMPEDANCE SELECTION FOR
PASSIVITY-BASED BILATERAL TELEOPERATION

by

Nicholas John D'Amore

Dissertation submitted to the Faculty of the Graduate School of the
University of Maryland, College Park in partial fulfillment
of the requirements for the degree of
Doctor of Philosophy
2016

Advisory Committee:
Professor David L. Akin, Chair/Advisor
Dr. Craig Carignan
Professor Nikhil Chopra
Professor Robert Sanner
Professor Raymond Sedwick

Acknowledgments

The work presented in this dissertation has benefited, directly and indirectly, from the input of too many people to list here. First and foremost, I want to thank my advisor, Dr. Dave Akin, for providing an educational experience in the Space Systems Laboratory that I could not have found anywhere else. Further thanks are due to all of the members of my dissertation committee for providing the time, support, and expertise to see this work through to completion. Particular thanks go to Dr. Robert Sanner and Dr. Craig Carignan, whose comments on an earlier draft of this dissertation were exceptionally thorough and contributed greatly to the final manuscript. Thanks are also owed to Dr. Nikhil Chopra, whose experience with wave-based systems proved useful on multiple occasions.

I am additionally grateful to Dr. Günter Niemeyer for sharing with me via e-mail some of his thoughts surrounding the present work.

Thank you to Brett Darcey of Heron Systems, as well as Gordon Roesler and Dave Barnhart of DARPA, for providing our lab with the opportunity to pursue this avenue of research. Thank you for sticking with us from phase one to phase two of this contract, even as the scope of the project had to be redefined in response to the constraints imposed by physical reality.

I thank all the subjects who each donated a not-inconsiderable amount of time to participate in the experimental trials that form Chapter 5 of this manuscript. They will remain anonymous here; but their acts of volunteerism despite the tedium are greatly appreciated. Thanks are also owed to Dr. Craig Carignan for providing

the use of the Phantom Omni device that made this experiment possible.

I thank all of the members, past and present, of the Space Systems Laboratory with whom I've had the privilege of working during my years here. Thank you to Kate McBryan for her effort to keep everyone moving forward. Thank you to Lem Carpenter and Josh Pugh for being there to drive the robots. Thank you to Nick Limparis and Chris Carlsen for dealing with the hardware. And thank you most especially to Kate Thorne (née Strickland) for being the voice of reason whenever things got a little chaotic.

I thank Kristin Kerns for her help refining the experiment plan for the human subjects study contained herein, and for helping me maintain an appropriate balance between work and play.

I also thank all the educators, from preschool through grad school, who each helped lay some small fraction of the foundation upon which this dissertation was built. In addition to the members of my dissertation committee (in every one of whose classrooms I have sat), I would like to thank Dan Doherty, Margaret Ritzel, and Beth Watson, to name but a few.

Last, but certainly not least, I thank my family—Mom, Dad, and Alex—for their support throughout this endeavor. And for hanging in there while this took a little longer than originally planned.

Table of Contents

List of Figures

List of Abbreviations

B	Wave impedance
b_{eq}	Equivalent linear damping perceived by the operator at low frequencies
F	Adaptation matrix
J	Manipulator Jacobian matrix
$\mathbf{K}_e$	Environmental stiffness
k_{eq}	Equivalent stiffness perceived by the operator at low frequencies
$\mathbf{K}_I$	Integral gain
$\mathbf{K}_P$	Proportional gain
k_{ref}	Reference stiffness
m_{eq}	Equivalent inertia perceived by the operator at low frequencies
$\underline{q}$	Manipulator joint angles
T	One-way communication delay
$\underline{u}$	Forward wave variable (from master to slave)
$\underline{v}$	Return wave variable (from slave to master)
α_f	Free motion coefficient
Φ	Optimization objective function

4C	Four channel
AMFC	Adaptive motion/force control
ANOVA	Analysis of variance
DOF	Degree(s) of freedom
FR	Force reflection
IPC	Intrinsically passive control
PC	Predictive control
PE	Position error
SCC	Shared compliance control
SMC	Sliding mode control

Chapter 1: Introduction

1.1 Motivation

Teleoperation is the extension of the influence of a human operator beyond the local site at which he or she is located. It can take the form of unilateral control (in which motion commands are transmitted from the master to the slave with no return commands from slave to master), bilateral control (in which force feedback is additionally transmitted from the slave to the master), or supervisory control (in which the slave acts with some degree of autonomy and the operator is not involved in the lowest level of command generation). This dissertation focuses on the challenge of bilateral teleoperation, which gives the operator a sense of touch for the remote site.

Teleoperation systems are of interest to practitioners in a variety of fields in which action is necessary in environments that are dangerous or difficult to access,

with applications including satellite servicing, undersea inspection and monitoring, hazardous materials handling, surgery, terrestrial mining, and emergency response. Using bilateral teleoperation technology, space robot operators could employ tactile perception to perform tasks in situations in which communication bandwidth is too limited to support visual imagery. Medical professionals could palpate a patient abdomen from a continent away. Emergency responders could begin patient rescue and stabilization before the scene of an accident is safe enough for them to physically enter. Moreover, developments in this area have potential applications beyond just the remote operation of physical robots. Its applications to virtual environments are equally exciting. Internet users could one day collaborate over tactile interaction with simulated objects, bringing participant immersion to unprecedented levels. Internet-based, multiplayer video games could involve cooperative tactile tasks, not only making current players feel even more as though they were truly touching the virtual environment but also opening access to these systems to the visually impaired. Teams of people could train to perform physical tasks together, or a physical therapist could physically guide a patient through a virtual rehabilitation task, all without devoting the time and expense necessary to travel to the same location. The results may even be applicable to systems that do not directly involve a human operator in the loop at all—for example, to guarantee stability of a distributed simulation scheme wherein contact dynamics are simulated on a test bed at one location while hardware under development at a different facility is kept in the loop. This could greatly aid collaboration across different institutions to develop satellites and other systems, enabling system-level testing while the individual components

are still geographically disparate.

The fundamental challenge of the systems described above is that, because the force reflection closes a feedback loop around the delayed communication channel, even delays as small as 50 milliseconds can easily destabilize systems that were not explicitly designed to tolerate the latency [1]. On Earth, this duration is of the same order as typical coast-to-coast message transit times within the United States; and random delays in internet traffic can often delay individual packets for considerably longer than this. In space applications, round-trip latencies to the ground may easily be on the order of several seconds for targets in Earth orbit or on the moon.

1.2   Background: Teleoperation with Delay

This section presents a brief overview of the history and present state of teleoperation with communication delay, focusing primarily on bilateral (i.e., force-feedback) teleoperation. A more detailed overview and discussion can be found in historical surveys by Sheridan [2], Hokayem and Spong [3], and Zhu et al. [4].

1.2.1   Operator-centric Studies

Early work on the problem of teleoperation in the presence of communication latency focused primarily on the behavior and performance of human operators under delayed-feedback conditions. Held et al. [5] found that the psychological mechanism whereby a human operator adapts to spatial displacement between their own hand and visual feedback of their movement breaks down when as little as 0.3

seconds of lag is introduced. Ferrell [6] found that human operators tend to adopt a "move-and-wait" strategy in the presence of perceptible time delay (1.0 - 2.3 seconds in the cited study), wherein they execute discrete motions and wait for feedback before proceeding further. Noyes [7] experimented with graphical overlays to provide updated manipulation configuration data when video feedback was intermittently delayed due to low frame rates of 0.55 and 1.6 frames per second. Performance scores (a linear function of performance time and number of errors) were generally improved by about 50% to 150% versus operation without the graphical overlay. Subsequent work in command and predictive displays have also shown graphical overlays to improve performance under conditions of delayed visual feedback.

The force-feedback problem of the present research presents a markedly different challenge than delayed visual feedback. Whereas visual feedback can be ignored by the operator when acting upon it is deemed inappropriate, a force applied to the operator's hand will necessarily affect the motion of that hand and thus necessarily close the control loop that in the previous scenario the operator could open at will. Ferrell [1] showed that direct force feedback to the operator in such a fashion could destabilize the teleoperation system. Operator-centric solutions have been to reopen the control loop by converting the remote forces to visual [8] or auditory or vibrational [9] cues rather than tactile feedback, or to use one of the operator's hands for force feedback while the other is used to drive the system [1]. These solutions effectively allow the human to once again sever the control loop and return to a move-and-wait strategy. Other means of reopening the control loop have included the use of (undelayed) predicted rather than (delayed) actual forces [8]. Supervi-

sory control has also been used remove the human from the low-level control loop completely, instead closing that loop at the remote site.

1.2.2 Control Theoretic Studies

Rather than opening the control loop, as in the studies of the preceeding subsection, the focus in more recent decades has tended toward control theoretic approaches guaranteeing stability despite the presence of latency in the closed loop. The following subsubsections present an overview of these schemes. For clarity, after introducing the classic Force Reflection (FR) approach, the four categories of bilateral control schemes used by Zhu et al. [4] are used to organize the discussion. These categories are Prediction-based, Sliding Mode, Passivity-based, and Other. Analytical results regarding the stability and transparency from Arcara and Melchiorri [10] are also summarized where relevant. The reader is cautioned that although the cited authors' conclusions are formally valid at low frequencies and in the limit as certain parameters become very large or very small, they present an incomplete picture of the performance such systems can achieve in practice.

1.2.2.1 The Classic Approach

The Force Reflection (FR) control scheme transmits position information from master to slave and force information from slave to master. It implements no special measures to mitigate the destabilizing effect of communication latency, and therefore represents the baseline for evaluation of the other schemes. The technique is

not intrinsically stable; indeed, it was instability issues with this technique that motivated the development of the controllers described in the following sections. In this simple approach, the operator will perceive double the actual robot inertia and damping (i.e., the sum total of the master and slave, which are assumed by Arcara and Melchiorri to be identical) and correct environmental stiffness, while master-slave position coordination error will be proportional to the magnitude of the communication delay [10].

1.2.2.2   Prediction-based Control

The Predictive Control (PC) scheme is an FR variant in which *a priori* knowledge of the slave dynamics and communication delay are used to predict the slave's response. Because, however, latency of perception is not one of the metrics considered by Arcara and Melchiorri [10], their transparency findings are much the same as in the FR case; and stability is dependent upon environmental parameters. (A variant of this technique additionally incorporates a guarantee of passivity and thus for the purpose of this manuscript is included in that portion of the discussion.) More sophisticated adaptive prediction schemes have been developed in the years since Arcara and Melchiorri's comparative study, making use of the Kalman and particle filters [11] and neural networks [12], [13].

In the Adaptive Motion/Force Control (AMFC) scheme, the master and slave each adaptively learn and cancel their own dynamics, theoretically allowing for perfect transparency in the absence of communication delay. Stability can be achieved

through proper selection of the controller parameters, assuming environmental parameters can be bounded [10].

1.2.2.3 Sliding Mode Control

Arcara and Melchiorri find that the Sliding Mode Controller (SMC) exhibits excellent transparency: accurate environmental stiffness, any desired inertia and damping perception by the operator, and vanishingly small master-slave coordination errors [10]. It is intrinsically stable in the case of free motion, but was at the time of Arcara and Melchiorri's study easily destabilized by environmental contact. This shortcoming has been greatly mitigated in subsequent work [14], [15]; and García-Valdovinos et al. [16] present a sliding mode scheme that (much like the classic formulation of the wave-based control) guarantees stability for unknown but constant time delays, although only in the case of linear robot dynamics. Nonlinear manipulators have been addressed more recently [17], although its implementation on uncertain manipulators relies upon an adaptive scheme for parameter identification.

1.2.2.4 Passivity-based Control

Passivity-based control is control that relies in some fashion upon the idea of a system that cannot have more energy than was initially present at time $t = 0$ plus the net work done on the system for $t > 0$. This is a natural property of mechanical systems, and has been exploited in various control laws for decades [18] [19].

Passivity-based control is intuitively appealing because it is analogous to concepts of mechanical or electrical power and energy, even when applied to more abstract algorithms with no physical instantiation themselves. Moreover, because the feedback interconnection of passive nodes is itself also passive, the notion lends itself quite readily to a building-block approach to control system design. Once individual pieces of a network have been shown to be passive, a wide variety of different interconnection schemes are immediately known to be stable [20]. In the realm of teleoperation specifically, this allows for widespread mixing and matching of various tools that have been developed, for example, to reduce master-slave position drift, to mitigate the effects of packet loss, or (as in the present work) to implement a time-varying choice of wave impedance. In contrast to the other strategies summarized here (with the partial exception of Sliding Mode Control), the three control schemes described here are the only considered schemes that are *intrinsically* stable—i.e., guaranteed to be stable regardless of the choice of system parameters and without requiring knowledge of environmental parameters or the (assumed-constant) magnitude of the communication delay. Nuño et al. [21] and Sun et al. [22] present surveys of work in wave-based teleoperation.

The critical insight that delay renders an otherwise passive communication channel nonpassive (thus introducing energy into the system) was first presented by Anderson and Spong [23]. This can most simply be addressed by introducing sufficient damping to overwhelm this energy generation. The most basic approach, as in the case of the Engineering Test Satellite VII [24], is to inject pure damping of the form $\tau = -b\dot{q}$ at both the master and slave locations. The authors present an anal-

ysis for the magnitude of damping b necessary to formally guarantee passivity, but employ a smaller value (due to practical limitations) that they found to be seemingly stable in practice. The Force Reflection with Passivity (FRP) scheme considered by Arcara and Melchiorri [10], and first presented by Niemeyer and Slotine [25], takes this one step further by formulating the dissipation in such a way that stability can be guaranteed (for arbitrary choice of their differently-defined damping parameter) without requiring knowledge of the master or slave dynamics, or of the magnitude of the (assumed-constant) time delay. This intrinsic stability is the primary appeal of most passivity-based teleoperation schemes, but is achieved in this particular case at substantial performance penalty. Perception of environmental stiffness is not possible; and master-slave coordination error is introduced [10].

The use of scattering (wave) variables from transmission line theory was the first truly viable solution (introduced by Anderson and Spong [26], [23], and developed into its modern formulation by Niemeyer and Slotine [25]) to maintaining stable teleoperation in the presence of communication latency, and remains a topic of considerable research attention to this day. Their approach, described in greater detail in Chapter 2, simulates an ideal transmission line and thus ensures that the communication delay cannot cause any addition of energy to the system. In this Intrinsically Passive Control (IPC) scheme, information is transmitted between master and slave in the form of waves, which make no distinction between force/torque and velocity[1]. This allows ready use of the same control law in both contact and free

---

[1]Niemeyer and Slotine [27] describe the forward wave, going from the master to the slave, as a "move or push command" which will be translated into either motion or force depending upon

motion (a feature of compliance control in general [28]). The transmission of velocity rather than position information introduces the possibility of large coordination errors between master and slave, but Arcara and Melchiorri conclude that this technique is similar in transparency to the classic FR scheme [10]. This is, however, one of the more obvious cases in their work of statements that are formally true in the limit but are lacking with regard to practical application: although the system provides double perceived inertia and accurate stiffness perception for vanishingly small time delay, these two results occur only under conflicting parameter choices at non-trivial latency. This conflict is the primary motivation behind the Cartesian-based framework proposed in the present work, which focuses on this IPC scheme.

Arcara and Melchiorri additionally analyze Predictive Control with Passivity (PCP), which uses an IPC-style approach incorporating wave variables in order to avoid PCP's vulnerability to destabilization by the environment; and thus achieves similar transparency to IPC [10].

Hirche et al. [29] describe the scattering/wave approach as "the most successful approach" to bilateral teleoperation with communication latency. It has been an active area of research since its introduction in 1989. Subsequent work in the area of wave-based teleoperation has sought to tackle the challenges of time-varying communication latency[2] [27] [30] [31] [32], position drift between master and slave [33] [34] [35], packet loss in the communication channel [36] [31], performance

_____

the circumstances encountered at the slave site.

[2]a significant challenge for internet-based teleoperation

degradation due to wave reflections [35] [37], transparency of high-frequency vibro-tactile force content [37], and multilateral teleoperation [38]. Moreover, passivity-based transmission of wave variables does not preclude combination with the other control strategies listed here. Fundamentally, wave variables provide a form of *communication*, not control, which can be usefully employed in a variety of different control schemes. Although the wave variables of the IPC scheme solve the latency problem and enable the use of simple proportional-integral (PI) controllers to drive the master and slave manipulators in their customary implementation, wave-based communication has been used in conjunction with adaptive [39] and sliding mode [40] controllers, blurring the lines between the categories of teleoperation schemes considered in Subsection 1.2.2.

In addition to its use in bilateral teleoperation as described above, wave-based control has also seen application in the realm of haptic interaction with virtual environments. Carignan and Olsson [41] explore cooperative control in which two masters interact with a virtual object. Diolaiti et al. [42] use wave variables to directly interact with motor current and voltage, thus achieving greater stiffness rendering than in more traditional means of driving the motors. The use of wave variables to passively connect a high-update-rate haptic feedback device to a lower-update-rate virtual environment simulation has also been a topic of research in recent years [43] [44].

Some passivity-based controllers have also been presented that do not rely upon the scattering transform [45] [46] [47] [48].

1.2.2.5 Other Control Schemes

The Position Error (PE) scheme is similar both in its simplicity and in its achieved transparency to the FR scheme, transmitting position information in the slave-to-master direction rather than force information. Smaller master-slave coordination errors result, but Arcara and Melchiorri [10] otherwise declare the techniques to be similar.

Shared Compliance Control (SCC) instead inserts a slave-side compliance controller to improve system behavior in contact. Such a scheme is, however, subject to the exact same stability limitations in free motion as the uncorrected FR scheme [10]. SCC exhibits similar transparency to the uncorrected FR approach: double perceived inertia and damping, tracking error proportional to communication delay, and correct perception of environmental stiffness.

The Four Channels (4C) scheme is a generic controller framework that could be used to describe and analyze almost any bilateral scheme (including the wave-based IPC [35]) in which force and motion information is transmitted between master and slave. Consequently, only a small subset of possible controller choices are considered by Arcara and Melchiorri [10]. The authors remark that their particular subset of 4C control can achieve perfect transparency in the case of zero time delay, but that there must otherwise be a trade-off. The 4C framework has seen use in design for transparency [49], robustness [50], and adaptive control [51].

1.2.3   Experimental Teleoperation Work

Many of the studies cited above include some aspect of experimental valida-
tion of their respective strategies. Often, this is done using single-degree-of-freedom
test beds and communication latencies on the order of 100 milliseconds. However,
Ferrell [1], who first drew widespread attention to the potential for instability even
at smaller latencies than this, conducted experiments on a single-DOF test bed with
round-trip delays as large as 3.0 seconds, and found some configurations of his PE-
style control system to remain sufficiently stable for task completion under some
circumstances even at this level of delay. That teleoperation can be achieved with
delays on the order of several seconds was further underscored by the experiment
of the Engineering Test Satellite VII. Launched in 1999 by the National Space De-
velopment Agency of Japan to an orbital altitude of approximately 550 km, this
satellite demonstrated the technology for ground-to-space teleoperation of a 6-DOF
robotic manipulator operating with round-trip communication latencies of 6 to 7 sec-
onds [24] [52] [53]. Their basic control approach was also that of the PE scheme, but
with damping injected in a manner reminiscent of the most basic form of passivity
based control.[3] A variety of two-dimensional tasks were performed in the horizontal
plane; and all of them proved feasible even in the absence of visual feedback [24].

More recently, Rodríguez-Seda et al. [54] performed an experimental study
comparing six different teleoperation schemes (five variants of the wave-based IPC

---

[3]As mentioned in Subsection 1.2.2.4, however, the damping employed was not of sufficient
magnitude to actually guarantee passivity of the system.

scheme and one PE-style approach with damping injection to provide passivity) in the presence of data loss and time-varying delay. The master and slave consisted of 2-DOF planar elbow manipulators; and mean round-trip latencies as large as 0.96 seconds were explored. All six controllers remained stable in the scenarios tested.

Although a number of telesurgery experiments have occurred to date, they largely fall outside the scope of the present study. Both the Zeus and the Da Vinci surgical systems are unilateral in nature, forcing the operator to rely on visual rather than haptic feedback, and typically situate both master and slave in the same room [55]. A significant exception to the latter condition has been that of Operation Lindbergh [56], in which a surgeon located in New York successfully performed laparascopic surgery on an actual human patient located in France using a specially modified Zeus telesurgical system. Round trip latency was approximately 155 milliseconds using a private virtual channel hosted on a translatlantic fiberoptic line. Experiments conducted in preparation for this surgery suggested that surgeons could comfortably accommodate at least 330 milliseconds of round-trip latency[4], with some able to function reasonably at levels as high as 500 milliseconds. As a unilateral teleoperation system, however, the control challenges that are the primary interest of the present work were largely avoided; and this technology demonstration relates much more closely to the operator-centric studies presented in Subsection 1.2.1 than to the bilateral schemes discussed above.

---

[4]A magnitude very close to the 0.3 seconds reported in the human perception findings of Held et al. [5]

1.3   Wave Impedance Selection Problem

The action of the waves in the IPC scheme is governed by a wave impedance parameter B that is the focus of the present work. It is widely recognized that a large impedance value is well suited to contact tasks and a low value is preferable for free motion. Beyond this basic observation, however, little guidance exists in the literature regarding the selection of this parameter. More significantly, almost no guidance exists in prior work regarding the simultaneous combination of contact (perpendicular to the constraint) and free motion (parallel to the constraint) that is an intrinsic part of almost any realistic contact task. This becomes particularly important in the context of wave-based control, which often struggles in practical implementation to handle contact effectively. Indeed, Lawn and Hannaford [57] were forced to abandon trials of a passivity-based approach in their greatest time-delay scenario (1 second) when the use of an impedance value sufficiently low to enable reasonable operation did not provide adequate stiffness perception in contact.

1.3.1   Motivating Example

The primary effects of wave-based communication with delay are to reduce the apparent stiffness of the environment and increase the apparent inertia of the teleoperation system. Within some basic assumptions as will be discussed in greater

detail in Chapter 2, these effects behave according to

$$m_{eq} = m_m + m_s + BT \tag{1.1}$$

$$k_{eq} = \frac{K_e B}{B + K_e T} \tag{1.2}$$

where m_{eq} and k_{eq} are the perceived inertia and stiffness (respectively) of the tele-operation system, m_m and m_s are respectively the inertia of the master and slave manipulators, B is the wave impedance, K_e is the environmental stiffness, and T is the one-way communication latency [58] [10] [59].

Consider a teleoperation system operating with $T = 1.5$ seconds one-way latency[5]. Suppose the environmental stiffness is 1 kN/m and 90% accurate stiffness perception is desired (i.e., $K_{eq} = 0.9$ kN/m). Applying this requirement to the above equations, this requires a minimum acceptable wave impedance of $B = 13.5$ kN $\cdot$ s/m. The inertial penalty BT contributed to M_{eq} then becomes more than 20 metric tons, clearly orders of magnitude mismatched with the capabilities of a human operator.

The large choices of B which are often necessary in order to facilitate adequate perception of the environment can easily inhibit free motion of the manipulator to such a degree as to make motion along the non-contact axes virtually impossible. As other researchers work to improve transparency of the system by reducing wave reflections and improving position tracking, this often-neglected limitation becomes

---

[5]This is approximately the time for a speed-of-light signal between the Earth and the Moon. Moreover, latencies of this level might easily occur in less efficient communication networks to satellites in Earth orbit.

an increasingly limiting implementation challenge. Uniform application of the same B value across all axes greatly limits the operating regimes in which wave-based teleoperation is feasible; and even the ability to assign different choices of B to each joint space degree of freedom[6] becomes of very limited utility when contact behaves in a Cartesian fashion.

1.3.2 Related Work

In a scope that far exceeds bilateral teleoperation specifically, the idea of treating different degrees of freedom differently during a contact task has existed for some time. Mason [60] stated that, clearly, position control is only appropriate when the manipulator is free to move and that force control is only appropriate when the manipulator is in contact with something against which to react forces, and that neither pure force control nor pure position control is appropriate in the case of constrained motion. Hybrid control schemes [61] [62] have been put forward which implement force-based control on those degrees of freedom most nearly normal to a motion constraint and position control on those degrees of freedom most nearly tangent to the constraint. Salisbury [63] instead proposed generating an appropriate Cartesian stiffness matrix to govern the behavior of the manipulator, wherein a low stiffness is chosen perpendicular to the constraint to ensure low contact force but a high stiffness is chosen parallel to the constraint to ensure good velocity tracking. The latter is an example of impedance control (See [28]), as is the wave-based scheme

---

[6]a capability that is widely acknowledged but seldom meaningfully discussed in the literature

that is the focus of the present work. Wang and Xie [64] explore the implementation of a (Jacobian-transpose) Cartesian-based control law on top of a passivity-based teleoperation scheme; however, their scheme is not wave-based. Moreover (reminiscent of [65]), their approach is not *intrinsically* passive, guaranteeing passivity by requiring that gains be selected within certain bounds on the basis of a presumed-known upper limit on communication latency; and this guarantee of passivity is for the teleoperation system as a whole, not its individual elements, complicating any attempts to use it in conjuction with other work in passivity-based teleoperation.

Despite the long-standing recognition of the utility of distinguishing constrained and unconstrained degrees of freedom in the larger field of compliance control, application of this notion to wave-based teleoperation specifically has been surprisingly lacking. Some works [25] [66] have acknowledged that a diagonal wave impedance matrix can be used to treat each of the joint degrees of freedom separately. Because nearly any realistic contact task would constrain motion in a Cartesian manner, however, this is not directly useful except in highly kinematically simple situations. It is this limitation in prior work which the present dissertation endeavors primarily to correct. Overcoming the conflict between free motion and contact tasks is of paramount importance, and represents one of the most significant impediments to the extension of recent teleoperation developments into practical application.

A second consideration of the present work is the question of what choice of impedance is appropriate for a given task. Prior work in the area of contact-noncontact transition in wave-based teleoperation has largely focused on the idea of

transitioning from a "small" to a "large" value of impedance when contact is detected [66] [67]. No guidance was given in these works as to the choice of appropriate small or large values, however. Hirche and Buss [59] present a linear, single-input-single-output (SISO), human-oriented analysis yielding upper and lower bounds on wave impedance selection such that the effect of the teleoperation system on transparency falls below human perceptual limits. Only in the case of very small time delays, however, can both of these bounds be satisfied simultaneously. What is needed is a formulation of appropriate compromise between these conflicting considerations when system limitations do not allow for quasi-perfect transparency to the user.

Because the mapping between joint torques and Cartesian forces and torques varies with joint angles, this scheme necessarily involves a time-varying choice of impedance. While not presented in a joint-configuration-dependent sense as in the present application, Rodríguez-Seda [68], Rodríguez-Seda and Spong [66], and Tanner and Niemeyer [67] have proposed methods for changing the wave impedance at runtime in response to transitions between contact and free motion, with the first two references proposing a continuously changing impedance and the final one investigating the effects of a discrete change between free-motion and contact values. In all cases, however, contact is treated in a binary fashion: either a joint is in contact and should have high impedance, or it is free and should have low impedance. No guidance is given as to the selection of appropriate high and low values for the system. Environmental constraints are treated with a simplicity that suggests one expects them to be either perfectly parallel to or perfectly perpendicular to each of the robot's degrees of freedom—a clearly simplistic line of thought.

1.4   The Present Work

1.4.1   Problem Statement

The present work aims to negotiate the trade between the conflicting requirements of contact and free motion by selecting a wave impedance on the basis of the Cartesian reality of the manipulation task, identifying a favorable wave impedance choice that takes full advantage of the freedom to choose a positive definite matrix rather than simply a scalar.

1.4.2   Contributions of the Present Work

Whereas previous work in wave-based teleoperation has generally taken the wave impedance to be a scalar or, occasionally, a diagonal matrix of positive values in the joint space[7], the present work extends thinking on this parameter into the duality between the joint and Cartesian spaces that is in an intrinsic part of any realistic contact task. Simultaneously addressing the conflicting requirements of contact and free motion is of critical importance to practical application of wave-based techniques. In contrast to scalar or diagonal matrix treatments, this scheme takes advantage of the freedom to choose any positive-definite matrix. Exploration of this capacity provides necessary insight into the bilateral-teleoperation-with-delay problem, since wave-based teleoperation cannot be meaningfully compared against

---

[7]Exceptions include Carignan and Ollson [41] and Kanno and Yokokohji [38], who treat the wave impedance as a scalar in the Cartesian space. Neither work, however, provides guidance on the selection of an appropriate value nor considers the possibility of a non-isotropic impedance distribution.

the other control schemes described in Section 1.2 if the system has not been tuned effectively.

To provide additional guidance and insight into the impedance selection problem, a quasi-optimal result from linear systems theory is explored within the proposed Cartesian framework. A Lyapunov-like analysis is presented to demonstrate that the passivity of the IPC system is unaffected by the proposed scheme even if such impedance updates are executed in an online fashion; and results from simulation and human factors studies are presented validating the technique. The effect of uncertain environmental parameters is also explored.

Chapter 2:   Wave-based teleoperation: Linear analysis

2.1   Overview

This chapter defines the concept of passivity and summarizes the wave-based bilateral teleoperation scheme. Transparency is considered in the case of linear manipulator dynamics, and an optimal choice of wave impedance is identified for the case of a single-input-single-output linear system. This provides general insight into the basic considerations associated with the design of a wave-based teleoperation system.

2.2   Passivity

A dynamic system with state $\underline{x}$ is said to be passive with $\underline{u}$ as input and $\underline{y}$ as output if there exists a positive semidefinite storage function $V(\underline{x})$ such that

$$\underline{u}^T(t)\underline{y}(t) \geq \dot{V}(\underline{x}, \underline{\dot{x}}) \tag{2.1}$$

An equivalent condition in integral form is

$$\int_0^t \underline{u}(k)^T \underline{y}(k) dk \geq -V_0 \tag{2.2}$$

where V_0 represents a stored potential in the component at time $t = 0$ and k is a dummy time variable introduced for integration.

The storage function $V(\underline{x})$ is analogous to physical energy. The condition above is essentially a statement that the system cannot generate energy, and that its total energy cannot increase unless work is done on the system via its input. It is not necessary that $V(\underline{x})$ be the actual mechanical or electrical energy of the system, nor that it have units of energy, although this is often a reasonable starting point in the analysis of the passivity of actual physical systems.

In the same way that the interconnection of passive mechanical or electrical elements (such as resistors, capacitors, and inductors) produces a system whose energy state cannot increase except due to input, systems that meet the definition of passivity given above can be placed in (negative) feedback with other passive elements to yield a network of components that is itself also passive [20] (also summarized in [69]). In the context of control of robotic systems, this amounts to a guarantee of stability (in the sense of Lyapunov) of the output variable. This means that the feedback interconnection of one or more passive physical systems with a passive controller, communication channel, etc., is immediately known to also be passive and therefore stable. This allows for widespread reuse of developed components that are known to be passive without requiring additional analysis of the stability of the overall network, enabling a virtual toolbox of robotic control components that may be used in a myriad of combinations.

2.3 Teleoperation scheme

Within the preceding considerations, the traditional force-reflection scheme of bilateral teleoperation can be shown to be passive in the absence of communication latency. When communication latency exists, however, it can also be readily shown that transmission of force and velocity information ceases to be passive. To this end, Anderson and Spong [23] suggested the use of the scattering transformation to exchange this information in the manner of a transmission line (developed into its present-day formulation by Niemeyer and Slotine [25]). Fig. 2.1 shows an overview of this teleoperation scheme, in which a scattering transform converts motion and torque variables $\dot{q}$ and τ into wave variables $\underline{u}$ and $\underline{v}$. These wave variables are transmitted across the latent channel before being converted back into suitable motion and torque values. $\underline{\tau}_h$ represents the torque due to the human operator, and $\underline{\tau}_e$ the torque due to the environment. The blocks labeled PI are proportional-integral[1] controllers operating on the velocity tracking error $\underline{e}_s = \dot{\underline{q}}_{sd} - \dot{\underline{q}}_s$ and $\underline{e}_m = \dot{\underline{q}}_{md} - \dot{\underline{q}}_m$.

---

[1]In some works, these controllers are referenced as PD rather than PI controllers. They are PI in the velocity space, which is mathematically equivalent to PD in the position space because position is the integral of velocity. The velocity space interpretation is favored here because the notion of impedance is conventionally defined as the mapping from velocity (not position) to force, and because velocity $\dot{q}$ is the motion variable employed in the wave transform.
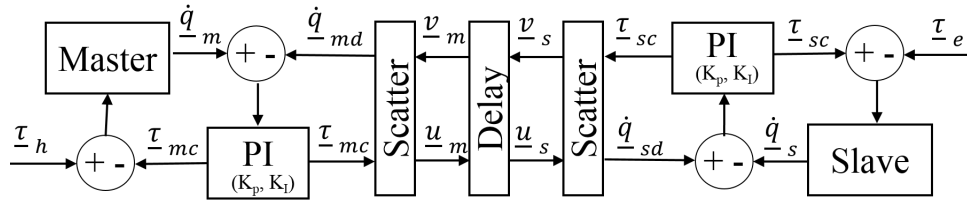
Figure 2.1: Overview of the passivity-based bilateral teleoperation scheme

This change of variables encodes position and velocity information into a wave, which is passed from one robot to the other. The transformation between this wave and torque/velocity information is given by [70]

$$\underline{u}_m = \frac{1}{\sqrt{2}} \left(\mathbf{B}_{1/2} \underline{\dot{q}}_{md} + \mathbf{B}_{1/2}^{-T} \underline{\tau}_{mc} \right) \tag{2.3}$$

$$\underline{v}_m = \frac{1}{\sqrt{2}} \left(\mathbf{B}_{1/2} \underline{\dot{q}}_{md} - \mathbf{B}_{1/2}^{-T} \underline{\tau}_{mc} \right) \tag{2.4}$$

$$\underline{u}_s = \frac{1}{\sqrt{2}} \left(\mathbf{B}_{1/2} \underline{\dot{q}}_{sd} + \mathbf{B}_{1/2}^{-T} \underline{\tau}_{sc} \right) \tag{2.5}$$

$$\underline{v}_s = \frac{1}{\sqrt{2}} \left(\mathbf{B}_{1/2} \underline{\dot{q}}_{sd} - \mathbf{B}_{1/2}^{-T} \underline{\tau}_{sc} \right) \tag{2.6}$$

where $\mathbf{B}_{1/2}$ is the square root of the wave impedance $\mathbf{B}$. Most previous work has taken the wave impedance parameter $\mathbf{B}$ to be a positive scalar or, occasionally, a diagonal matrix of positive values; and in either case the definition of the square root is unambiguous. It is well known, however, that any positive definite matrix will preserve passivity of the communication channel in the case of constant communication latency [71]; and Alise et al. [70] provide conditions that are still more general. Alise et al. adopt the interpretation that $\mathbf{B}_{1/2}$ is the positive definite matrix square root (i.e., $\mathbf{B}_{1/2}$ is the matrix satisfying $\mathbf{B}_{1/2}\mathbf{B}_{1/2} = \mathbf{B}$). The present work follows in this same interpretation for the simulation and experimental results to be presented here and in subsequent chapters, but has transposed $\mathbf{B}_{1/2}^{-1}$ in the above expressions so as to achieve a formulation that is additionally compatible with the use of the Cholesky decomposition (i.e., the upper-triangular[2] matrix sat-

---

[2]The MATLAB function `chol` follows this convention of an upper-triangular matrix by default,

isfying $\mathbf{B}_{1/2}^T\mathbf{B}_{1/2} = \mathbf{B}$). The stability discussion to be presented in Section 3.2.1.3 applies equally to either approach, as does the analysis of steady-state mechanical characteristics in Section 3.4.

The wave variables given above make no distinction between forces (torques) and velocities (angular rates); the system designer may choose to extract commands for each of the master and slave in the form of either a desired velocity or a commanded torque [58]. Fig. 2.1 shows the velocity-velocity configuration, as is the most common implementation. In the force-force configuration, the PI controllers would be omitted; and the wave-based communication channel (the scatter-delay-scatter portion of the diagram) would connect directly to the master and slave systems.

Because this scheme transmits velocity rather than absolute position information, it is known to exhibit a gradual accumulation of coordination error between master and slave. Feedback passivation has been used to allow transmission of absolute position information in an effort to mitigate this [34], but this requires either a priori knowledge of the system dynamics or an adaptation scheme for learning this model. For simplicity, the present study considers the traditional case of velocity transmission. Techniques exist for mitigating the accumulation of coordination error within such a scheme without violating passivity for the overall teleoperation system [33], [36], [25]; however, these techniques (and in particular their effect on transparency) are beyond the scope of the present study.

───────────────────────────

although some treatments instead employ a lower-triangular matrix that should be transposed before use in the expressions given here.

2.3.1 Mechanical characteristics displayed to the operator

Arcara and Melchiorri [10] identify the equivalent mass, damping, and stiffness displayed to the operator of a variety of teleoperation schemes, including the Intrinsically Passive Controller (IPC) shown in Fig. 2.1. Their approach is to identify the transfer function governing the relationship between the force applied by the human operator and the motion of the master manipulator, assuming linear SISO dynamics:

$$G(s) = \left(\frac{X_m(s)}{F_h(s)} \right)^{-1} \qquad (2.7)$$

where $X_m(s) = \mathcal{L}(x_m(t))$ and $F_h(s) = \mathcal{L}(F_h(t))$ represent the Laplace transforms of their respective time-domain quantities. Containing delay terms e^{-sT}, this transfer function has infinitely many poles and zeros and thus cannot truly be mapped to an equivalent mass-spring-damper combination. The authors' approach is therefore to neglect terms of order s^3 and higher, thus identifying the second-order system that approximates the teleoperator at low frequencies ($\omega << 1$). Equivalent mass m_{eq} and damping b_{eq} are identified for free motion, decomposing the transfer function as:

$$G(s)|_{F_e=0} = m_{eq}s^2 + b_{eq}s + G^*(s) \qquad (2.8)$$

where $G^*(s)$ contains terms of order s^3 and higher (neglected to approximate behavior at lower frequencies); and equivalent stiffness k_{eq} is identified for contact:

$$k_{eq} = \lim_{s \to 0} \left(G(s)|_{F_e=-K_e x_s} \right) \qquad (2.9)$$

27

The master and slave manipulators are modeled as linear mass-dampers. Whereas Arcara and Melchiorri assumed the master and slave were identical, the more general case is considered presently:

$$m_m \ddot{q}_m + b_m \dot{q}_m = \tau_m \qquad (2.10)$$

$$m_s \ddot{q}_s + b_s \dot{q}_s = \tau_s \qquad (2.11)$$

where τ_m and τ_s represent the net force (or torque) acting on the master and slave, respectively.

Arcara and Melchiorri consider a much more general control law than the PI controllers of the typical implementation shown in Fig. 2.1. In their formulation, the controllers are permitted to add virtual inertia to the system, which is permitted to have a damping coefficient of its own and connects to the other elements of the teleoperator with a designer-selectable stiffness. Although this serves to better capture the breadth of passive linear controllers that one could, in principle, choose to implement, PI controllers are by far the most conventional configuration. As will be shown shortly, the wave-based teleoperation scheme already serves to encumber the system with added virtual inertia. It will also be shown in Section 3.2 that the PI controllers introduce dissipativity into the system (which does not appear in the results below because it does not take the form of a linear damper). The system designer is therefore left with little motivation to implement these additional control features. The remainder of the analysis below therefore assumes ordinary PI controllers; and the reader is referred to the authors' original work [10] for the

full general result.

Fig. 2.2 defines four subsystems within the overall teleoperation system presented in Fig. 2.1. Below, the transfer functions of these subsystems are presented (assuming $K_p = B$ for impedance-matching purposes[3]), followed by the total system. These transfer functions are expressed with regard to position rather than velocity variables for consistency with Arcara and Melchiorri's approach ($\mathcal{L}\{\dot{q}(t)\} = s\mathcal{L}\{q(t)\}$). T represents the one-way communication delay.

$$G_1(s) = \frac{\tau_{sc}}{q_{sd}} = \frac{(K_p + K_I/s)(m_s s^2 + b_s s + K_e)}{m_s s^2 + b_s s + K_p s + K_e + K_I} \tag{2.12}$$

$$G_2(s) = \frac{v_m}{u_m} = e^{-2sT}\frac{B - G_1(s)}{B + G_1(s)} \tag{2.13}$$

$$G_3(s) = \frac{\dot{q}_{md}}{\tau_{mc}} = \frac{G_2^{-1}(s) + 1}{B(G_2^{-1}(s) - 1)} \tag{2.14}$$

$$G_4(s) = \frac{\tau_{mc}}{q_m} = \frac{(K_p + K_I/s)s}{1 + (K_p + K_I/s)G_3(s)} \tag{2.15}$$

$$G_{tot}(s) = \frac{\tau_h}{q_m} = m_m s^2 + b_m s + G_4(s) \tag{2.16}$$

G_{tot} is then analyzed according to (2.8) and (2.9), yielding equivalent mechanical parameters as follow:

$$m_{eq} = m_m + m_s + BT - \frac{b_s^2 T}{B} - \frac{2b_s^2}{K_I} \tag{2.17}$$

$$b_{eq} = b_m + b_s \tag{2.18}$$

$$k_{eq} = \frac{K_e K_I B}{B(K_I + 2K_e) + K_e K_I T} \tag{2.19}$$

---

[3]An impedance mismatch can cause wave reflections in the communication channel, resulting in oscillation of the system [25] that (although stable) is generally undesirable.

These results are consistent with those derived by Niemeyer and Slotine [58] and Hirche and Buss[4] [59] for the effect of the communication channel alone, neglecting slave joint friction. Taking the limit of the above expressions as $K_I \to \infty$ and $b_s \to 0$,

$$m'_{eq} = m_m + m_s + BT \tag{2.20}$$

$$k'_{eq} = \frac{K_e B}{B + K_e T} \tag{2.21}$$

These values are equivalent to combining the master and slave systems in series[5] with an element having inertia BT and stiffness B/T. They may be taken as exact results for the force-force wave teleoperator configuration, or as approximate relations (assuming large integral gain) in the velocity-velocity configuration with PI controllers.

The equivalent damping b_{eq} derived above in the manner of Arcara and Mel-

---

[4]Note that this reference follows the convention that T is the *round-trip* communication delay

[5]In which case inertias add directly ($m_{1+2} = m_1 + m_2$) and stiffnesses add inversely ($k_{1+2}^{-1} = k_1^{-1} + k_2^{-1}$).
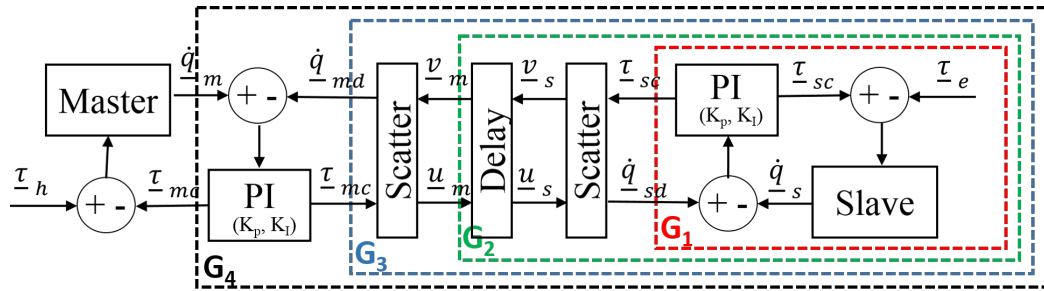
Figure 2.2: Diagram of teleoperation system subcomponents for which transfer functions are presented.

chiorri differs from that presented by Niemeyer and Slotine [58] because the former seeks to identify a linear damping term that is directly proportional to the master velocity. Damping of this form appears in the system at low frequency only as a result of joint friction in the master and/or slave (unless, of course, additional damping is deliberately injected as part of the control law). Niemeyer and Slotine do not consider such joint friction, and report instead a damping of $2B$, ostensibly referring to the dissipation introduced by the PI controllers (to be discussed in Section 3.2).

2.4 Optimization of Wave Impedance

The system designer has considerable latitude to select the wave impedance **B** with transparency as very nearly the sole consideration beyond the requirement of positive definiteness given in the previous section. Beyond the basic recognition that high impedance is well suited to contact tasks and low impedance is well suited to free motion, however, little guidance exists in the literature regarding selection of this parameter. Hirche and Buss [59] present a human-oriented analysis yielding upper and lower bounds on the wave impedance such that the effect of the teleoperation system will fall below human perceptual limits; but only in the case of very small time delays can both bounds be satisfied simultaneously. Niemeyer et al. [58] acknowledge that perfect transparency is impossible, and instead propose treating the teleoperator as a "virtual tool" to which desired properties can be assigned rather than a link with the remote environment that is expected to transparently vanish from the operator's perception. Both of these prior works address the wave

impedance in only a scalar sense. In order to address the more general case in which one must compromise in a non-neglible sense between the conflicting design goals, and continuing (for the present chapter) in this scalar analysis regime, this section considers an optimization based upon the results of the preceding section.

For the purpose of the present dissertation, the problem of teleoperation can be separated into two parts: the control of the robots themselves, and the communication of information between the master and slave sites. In the case of the conventional wave-based configuration shown in Fig. 2.1, control is provided by the PI controllers while communication is provided by the wave transformation (scatter-delay-scatter in the figure).[6] The utility of wave-based communication is precisely in this latter arena; and the following analysis focuses on the contribution of the communication channel specifically (treating it as a "virtual tool" in the manner of Niemeyer and Slotine [58] and employing the simplified relations m'_{eq} (2.20) and k'_{eq} (2.21)) rather than deriving an optimum that is applicable only to a specific configuration among an infinite number of possible configurations.[7] (For completeness, however, the overall operator experience provided by the conventional configuration shown in Fig. 2.1 is additionally analyzed in Subsection 2.4.4.) In much the

---

[6]These two components need not decouple in all cases. The wave variable equations can, for example, be solved for forces rather than velocities [25], thus eliminating the PI controllers and subsuming the control aspect into the wave transformation as well—although this is not usually done because the PI controllers provide a convenient means of impedance matching. Additionally, many of the other schemes discussed in Chapter 1 close a single control loop *around* the communication channel rather than having separate loops on either side.

[7]Indeed, Mendoza et al. [39] entirely replace the PI controllers of Fig. 2.1 with their own adaptive impedance controllers to improve regulation of contact forces; and Sun et al. [40] combine a sliding mode controller with a modified wave based communication channel.

same way as PD position and PI velocity controllers (which are also intrinsically passive when gains are constant) are so widely used throughout robotics because of their usefulness across an incredible variety of systems, the passive communication channel provided by the wave transformation has a similar capacity to be the go-to communication scheme[8] for a wide variety of control-with-delay applications.

Several different formulations of the optimization problem are considered in the following subsections. The results are then tabulated in Table 2.1 in the end-of-chapter summary presented in Section 2.6.

2.4.1 Formulation of the Optimization Problem

Weber's Law [72] states that the just noticeable difference (JND) for a sensory stimulus will be a fixed fraction of the base stimulus. For example, if a subject can detect at minimum a one-pound variation on a ten-pound load, then one would expect a two-pound variation to be the just noticeable difference on a twenty-pound load. This suggests objective functions comparing the fractional (rather than absolute) error in the perception of the two quantities given above (which directly relate to the force/torque perceived by the user and to the motion of the system via

---

[8]In the sense of being a simple, widely applicable scheme with minimal knowledge burden associated with successful implementation

Newton's second law and Hooke's law, respectively):

$$\phi_M = \frac{m'_{eq}}{m_m + m_s} \tag{2.22}$$

$$\phi_K = \frac{K_e}{k'_{eq}} \tag{2.23}$$

Each of these fractions is written with the larger quantity in the numerator, such that transparency is maximal when these expressions are minimal. It is clear from inspection of the relations for m'_{eq} (2.20) and k'_{eq} (2.21) that in general (for $T \neq 0$) ϕ_M is minimal when $B \to 0$, whereas ϕ_K is minimal when $B \to \infty$. This is therefore a two-objective optimization problem in which the objectives are in direct conflict; and the Pareto frontier consists of the entire design space $B \in (0, \infty)$.

In a high-stiffness environment, little motion will be possible and force transparency concerns will far outweigh velocity motion transparency. Conversely, in a low-stiffness environment, there will be little contact force for the operator to feel and motion transparency will be the primary concern. To this end, a free motion coefficient is defined as

$$\alpha_f = \frac{k_{ref}}{k_{ref} + K_e} \tag{2.24}$$

which will vary between 0 (when $K_e = \infty$, i.e., when in contact with a perfectly rigid environment) and 1 (when $K_e = 0$, i.e., when in completely free motion). This coefficient (which can vary during operation as the robot encounters changing environmental conditions) is used as a weighting factor to define a combined objective function that is a weighted combination of the two principal considerations given

by ϕ_M and ϕ_K. The reference stiffness $k_{ref} > 0$ is an application-specific parameter that must be selected by the end user, representing the stiffness at which these two conflicting transparency considerations are weighted evenly (i.e., $\alpha_f = 0.5$). Some additional discussion of this parameter is provided in Subsection 2.4.3. Using this measure of the degree to which the system is in a state of free motion, one may then codify the preceding transparency concerns into the following objective function, which will emphasize inertia transparency in free motion but stiffness perception when in contact:

$$\Phi = \frac{m'_{eq}}{m_m + m_s}\alpha_f + \frac{K_e}{k'_{eq}}(1 - \alpha_f) \tag{2.25}$$

Inertia perception becomes the sole consideration at zero stiffness; and pure stiffness consideration is smoothly and asymptotically approached as K_e becomes large.

2.4.2   Optimization

Substituting the proposed free motion coefficient (2.24) into the objective function (2.25):

$$\Phi = \frac{m'_{eq}}{m_m + m_s}\alpha_f + \frac{K_e}{k'_{eq}}(1 - \alpha_f) \tag{2.26}$$

$$= \frac{m'_{eq}}{m_m + m_s}\left(\frac{k_{ref}}{k_{ref} + K_e}\right) + \frac{K_e}{k'_{eq}}\left(1 - \frac{k_{ref}}{k_{ref} + K_e}\right) \tag{2.27}$$

$$= \frac{m'_{eq}}{m_m + m_s}\left(\frac{k_{ref}}{k_{ref} + K_e}\right) + \frac{K_e}{k'_{eq}}\left(\frac{K_e}{k_{ref} + K_e}\right) \tag{2.28}$$

This function is to be optimized with respect to the choice of wave impedance B.

Substituting the expressions for equivalent mass (2.20) and stiffness (2.21) into

(2.28) in order to make the dependence on B explicit:

$$\Phi = \frac{m_m + m_s + BT}{m_m + m_s}\left(\frac{k_{ref}}{k_{ref} + K_e}\right) + \frac{B + K_eT}{B}\left(\frac{K_e}{k_{ref} + K_e}\right) \tag{2.29}$$

The denominator quantity $k_{ref} + K_e$ is a constant for the purpose of this optimization and will not affect the value of B at which Φ is minimal. One can therefore consider the equivalent optimization of the simpler cost function Φ':

$$\begin{aligned}
\Phi' &= (k_{ref} + K_e) \cdot \Phi \\
&= \frac{k_{ref}(m_m + m_s + BT)}{m_m + m_s} + \frac{K_e(B + K_eT)}{B} \\
&= k_{ref} + \frac{k_{ref}BT}{m_m + m_s} + K_e + \frac{K_e^2T}{B}
\end{aligned} \tag{2.30}$$

The constant terms and factors in this expression may similarly be dropped, reducing the equivalent objective function as

$$\Phi'' = k_{ref}\frac{BT}{m_m + m_s} + \frac{K_e^2T}{B} \tag{2.31}$$

$$\Phi''' = k_{ref}\frac{B}{m_m + m_s} + \frac{K_e^2}{B} \tag{2.32}$$

The general shape of this reduced objective function is given in Fig. 2.3. For $B > 0$, it has a single global minimum B^* and approaches infinity as B approaches either zero or infinity. The minimum B^* can be identified by differentiating the

expression and setting it equal to zero:

$$\frac{d}{dB}\left(\Phi'''\right) = \frac{k_{ref}}{m_m + m_s} - \frac{K_e^2}{B^2} = 0 \tag{2.33}$$

$$\rightarrow \boxed{B^* = K_e\sqrt{\frac{m_m + m_s}{k_{ref}}}} \tag{2.34}$$

That this result is a minimum (rather than a maximum or inflection point) of Φ''' can be verified by inspection of the second derivative:

$$\frac{d\Phi'''}{dB^2} = 2\frac{K_e^2}{B^3} > 0 \tag{2.35}$$

Note that this minimum (2.34) is independent of delay time T, which may in general be unknown.

This is an unconstrained minimization; and caution is warranted in the application of its result. See Subsection 2.4.5 for further discussion.
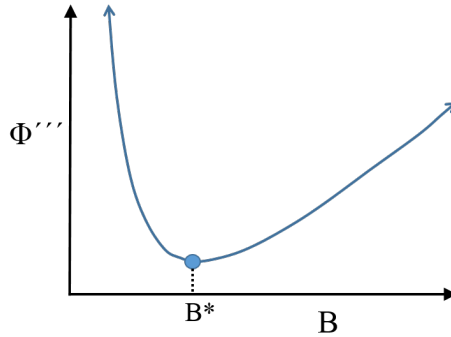
Figure 2.3: General shape of Φ'''

2.4.3 Choice of k_{ref}

The parameter k_{ref} gives the end user the freedom to specify at what stiffness the contact/free-motion trade becomes significant. Directly, k_{ref} is the stiffness at which $\alpha_f = 0.5$, and thus the two conflicting considerations are weighted evenly. Using (2.24), however, one could easily instead choose k_{ref} so as to achieve a particular weighting at a particular stiffness level—e.g. to attain $\alpha_f = 0.95$ at some stiffness that is considered essentially indistinguishable from rigid contact. The choice of k_{ref} will necessarily be task-specific. Tasks consisting largely of free motion and requiring only the ability for the operator to crudely distinguish contact from non-contact (as in simple assembly and servicing tasks) would motivate a large choice of k_{ref}. Tasks requiring more precise assessment of subtle environmental characteristics (as when palpating a patient abdomen in medical applications) would motivate a smaller choice of k_{ref}. In practice, one might give the operator the ability to adjust this parameter during runtime as different subtasks skew the emphasis toward one or the other of the two conflicting goals of stiffness and inertia transparency.

In addition to the foregoing task-specific considerations, the perceptual system of the human operator also merits consideration. From inspection of the literature (for example, see [73]), one might conclude that humans are roughly twice as sensitive to changes in stiffness as compared to changes in inertia. This might argue for doubling the weight of the stiffness perception term in Φ; however, the effect of this is only to change the final expression for B^* by a factor of $\sqrt{2}$ and is algebraically equivalent to choosing a value of k_{ref} that is half the stiffness value at which it is

desired to have equal *perceived* inertia and stiffness fidelity. Because the choice of k_{ref} is already application specific, this facet of human perception is not particularly relevant to the present study but may be relevant to future work.

Although mathematically k_{ref} could take on any finite positive value, one might additionally expect human perceptual systems to render sufficiently extreme choices inappropriate. Tan et al. [74] found subjects in contact with a rectangular aluminum beam to report no perceptible difference from complete rigidity beginning at stiffnesses ranging between 15 and 42 kN/m (although subjects had their eyes closed and visible deflections still occurred in this experiment). Under ordinary teleoperation circumstances (with a human operator and the goal of maximizing transparency), one should therefore employ a k_{ref} well below this threshold. In principle, however, one could choose a higher value of k_{ref} so as to effectively translate higher environmental stiffness into the human perceptual regime; or one could replace the human operator entirely with some passive computer-based controller for which questions of human perception are not relevant.

2.4.4   Effect of the controllers

The preceding analysis considers only the effect of the communication channel itself. In actuality, the system designer would ideally like to optimize the user experience when interacting with the full teleoperation system rather than the communication channel alone. In any reasonable configuration, though, the goal is to tune the communication channel such that it accurately transmits force information

without unduly burdening the system with added inertia. Indeed, the "virtual tool" representation proposed by Niemeyer and Slotine [58] considers the communication channel as a piece of the system whose inertia and stiffness add to those of the other components of a teleoperation system (whatever they may be) in the same way that physical mass-spring-damper properties would add when combined in series. Thus, one might expect the foregoing optimization of the choice of B to be a reasonable rule-of-thumb choice—yielding a communication channel appropriately designed as a virtual tool for the job—even when combined with other components in a larger teleoperation system. The present subsection explores this question in greater detail, showing the effect on the optimal (with respect to the chosen objective function (2.25)) choice of B as well as exploring the choice of controller gains.

A feature of passivity-based control is that passive components such as the wave-based communication channel may be used in (negative) feedback with any other passive components and still maintain passivity of the overall system [20] (also summarized in [69]). It would, naturally, be impossible to consider every possible configuration of a wave-based teleoperation scheme in the present analysis. This subsection considers case presented in Fig. 2.1, utilizing the full results m_{eq} and k_{eq} presented in Subsecton 2.3.1, including the effects of the controllers that were neglected in the preceding analysis.

Replacing the simplified mass and stiffness expressions in (2.25) with the full

expressions (2.17) and (2.19) yields the full objective function

$$\Phi_{full} = \frac{m_{eq}}{m_m + m_s}\alpha_f + \frac{K_e}{k_{eq}}(1 - \alpha_f) \tag{2.36}$$

The derivative with respect to the design variables of this proposed objective function are given by:

$$\frac{d\Phi_{full}}{dB} = \frac{\left[b_s^2 k_{ref} + B^2 k_{ref} - K_e^2(m_m + m_s)\right]T}{B^2(K_e + k_{ref})(m_m + m_s)} \tag{2.37}$$

$$\frac{d\Phi_{full}}{dK_I} = \frac{2b_s^2 k_{ref} - 2K_e^2(m_m + m_s)}{K_I^2(K_e + k_{ref})(m_m + m_s)} \tag{2.38}$$

Because the derivative of Φ_{full} with respect to each design variable is independent of the other, this two-variable optimization problem reduces to two independent single-variable optimizations discussed in Subsubsections 2.4.4.1 and 2.4.4.2, respectively.

2.4.4.1 Choice of B

The foregoing expressions for the full-system m_{eq} and k_{eq} modify the optimal (with respect to the proposed form of Φ) choice of B only slightly:

$$B_{full}^* = \sqrt{\frac{K_e^2(m_m + m_s)}{k_{ref}} - b_s^2} \tag{2.39}$$

In the event that no joint friction is present in the slave manipulator ($b_s = 0$), this reduces to the exact same choice of B^* as derived above (2.34) for the communication channel alone. This result is independent of K_I and, as before, independent of T.

2.4.4.2 Choice of K_I

From evaluation of the derivatives of (2.17) and (2.19) with respect to K_I, it is observed that small K_I will decrease the inertia penalty whereas large K_I will decrease the stiffness penalty (Recall that $m_{eq} > m$ and $k_{eq} < K_e$).

$$\frac{dm_{eq}}{dK_I} = \frac{2b_s^2}{K_I^2} \geq 0 \tag{2.40}$$

$$\frac{dk_{eq}}{dK_I} = \frac{2B^2 K_e^2}{[B(2K_e + K_I) + K_e K_I T]^2} \geq 0 \tag{2.41}$$

Similar to the general advice for B, this would then imply that (for the sole considerations of providing accurate stiffness and inertia perception[9]) a small K_I is best suited for free motion and a large K_I is best suited for contact. (A suitable definition of "large" is discussed in subsection 2.4.5.) As in the case of choosing B, it is again necessary to define a reasonable trade between the conflicting considerations in scenarios in which neither pure contact nor pure free motion considerations are entirely appropriate.

In contrast to the case seen in the impedance selection problem, this formulation of Φ admits no unique, finite optimum for the choice of $K_I > 0$. From inspection of the expression given for $d\Phi/dK_I$, one can see that (for given b_s, k_{ref}, and K_e) the derivative of Φ with respect to this design variable will always have constant sign regardless of choice of $K_I > 0$. If $k_{ref} > \frac{K_e^2(m_m + m_s)}{b_s^2}$, then Φ is minimized as $K_I \to 0$. If $k_{ref} < \frac{K_e^2(m_m + m_s)}{b_s^2}$, then Φ is minimized as $K_I \to \infty$. If $k_{ref} = \frac{K_e^2(m_m + m_s)}{b_s^2}$, then

---

[9]This neglects coordination error, the topic of Subsubsection 2.4.4.3.

the minimization problem is insensitive to K_I. For the ideal case in which joint friction is negligible, these considerations motivate a large choice of K_I. When in contact ($K_e > 0$), this choice will reduce the value of Φ; and when in free motion ($K_e = 0$), the value of Φ will be insensitive to K_I.

2.4.4.3 Coordination Error

Not considered in the foregoing definition (2.36) of Φ is the coordination error between the master and slave robots. Arcara and Melchiorri's expression for master-slave "drift" (at low frequencies when in contact with a remote environment) becomes, again for the case shown in Fig. 2.1,

$$\delta = \lim_{s \to 0} \left(\frac{X_m(s) - X_s(s)}{F_h(s)} \right) = \frac{2}{K_I} + \frac{T}{B} \tag{2.42}$$

In the absence of the integral control term (i.e., in the limit as $K_I \to 0$), coordination error can become unboundedly large because no correction for position drift is implemented. Pure minimization of coordination error (without consideration of the transparency concerns codified in Φ above) would therefore motivate the choice of both B and K_I as large as possible.[10] The reader is additionally reminded that techniques exist outside of the impedance selection problem for mitigation of coordination error [33], [36], [25], and that the following discussion may be used in conjunction with those techniques.

---

[10]One will note, however, that as $B \to \infty$, $m_{eq} \to \infty$ and motion becomes impossible. This clearly defeats the purpose of a teleoperation system.

In the most general treatment, coordination error would be codified in a third objective function in addition to ϕ_M and ϕ_K. Inclusion of its effect in the definition of Φ, however, is not entirely straightforward or appropriate. The expression for δ does not depend upon the magnitude of any reference drift, nor is this error something that will be directly perceptible to the operator in any case. It therefore cannot readily be written in terms of Weber's Law and has no direct effect on the impedance experienced by the operator (which is the quantity of concern in the classical definition of transparency [75]). If, however, one wished to define a Δ_{ref} representing a nominal system drift and to add this drift ratio as an additional contact consideration in the original definition of Φ, then the resulting alternative objective function to that given in (2.36) [11]

$$\Phi_{alt} = \frac{m_{eq}}{m_m + m_s}\alpha_f + \left[\frac{K_e}{k_{eq}} + \frac{\delta}{\Delta_{ref}}\right](1 - \alpha_f) \tag{2.43}$$

yields an optimum impedance choice of:

$$B_{alt}^* = \sqrt{\frac{K_e^2(m_m + m_s)}{k_{ref}} - b_s^2} + \frac{K_e(m_m + m_s)}{k_{ref}\Delta_{ref}} \tag{2.44}$$

In this case the boundary between preference for $K_I \to 0$ and $K_I \to \infty$

---

[11]Note that this objective function in some sense lends double weight to contact considerations versus those of free motion (assuming Δ_{ref} scales the coordination error fraction similarly to the other fractions), since two error measures are summed for the former case and only one for the latter. This simple approach is taken here to facilitate more direct comparison with the optimality conditions derived above. A more rigorous multi-objective treatment remains for future work.

becomes

$$k_{ref,boundary} = \frac{(m_m + m_s)}{b_s^2} \left[K_e^2 + \frac{K_e}{\Delta_{ref}} \right] \qquad (2.45)$$

As previously, small K_I is preferred when k_{ref} is larger than this boundary quantity, large K_I is preferred when k_{ref} is less than this boundary quantity, and the optimization is insensitive to choice of K_I when k_{ref} is equal to this boundary quantity. Once again, this means a large K_I is preferred in the ideal situation in which slave joint friction b_s is negligible.

2.4.5   Suitable Bounds on B and K_I

The results (2.34) and (2.39) for the choice of B stem from an unconstrained optimization of the objective function, and suggest that zero impedance be employed in completely free motion and infinite impedance when in contact with a perfectly rigid object. Obviously, neither of these conditions would be achievable or desirable in practice; and the trade-off codified in (2.26) only makes sense when K_e is of such a value that both stiffness and inertia perception are relevant. Similarly, the foregoing conclusion that it is typically desired to have K_I "large" leaves the system designer with equally little guidance. This subsection attempts to provide some additional guidelines with respect to constraints (particularly upper and lower parameter bounds) that might be reasonably imposed upon the foregoing optimization.

For both B and K_I, substantially limiting factors regarding the maximum acceptable parameter choice will be the effects of discrete implementation in a digital

45

control system and of unmodeled sensor and actuator dynamics. These phenomena threaten the stability of the system, and are discussed briefly in Section 3.7. Ultimately, however, these limitations hinge heavily upon the precise dynamics of the underlying implementation and cannot be addressed in detail in the present general discussion. The following therefore seeks to address only questions of suitable parameter choice that are relevant to the ideal case, in which all system components behave perfectly in accordance with the above-considered equations.

It was remarked in Subsection 2.4.3 that above some threshold K_{max} (which may be somewhere in the tens of kN/m) humans find a spring to be essentially indistinguishable from a rigid object. Thus, although (2.34) may prescribe extremely high choices of B in the presence of extreme stiffnesses K_e, it will be detrimental to encumber the system with an added inertia penalty when the rendered stiffness to the operator already differs imperceptibly from rigid contact. One could certainly (if K_e is known) rearrange (2.19) to identify the B_{max} at which $k_{eq} = K_{max}$. See [59] for a similar human-oriented analysis on impedance bounds. Without appeal to a specific K_e, however, the system designer may wish to enforce an upper bound on B such that the stiffness of the "virtual tool" represented by the wave communication channel ($K_{comm} = B/T$) does not exceed this K_{max}:

$$B_{high} = K_{max}T \tag{2.46}$$

To explore the need for large integral gain, consider the sensitivity of the

objective function to K_I:

$$\frac{d\Phi}{dK_I} = \frac{2\left[b_s^2 k_{ref} - K_e^2(m_m + m_s)\right]}{K_I^2\left(K_e + k_{ref}\right)\left(m_m + m_s\right)} \qquad (2.47)$$

If joint friction b_s is negligible, this becomes

$$\left.\frac{d\Phi}{dK_I}\right|_{b_s \to 0} = \frac{-2K_e^2}{K_I^2\left(K_e + k_{ref}\right)} \qquad (2.48)$$

The effect of K_I was noted to be significant in contact scenarios. When $K_e >> k_{ref}$, this becomes

$$\left.\frac{d\Phi}{dK_I}\right|_{contact} \approx -\frac{2K_e}{K_I^2} \qquad (2.49)$$

Thus, when K_I is chosen comparable to K_e, this derivative becomes approximately $-2/K_I$ (For comparison, recall that $\Phi > 1$) and further increases in integral gain will yield little improvement in the value of Φ. The choice $K_{I,high} = K_e$ may therefore be taken as an approximate guideline for the point at which increases in K_I yield diminished returns; and one may choose to enforce an upper bound on K_I at approximately this level.

With regard to minimum acceptable impedance choice (motivated in free motion scenarios), coordination error will be a substantial consideration. If a maximum acceptable value δ_{max} is identified for the drift quantity defined in (2.42), then that equation may be rearranged to yield

$$B_{low} = \frac{T}{\delta_{max} - (2/K_I)} \qquad (2.50)$$

47

and becomes ill-defined if the first term on the right hand side of (2.42) itself violates δ_{max} (i.e., if K_I is too small to allow satisfaction of this constraint). The choice of δ_{max}, the ratio of the maximum acceptable steady-state coordination error to the maximum anticipated operator force, is necessarily task-specific. The former might be dictated by the minimum feature size of the environment or mechanical tolerances of the task at the remote site; and the latter might be dictated by limitations of either the master haptic device or of the human operator.

A further source of a lower bound on B may (much as the upper bound given above) be extracted from human perceptual considerations. Just as it does little good to increase B above B_{high} to generate an improvement in stiffness rendering that the operator will be unable to detect, reducing B below the operator's just noticeable inertia difference will increase coordination error with no perceptible transparency improvement. If there exists some Δm_{JND} that represents the just noticeable inertia change relative to $m_m + m_s$, then setting this equal to the minimum inertia penalty $B_{min}T$ yields

$$B_{min} = \frac{\Delta m_{JND}}{T} \tag{2.51}$$

where Δm_{JND} would be expected (as with other Weber fractions) to be a fixed ratio of $m_m + m_s$. Beauregard, Srinivasan, and Durlach [76] found this fraction to be approximately 21%.

2.4.6 The Use of General Weights

Choices of objective function other than the one considered here are certainly possible; and the given form of α_f in particular was chosen with the primary goal of defining an algebraically simple function smoothly joining the points $(K_e = 0, \alpha_f = 1)$ and $(K_e = \infty, \alpha_f = 0)$ with a scalable break-even stiffness (via k_{ref}). Presented in this fashion, for given manipulators and environmental parameters, the sole designer-selected input parameter (k_{ref}) to the optimization is a quantity having direct physical meaning—the stiffness above which accurate perception of contact forces is more important than accurate perception of system inertia. In some cases, however, one might wish to combine the Weber fractions ϕ_M (2.22) and ϕ_K (2.23) according to more general, designer-chosen weights. Consider, then, the general weighted combination of these two objectives:

$$\Phi_{gen} = \frac{m_{eq}}{m_m + m_s} w_M + \frac{K_e}{k_{eq}} w_K \tag{2.52}$$

This choice of objective function is minimized when the wave impedance is chosen according to

$$B^*_{gen} = \sqrt{K_e(m_m + m_s) \frac{w_K}{w_M} - b_s^2 w_M} \tag{2.53}$$

This reduces to the previous results (2.34) and (2.39) when $w_M = 1$ and $w_K = K_e/k_{ref}$.

In any event, the optimal results (2.34), (2.39), and (2.53) presented here provide at the very least some basic rules of thumb for the impedance selection

49

problem—guidance that has been lacking in the existing literature. In general, one might expect good results if the chosen wave impedance scales roughly with the environmental stiffness[12] and with the square root of the system inertia. For example, if a teleoperation system that has historically functioned well at some wave impedance choice B_1 picks up a payload that doubles the system's inertia, then one might expect $\sqrt{2}B_1$ to be an appropriate new choice in order to make this new mass apparent to the user. If instead the system mass is left unchanged but the environmental stiffness is reduced by a factor of two, then one might use $B_1/2$ as a starting point for tuning the new system so as to not unduly inhibit motion now that greater displacements are possible. Similarly, in the case of a multi-DOF robot, a simple effort to move beyond the common scalar-impedance implementation would be to choose an impedance for each joint that is proportional to the square root of the effective system inertia at that joint. Thus, more distal joints on a serial-link manipulator might tend to warrant smaller choices of B.

2.5   A Purely Joint Space Implementation

Using the result of the previous section, one can now begin to assess the benefit of systematically associating different choices of wave impedance with different degrees of freedom of the robotic system. Consider a pair of planar, two-link elbow manipulators of the form depicted in Fig. 2.4, each having two links that are 1 m in length, 10 kg in mass, and 3.33 kg-m^2 in rotational inertia. Suppose, for the purpose

---

[12]Or with the square root of stiffness if w_K is not proportional to K_e, and stiffness perception is therefore uniformly weighted regardless of its magnitude

of confining behaviors to the joint space, that the slave's environment consists of torsional springs attached to the manipulator's joints and applying restoring forces $\underline{\tau} = -\mathbf{K}_j\underline{q}$ where the stiffness is given by

$$\mathbf{K}_j = \begin{pmatrix} 1,000 & 0 \\ 0 & 10 \end{pmatrix} \text{N} \cdot \text{m/rad}$$

The human operator, modeled as a PD controller with $K_p = K_d = 100$, drives the robot from an initial pose of $\underline{q}(t = 0) = \begin{bmatrix} 0 & 0 \end{bmatrix}^T$ along a desired trajectory of $\underline{q}_{des}(t) = \begin{bmatrix} 0.5\sin(t) & 0.5\sin(t) \end{bmatrix}^T$. Round trip communication latency is taken to be 100 milliseconds.

The joint space inertia matrix for the given manipulator in its initial pose is given by:

$$\mathbf{M} = \begin{pmatrix} 31.67 & 10.83 \\ 10.83 & 5.833 \end{pmatrix} \text{kg} \cdot \text{m}^2$$

Because the analysis of Section 2.4 was single-DOF in nature, wave impedance for each joint will be chosen on the basis of the corresponding diagonal element of the above matrix (i.e., the inertia associated with motion purely in that joint axis). Choosing $k_{ref} = 100 \text{ N} \cdot \text{m/rad}$, this dictates impedance choices of 795.8 and 3.416 kg $\cdot$ m^2/s for the first and second joints, respectively. Due to the very small environmental stiffness on the second axis, the latter of these quantities is sufficiently small as to cause substantial numerical difficulties in practice. For this reason, 75 kg $\cdot$ m^2/s is taken to be the minimum allowable wave impedance.
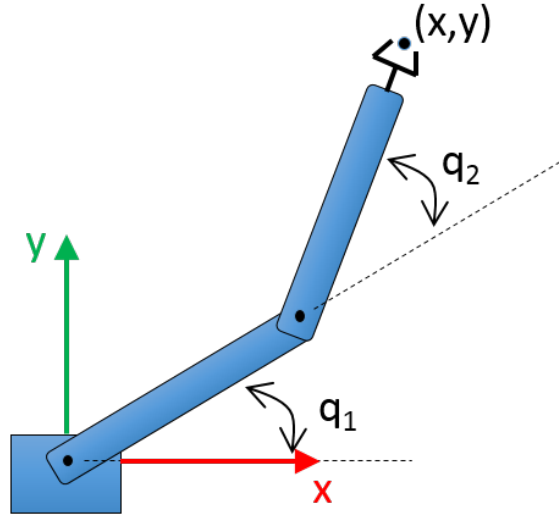
Figure 2.4: 2-degree-of-freedom planar elbow manipulator model

This scenario is simulated under three impedance choices: (1) $B_{low} = 75 \text{ kg} \cdot \text{m}^2/\text{s}$ on both joints, (2) $B_{high} = 795.8 \text{ kg} \cdot \text{m}^2/\text{s}$ on both joints, and (3) $B_1 = B_{high}$ on the first joint while $B_2 = B_{low}$ on the second joint[13]. The proportional gain of the PI controllers is taken to match the corresponding wave impedance to avoid wave reflections[14]; and the integral gain $K_I = 20$.

Fig. 2.5 shows the evolution of the master and slave joint angles during the course of this maneuver. In the low-impedance case of Fig. 2.5a, both of the master joint angles (the solid curves) follow something resembling the desired trajectory, albeit at somewhat diminished amplitude. Joint 2 of the slave, which experiences a small environmental stiffness driving it back toward 0, also tracks the desired

---

[13]i.e., the wave impedance is given by the matrix quantity $\mathbf{B} = \begin{pmatrix} 795.8 & 0 \\ 0 & 75.0 \end{pmatrix} \text{ kg} \cdot \text{m}^2/\text{s}$

[14]An impedance mismatch can cause wave reflections in the communication channel, resulting in oscillation of the system [25] that (although stable) is generally undesirable.

trajectory similarly. Joint 1 of the slave, however, which experiences a large environmental stiffness, exhibits motion at greatly reduced amplitude. That joint 1 of the master was unaffected by this stiffness is typical of teleoperation with insufficient wave impedance—the contact is not made apparent to the operator, who continues to move the master essentially unimpeded (resulting in large master-slave coordination errors). It is for this reason that contact considerations would generally motivate a larger choice of wave impedance, as in Fig. 2.5b. Here, motion in joint 1 is successfully inhibited at the master site; but joint 2 motion is impeded as well. The distinct choices of wave impedance (as in Fig. 2.5c) result in simultaneous satisfaction of the relevant goals: permitting motion of the second joint while inhibiting motion of the first joint.

Fig. 2.6 similarly shows the effect of these impedance choices on the joint torque due to operator effort. In the low- and high-impedance cases of Fig. 2.6a and b, the operator exerts near-identical effort on the two joints, suggesting no substantial difference in the way he or she perceives these two degrees of freedom. In the case of Fig. 2.6c, however, substantially more torque is required along the first joint than the second. Despite the nonlinear and coupled nature of the joint degrees of freedom considered here, the results qualitatively align with the SISO analytical results: Increasing wave impedance reduces coordination error while increasing necessary forces.

This example was grounded in the joint space, but hints at more realistic applications that are founded in Cartesian space. A 2-DOF manipulator whose degrees of freedom dynamically couple, with one experiencing a large stiffness and one
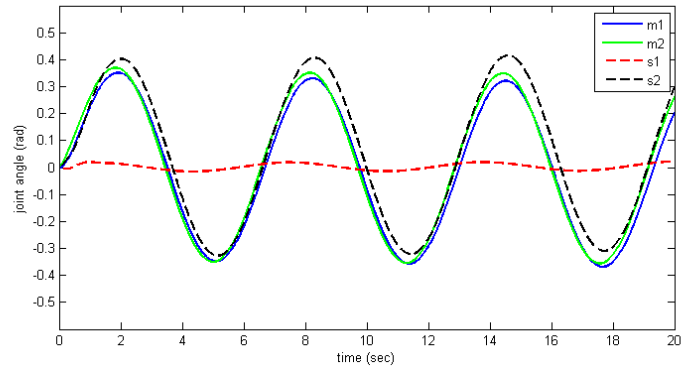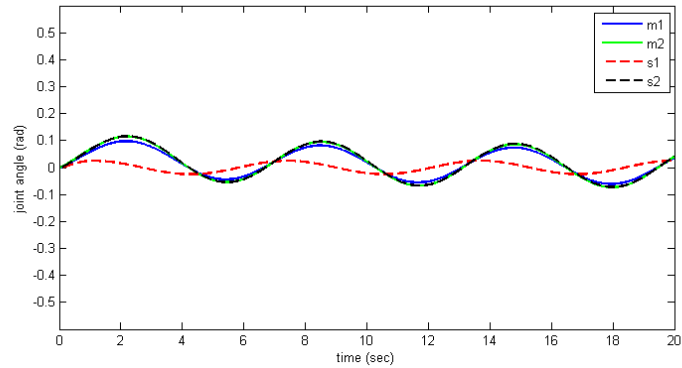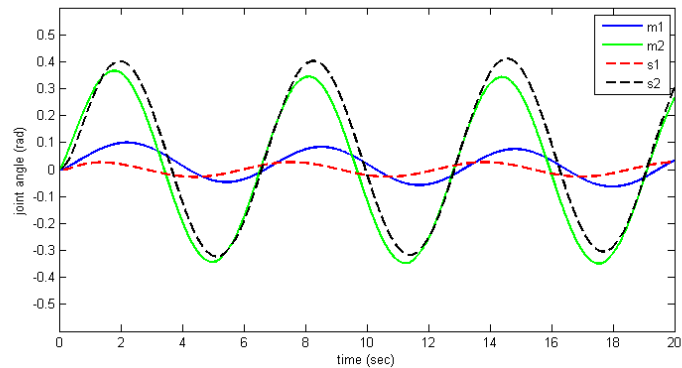
Figure 2.5: Comparison, in simulation, of master and slave joint angles for (a) uniform $B_{low} = 75$, (b) uniform $B_{high} = 795.8$, (c) $B_1 = B_{high}$ while $B_2 = B_{low}$
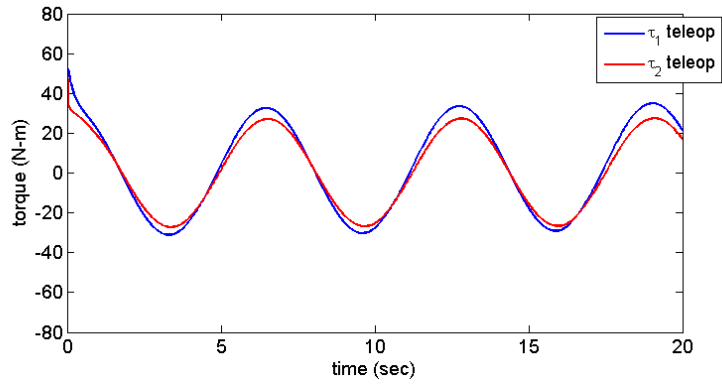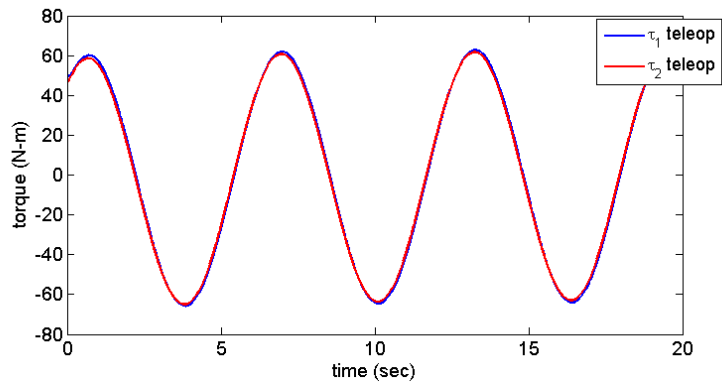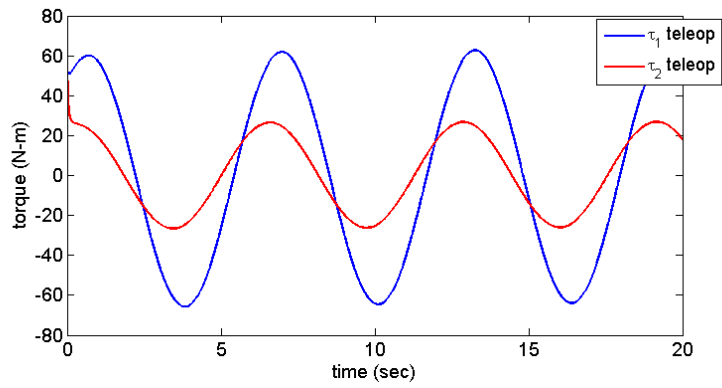
Figure 2.6: Comparison, in simulation, of master and slave joint torques due to operator effort for (a) uniform $B_{low} = 75$, (b) uniform $B_{high} = 795.8$, (c) $B_1 = B_{high}$ while $B_2 = B_{low}$

experiencing a small stiffness, resembles the more conventional manipulation task in which one joint is approximately normal to a motion constraint while another is more nearly parallel. Extension to such Cartesian reality is explored in the following chapter.

2.6 Chapter Summary

Passivity-based teleoperation has been described briefly, and an optimization problem was formulated in which the master and slave manipulators are modeled as linear, single-input-single-output (SISO) systems. With an objective function defined as a weighted sum of the two conflicting principal considerations of stiffness and inertia perception at the operator (master) site, several optimal choices of wave impedance were derived corresponding to different choices of objective function. Consideration was also given to controller gains for the velocity-velocity configuration, in which case it is typically desirable that $K_p = B$ (to avoid wave reflections) and K_I be comparable to K_e (or as large as reasonably achievable, in the likely scenario that numerical limitations and/or unmodeled dynamics destabilize the system for so large a choice). Simulation on a nonlinear planar manipulator demonstrate reasonable results even when applied to a non-SISO, nonlinear system.

Table 2.1 presents an overview of the objective functions and resulting optimal choices of wave impedance identified in this chapter, with equation numbers referenced for each. The expression (2.34) was identified through optimization of the basic force-force configuration. In (2.39), the result for the velocity-velocity

configuration employing PI controllers differs only through the inclusion of a term depending upon the slave joint friction b_s. Thus, in either configuration, the optimal results are identical for the ideal scenario in which slave joint friction is negligible; and (2.34) is the optimal result favored throughout the remainder of this dissertation. Consideration was also given to the inclusion of master-slave coordination error in the objective function, which manifested in (2.44) through the inclusion of another corrective term within the square root. Finally, the general case was considered in which the designer specifies explicit weights for each of the inertia and stiffness considerations, resulting in the optimal wave impedance (2.53).

Table 2.1: Summary of Optimal Wave Impedance Choices

Purpose	Objective Function, Φ	Optimal Impedance, B^*
Force-force configuration	$\frac{m'_{eq}}{m_m+m_s}\alpha_f + \frac{K_e}{k'_{eq}}(1-\alpha_f)$ (2.25)	$\sqrt{\frac{K_e^2(m_m+m_s)}{k_{ref}}}$ (2.34)
Velocity-velocity configuration	$\frac{m_{eq}}{m_m+m_s}\alpha_f + \frac{K_e}{k_{eq}}(1-\alpha_f)$ (2.36)	$\sqrt{\frac{K_e^2(m_m+m_s)}{k_{ref}} - b_s^2}$ (2.39)
Inclusion of a measure of coordination error in the contact objective	$\frac{m_{eq}}{m_m+m_s}\alpha_f + \left[\frac{K_e}{k_{eq}} + \frac{\delta}{\Delta_{ref}}\right](1-\alpha_f)$ (2.43)	$\sqrt{\frac{K_e^2(m_m+m_s)}{k_{ref}} - b_s^2 + \frac{K_e(m_m+m_s)}{k_{ref}\Delta_{ref}}}$ (2.44)
General weights rather than free motion coefficient	$\frac{m_{eq}}{m_m+m_s}w_M + \frac{K_e}{k_{eq}}w_K$ (2.52)	$\sqrt{K_e(m_m+m_s)\frac{w_K}{w_M} - b_s^2 w_M}$ (2.53)

Chapter 3: Application to nonlinear robotic manipulators

3.1 Overview

This chapter extends the discussion of simplified linear systems from the previous chapter into the realm of nonlinear, multiple-degree-of-freedom manipulators. First, it is shown that the wave-based teleoperation scheme discussed in Chapter 2 is compatible with time-varying choices of wave impedance. (The advice contained herein applies equally, however, to the selection of a constant wave impedance matrix for tasks executed in the neighborhood of a given reference pose.) Then, the optimal result (2.34) derived therein for a linear, decoupled system is applied quasi-optimally to nonlinear manipulators; and management of the duality between the Cartesian task space and the joint configuration space is considered.

3.2 Stability Effects of Time-varying Impedance

The subsequent sections of this chapter present a scheme for choosing the wave impedance parameter in a state-dependent fashion. Although one might choose to implement on the basis of these results a constant impedance value chosen for operation in the vicinity of a reference pose, attention is also given to the capacity

to update this impedance choice online. Before proposing such a scheme, it is therefore necessary to establish that a time-varying choice of $\mathbf{B}$ does not violate the passivity condition and does not destabilize the teleoperator. Niemeyer and Slotine [25] originally remarked on the acceptability of time-varying and/or state-dependent choices of wave impedance; and the present derivation demonstrates this fact in greater detail. This analysis closely follows the general Lyapunov-like analysis presented by Nuño et al. [21], although the case of time-varying controller gains was not directly considered in that work.

The teleoperation system consists of master and slave manipulators, master and slave PI controllers, and a wave-based communication channel. First it will be shown that these individual components of the teleoperation system behave passively, and then that the combined system has nonincreasing total energy. The consequences of a time-varying impedance choice are considered both in the wave-based communication channel itself and in the PI controllers (which, for impedance matching purposes[1], set $\mathbf{K}_p = \mathbf{B}$).

3.2.1 Component-level relations

Passivity of each component is shown by demonstrating that it satisfies either (2.1) or (2.2) with the inputs and outputs shown in Fig. 2.1. The communication channel is a two-port element, having an input-output pair on both its left and right

---

[1]An impedance mismatch can cause wave reflections in the communication channel, resulting in oscillation of the system [25] that (although stable) is generally undesirable.

sides. In this case, the condition (2.2) takes the form:

$$\int_0^t (\underline{u}_L^T \underline{y}_L - \underline{u}_R^T \underline{y}_R) dt \geq -V(0) \qquad (3.1)$$

where subscripts L and R denote the left and right ports, respectively.

3.2.1.1   Master and Slave Manipulators

The dynamic equations of motion of a robotic manipulator are given by

$$\mathbf{M}(\underline{q})\underline{\ddot{q}} + \mathbf{C}(\underline{q}, \underline{\dot{q}})\underline{\dot{q}} + \underline{g}(\underline{q}) = \underline{\tau} \qquad (3.2)$$

where $\underline{q}$ is the vector of joint angles, $\mathbf{M}$ is the inertia matrix, $\mathbf{C}$ contains the Centripetal and Coriolis terms, $\underline{g}$ contains the effect of gravity, and the control input $\underline{\tau}$ represents the applied joint torques [77]. Taking $V(\underline{q}, \underline{\dot{q}})$ as the total mechanical energy of the manipulator and carrying out the appropriate derivatives, it can be shown that such a manipulator satisfies the passivity criterion with $\underline{\dot{q}}$ as output and $\underline{\tau}$ as input.

Using the subscript $i = m, s$ to denote master and slave, the kinetic energy of these systems can be written as

$$KE_i = \frac{1}{2}\underline{\dot{q}}_i^T \mathbf{M}_i(\underline{q}_i)\underline{\dot{q}}_i \qquad (3.3)$$

And it can be shown by substitution of the dynamic equations of motion that this

energy can increase only as a result of work done on the robot:

$$\frac{d}{dt}(KE_i) = \underline{\dot{q}}_i^T \mathbf{M}_i(\underline{q}_i)\underline{\ddot{q}}_i + \frac{1}{2}\underline{\dot{q}}_i^T \dot{\mathbf{M}}_i(\underline{q}_i)\underline{\dot{q}}_i \tag{3.4}$$

$$= \underline{\dot{q}}_i^T(-\mathbf{C}_i\underline{\dot{q}}_i + \underline{\tau}_{net,i})\frac{1}{2}\underline{\dot{q}}_i^T\dot{\mathbf{M}}_i(\underline{q}_i)\underline{\dot{q}}_i \tag{3.5}$$

$$= \underline{\dot{q}}_i^T\left[\frac{1}{2}\dot{\mathbf{M}}_i - \mathbf{C}_i\right]\underline{\dot{q}}_i + \underline{\dot{q}}^T\underline{\tau}_{net,i} \tag{3.6}$$

$$= \underline{\dot{q}}^T\underline{\tau}_{net,i} \tag{3.7}$$

where the quadratic term containing $\frac{1}{2}\dot{\mathbf{M}}_i - \mathbf{C}_i$ vanishes because the matrix is skew symmetric [77] and the net torque acting on each manipulator is given by:

$$\underline{\tau}_{net,m} = \underline{\tau}_h - \underline{\tau}_{mc} \tag{3.8}$$

$$\underline{\tau}_{net,s} = \underline{\tau}_{sc} + \underline{\tau}_e \tag{3.9}$$

Thus, the rate of change of the energy of either robot is simply the rate at which work is being done on it.

3.2.1.2 PI Controllers

Because the PI controllers operate in part on the integral of the tracking error, they have an internal state variable corresponding to the integral error. The total energy is represented as the net work done on the controller (i.e., the work done on

the controller minus the work done *by* the controller):

$$W_{net,ic} = \int \underline{\tau}_c^T(k)\underline{\dot{q}}_{id}(k) - \underline{\tau}_c^T(k)\underline{\dot{q}}_i(k))dk \tag{3.10}$$

$$= \int_0^t \mathbf{K}_p(\underline{\dot{q}}_{i,d} - \underline{\dot{q}}_i) + \mathbf{K}_i \underline{x}_{ic})^T(\underline{\dot{q}}_{id} - \underline{\dot{q}}_i)dk \tag{3.11}$$

$$= \int_0^t \left[(\underline{\dot{q}}_{id} - \underline{\dot{q}}_i)^T \mathbf{K}_p(\underline{\dot{q}}_{id} - \underline{\dot{q}}_i) + \underline{x}_{ic}^T(\underline{\dot{q}}_{id} - \underline{\dot{q}}_i) \right] dk \tag{3.12}$$

$$= \int_0^t \left(\mathbf{K}_p(\underline{\dot{q}}_{id} - \underline{\dot{q}}_i) + \mathbf{K}_I \underline{x}_{ic} \right)^T (\underline{\dot{q}}_{id} - \underline{\dot{q}}_i)dk \tag{3.13}$$

where $\underline{x}_{ic} = \int_0^t (\underline{\dot{q}}_{i,d} - \underline{\dot{q}}_i)dk$, k is a dummy time variable introduced for the purpose of integration, and $i = m, s$ refers to the master or slave controller. Expanding (3.13) and realizing that the potential energy of the controller is $PE_{ic} = \frac{1}{2}\underline{x}_{ic}^T \mathbf{K}_I \underline{x}_{ic}$,

$$W_{net,ic} = \int_0^t \left[(\underline{\dot{q}}_{id} - \underline{\dot{q}}_i)^T \mathbf{K}_p(\underline{\dot{q}}_{id} - \underline{\dot{q}}_i) \right] dk + PE_{ic}(t) - PE_{ic}(0) \tag{3.14}$$

Thus, the controller is incapable of doing more work than was done on it, except insofar as it might have initial energy at $t = 0$. Note that, because $\mathbf{K}_I$ (unlike $\mathbf{K}_p$) appears in the definition of the controller's potential energy, one could *not* (without some corrective measure) allow $\mathbf{K}_I$ to vary with time and still guarantee passivity without introducing some other source of dissipation. On the face of it, this is not a problem because only $\mathbf{K}_p$ is required to vary in time in order to provide impedance matching as $\mathbf{B}$ changes. In the event that a time-varying choice of $\mathbf{K}_I$ is desired, however, the following PI-like control law will maintain passivity under

such conditions:

$$\underline{\tau} = \mathbf{K}_{P,i}\underline{e}_i + \mathbf{K}_{I,i}\underline{\epsilon}_i \tag{3.15}$$

$$\underline{\epsilon}_i = \int_0^t \left(\underline{e}_i - \frac{1}{2}\mathbf{K}_{I,i}^{-1}\dot{\mathbf{K}}_{I,i}\underline{\epsilon}_i \right) dk \tag{3.16}$$

This reduces to the conventional PI controller for $\dot{\mathbf{K}}_{I,i} = \mathbf{0}$ but may be useful in maintaining a choice of $\mathbf{K}_I$ that is appropriate to the operating conditions of the robot as those conditions change. It is not theoretically mandatory; and the integral gain may be taken as a constant if the traditional PI law is preferred.

3.2.1.3 Communication Channel

Before considering the energy stored in the communication channel, it is useful to derive some relations involving the wave variables. Recall that definition of scattering wave variables is:

$$\underline{u}_m = \frac{1}{\sqrt{2}} \left(\mathbf{B}_{m,1/2}\dot{\underline{q}}_{md} + \mathbf{B}_{m,1/2}^{-T}\underline{\tau}_{mc} \right) \quad \underline{v}_m = \frac{1}{\sqrt{2}} \left(\mathbf{B}_{m,1/2}\dot{\underline{q}}_{md} - \mathbf{B}_{m,1/2}^{-T}\underline{\tau}_{mc} \right) \tag{3.17}$$

$$\underline{u}_s = \frac{1}{\sqrt{2}} \left(\mathbf{B}_{s,1/2}\dot{\underline{q}}_{sd} + \mathbf{B}_{s,1/2}^{-T}\underline{\tau}_{sc} \right) \quad \underline{v}_s = \frac{1}{\sqrt{2}} \left(\mathbf{B}_{s,1/2}\dot{\underline{q}}_{sd} - \mathbf{B}_{s,1/2}^{-T}\underline{\tau}_{sc} \right) \tag{3.18}$$

where $\mathbf{B}_m$ and $\mathbf{B}_s$ represent the wave impedance on the master and slave sides, respectively, and subscript 1/2 denotes an appropriate choice of square root as dis-

cussed in Section 2.3. It follows from these definitions that

$$\underline{u}_m^T \underline{u}_m = \frac{1}{2} \left(\mathbf{B}_{m,1/2} \dot{\underline{q}}_{md} + \mathbf{B}_{m,1/2}^{-T} \underline{\tau}_{mc} \right)^T \left(\mathbf{B}_{m,1/2} \dot{\underline{q}}_{md} + \mathbf{B}_{m,1/2}^{-T} \underline{\tau}_{mc} \right) \tag{3.19}$$

$$= \frac{1}{2} \left(\dot{\underline{q}}_{md}^T \mathbf{B}_m \dot{\underline{q}}_{md} + 2 \underline{\tau}_{mc}^T \dot{\underline{q}}_{md} + \underline{\tau}_{mc}^T \mathbf{B}_m^{-1} \underline{\tau}_{mc} \right) \tag{3.20}$$

$$\underline{v}_m^T \underline{v}_m = \frac{1}{2} \left(\mathbf{B}_{m,1/2} \dot{\underline{q}}_{md} - \mathbf{B}_{m,1/2}^{-T} \underline{\tau}_{mc} \right)^T \left(\mathbf{B}_{m,1/2} \dot{\underline{q}}_{md} - \mathbf{B}_{m,1/2}^{-T} \underline{\tau}_{mc} \right) \tag{3.21}$$

$$= \frac{1}{2} \left(\dot{\underline{q}}_{md}^T \mathbf{B}_m \dot{\underline{q}}_{md} - 2 \underline{\tau}_{mc}^T \dot{\underline{q}}_{md} + \underline{\tau}_{mc}^T \mathbf{B}_m^{-1} \underline{\tau}_{mc} \right) \tag{3.22}$$

$$\rightarrow \underline{u}_m^T \underline{u}_m - \underline{v}_m^T \underline{v}_m = 2 \underline{\tau}_{mc}^T \dot{\underline{q}}_{md} \tag{3.23}$$

Following a similar derivation,

$$\underline{u}_s^T \underline{u}_s - \underline{v}_s^T \underline{v}_s = 2 \underline{\tau}_{sc}^T \dot{\underline{q}}_{sd} \tag{3.24}$$

Note that these results are independent of impedance choices, $\mathbf{B}_m$ and $\mathbf{B}_s$, even if those choices are time-varying and regardless of any impedance mismatch between the master and slave ends of the channel.

Consider now the net work done on the communication channel, which is the work by the master controller on the channel minus the work by the channel on the slave controller. Niemeyer and Slotine [25] showed that it is here, in the communication channel, that the wave transformation prevents energy generation that would otherwise occur in the case of delayed transmission of power variables, velocity and force:

$$\int_0^t \left(\underline{\tau}_{mc}^T(k) \dot{\underline{q}}_{md}(k) - \underline{\tau}_{sc}^T(k) \dot{\underline{q}}_{sd}(k) \right) dk \tag{3.25}$$

Employing the relations (3.23) and (3.24) derived above, this becomes

$$\frac{1}{2} \int_0^t \left(\underline{u}_m^T \underline{u}_m - \underline{v}_m^T \underline{v}_m - \underline{u}_s^T \underline{u}_s + \underline{v}_s^T \underline{v}_s \right) dk \qquad (3.26)$$

Substituting $\underline{u}_s(k) = \underline{u}_m(k - T)$ and $\underline{v}_m(k) = \underline{v}_s(k - T)$, this becomes

$$\frac{1}{2} \int_0^t \left[\underline{u}_m^T(k)\underline{u}_m(k) - \underline{v}_m(k)^T \underline{v}_m(k) - \underline{u}_m^T(k - T)\underline{u}_m(k - T) + \underline{v}_m^T(k - T)\underline{v}_m(k - T) \right] dk$$

$$(3.27)$$

which reduces to

$$\frac{1}{2} \int_{t-T}^t \left(\underline{u}_m^T \underline{u}_m + \underline{v}_s^T \underline{v}_s \right) dk \geq 0 \qquad (3.28)$$

Since this quantity is the integral of a strictly nonnegative value (the sum of two dot products), the communication channel can therefore never do more work than was done on it—again except insofar as it may have had some stored energy at time $t = 0$.

3.2.2   Total System

The foregoing definition of passivity is usually discussed in the context of a time-*invariant* system [20]; and a note of caution is warranted before concluding that the feedback interconnection of this time-varying "passive" system with arbitrary other passive elements will remain stable. In the interest of completeness, the total energy contained in the teleoperation system is therefore considered below.

First consider the teleoperation system itself, excluding the human operator and the environment. KE_m and KE_s denote the kinetic energy of the master and

slave, respectively; and PE_{chan} and PE_{ic} (i = m,s) are the potential energy of the communication channel and controllers, respectively.

$$\frac{d}{dt}(E_{sys}) = \frac{d}{dt}(KE_m + KE_s + PE_{chan} + PE_{mc} + PE_{sc}) \tag{3.29}$$

$$= \frac{d}{dt}\left(\frac{1}{2}\dot{\underline{q}}_m^T \mathbf{M}_m \dot{\underline{q}}_m + \frac{1}{2}\dot{\underline{q}}_s^T \mathbf{M}_s \dot{\underline{q}}_s + PE_{chan} + PE_{mc} + PE_{sc}\right) \tag{3.30}$$

$$= \dot{\underline{q}}_m^T \underline{\tau}_{net,m} + \dot{\underline{q}}_s^T \underline{\tau}_{net,s} + \frac{d}{dt}(PE_{chan}) + \frac{d}{dt}(PE_{mc}) + \frac{d}{dt}(PE_{sc}) \tag{3.31}$$

$$= \dot{\underline{q}}_m^T (\underline{\tau}_h - \underline{\tau}_{mc}) + \dot{\underline{q}}_s^T (\underline{\tau}_{sc} - \underline{\tau}_e) + \left(\underline{\tau}_{mc}^T \dot{\underline{q}}_{md} - \underline{\tau}_{sc}^T \dot{\underline{q}}_{sd}\right)$$
$$+ \frac{d}{dt}\left(\frac{1}{2}\underline{x}_{mc}^T \mathbf{K}_I \underline{x}_{mc}\right) + \frac{d}{dt}\left(\frac{1}{2}\underline{x}_{sc}^T \mathbf{K}_I \underline{x}_{sc}\right) \tag{3.32}$$

$$= \dot{\underline{q}}_m^T (\underline{\tau}_h - \underline{\tau}_{mc}) + \dot{\underline{q}}_s^T (\underline{\tau}_{sc} - \underline{\tau}_e) + \left(\underline{\tau}_{mc}^T \dot{\underline{q}}_{md} - \underline{\tau}_{sc}^T \dot{\underline{q}}_{sd}\right)$$
$$+ \underline{x}_{mc}^T \mathbf{K}_I (\dot{\underline{q}}_{md} - \dot{\underline{q}}_m) + \underline{x}_{sc}^T \mathbf{K}_I (\dot{\underline{q}}_{sd} - \dot{\underline{q}}_s) \tag{3.33}$$

where $\mathbf{K}_I$ is assumed constant and $\underline{x}_{mc}$ and $\underline{x}_{sc}$ are the integral errors as defined in Subsubsection 3.2.1.2. If gravity is present, then the potential energy terms for the master and slave must also be included.

The control laws are given by

$$\underline{\tau}_{sc} = \mathbf{K}_{p,s}(\dot{\underline{q}}_{sd} - \dot{\underline{q}}_s) + \mathbf{K}_I \underline{x}_{sc} \tag{3.34}$$

$$\underline{\tau}_{mc} = -\mathbf{K}_{p,m}(\dot{\underline{q}}_{md} - \dot{\underline{q}}_m) - \mathbf{K}_I \underline{x}_{mc} \tag{3.35}$$

Substituting these laws into (3.33) gives

$$\frac{d}{dt}(E_{sys}) = \underline{\dot{q}}_m^T \left(\underline{\tau}_h + \mathbf{K}_{p,m}(\underline{\dot{q}}_{md} - \underline{\dot{q}}_m) + \mathbf{K}_I \underline{x}_{mc} \right) + \underline{\dot{q}}_s^T \left(\mathbf{K}_{p,s}(\underline{\dot{q}}_{sd} - \underline{\dot{q}}_s) + \mathbf{K}_I \underline{x}_{sc} - \underline{\tau}_e \right)$$

$$- (\mathbf{K}_{p,m}(\underline{\dot{q}}_{md} - \underline{\dot{q}}_m) + \mathbf{K}_I \underline{x}_{mc})^T \underline{\dot{q}}_{md} - (\mathbf{K}_{p,s}(\underline{\dot{q}}_{sd} - \underline{\dot{q}}_s) + \mathbf{K}_I \underline{x}_{sc})^T \underline{\dot{q}}_{sd}$$

$$+ \underline{x}_{mc}^T \mathbf{K}_I (\underline{\dot{q}}_{md} - \underline{\dot{q}}_m) + \underline{x}_{sc}^T \mathbf{K}_I (\underline{\dot{q}}_{sd} - \underline{\dot{q}}_s) \qquad (3.36)$$

Expanding and simplifying, (3.36) becomes

$$\frac{d}{dt}(E_{sys}) = \underline{\dot{q}}_m^T \underline{\tau}_h - \underline{\dot{q}}_s^T \underline{\tau}_e - \left(\underline{\dot{q}}_m - \underline{\dot{q}}_{md} \right)^T \mathbf{K}_{p,m} \left(\underline{\dot{q}}_m - \underline{\dot{q}}_{md} \right) - \left(\underline{\dot{q}}_s - \underline{\dot{q}}_{sd} \right)^T \mathbf{K}_{p,s} \left(\underline{\dot{q}}_s - \underline{\dot{q}}_{sd} \right)$$

The first two terms on the right hand side represent the work done on the tele-operation system by the human operator and the environment, respectively. The remaining terms are pure dissipation introduced by the master and slave controllers. Thus, the only way the total energy of the teleoperation system can increase is via work done on the system by the operator and/or environment.

Consider now the total energy of the entire system, including the operator and environment

$$\frac{d}{dt}(E_{tot}) = \frac{d}{dt} \left(KE_m + KE_s + PE_{chan} + PE_{mc} + PE_{sc} + PE_h + PE_e \right)$$

$$= \frac{d}{dt}(E_{sys}) + \frac{d}{dt}(PE_h + PE_e)$$

If the operator and environment are both assumed to be passive systems, then

$\frac{d}{dt}(PE_h) \leq -\underline{\dot{q}}_m^T \underline{\tau}_h$ and $\frac{d}{dt}(PE_e) \leq \underline{\dot{q}}_s^T \underline{\tau}_e$:

$$\frac{d}{dt}(E_{tot}) \leq -\left(\underline{\dot{q}}_m - \underline{\dot{q}}_{md}\right)^T \mathbf{K}_{p,m} \left(\underline{\dot{q}}_m - \underline{\dot{q}}_{md}\right)$$
$$-\left(\underline{\dot{q}}_s - \underline{\dot{q}}_{sd}\right)^T \mathbf{K}_{p,s} \left(\underline{\dot{q}}_s - \underline{\dot{q}}_{sd}\right) \tag{3.37}$$

The total energy of the system can therefore never increase; and it can only remain constant in the event of perfect velocity tracking of both the master and slave (and then only if the operator and environment do not dissipate any energy). This result holds regardless of time variation in the choice of wave impedance.

3.3   Performance Effects of Time-varying Impedance

Rodriguez-Seda [68] observed in simulation that rapid or abrupt changes in wave impedance could cause undesirable (but stable) oscillations; however, this occurred under a feedback-passivized, position-transmission scheme in the manner of Chopra et al. [34]. No theoretical explanation for these oscillations was identified; and the simulations of Section 4.6 do not demonstrate the same phenomenon in the present scheme, which relies instead on classical, velocity-based wave transmission.

A consideration that is of relevance to the present scheme, however, is that of coordination error between the master and the slave. Because only velocity information is transmitted in classical wave-based teleoperation, there is in general no correction for any positional mismatch between the two systems. Consider the positions tracked by the PI controllers (or, equivalently, the master and slave positions

themselves in the force-force implementation). Combining (2.3)-(2.6):

$$\underline{\dot{q}}_{md} = \sqrt{2}\mathbf{B}_{m,1/2}^{-1}\left(\underline{u}_m + \underline{v}_m\right) \tag{3.38}$$

$$\underline{\dot{q}}_{sd} = \sqrt{2}\mathbf{B}_{s,1/2}^{-1}\left(\underline{u}_s + \underline{v}_s\right) \tag{3.39}$$

Thus, the theoretical master-slave coordination error is given by (where k is a dummy time variable):

$$\Delta q = \int_0^t \left(\underline{\dot{q}}_{md}(k) - \underline{\dot{q}}_{sd}(k)\right) dk \tag{3.40}$$

$$= \sqrt{2}\int_0^t \left[\mathbf{B}_{m,1/2}^{-1}(k)\left(\underline{u}_m(k) + \underline{v}_m(k)\right) - \mathbf{B}_{s,1/2}^{-1}(k)\left(\underline{u}_s(k) + \underline{v}_s(k)\right)\right] dk \tag{3.41}$$

$$= \sqrt{2}\int_0^t \left[\mathbf{B}_{m,1/2}^{-1}(k)\left(\underline{u}_m(k) + \underline{v}_s(k-T)\right) - \mathbf{B}_{s,1/2}^{-1}(k)\left(\underline{u}_m(k-T) + \underline{v}_s(k)\right)\right] dk$$

$$\tag{3.42}$$

In the case in which $\mathbf{B}_m = \mathbf{B}_s = $ const, this reduces to the case considered by Niemeyer and Slotine [78]:

$$\Delta q = \sqrt{2}\int_0^t \left[\mathbf{B}_{1/2}^{-1}\left(\underline{u}_m(k) + \underline{v}_s(k-T)\right) - \mathbf{B}_{1/2}^{-1}\left(\underline{u}_m(k-T) + \underline{v}_s(k)\right)\right] dk \tag{3.43}$$

$$= \sqrt{2}\mathbf{B}_{1/2}^{-1}\int_0^t \left(\underline{u}_m(k) - \underline{u}_m(k-T) - \underline{v}_s(k) + \underline{v}_s(k-T)\right) dk \tag{3.44}$$

$$= \sqrt{2}\mathbf{B}_{1/2}^{-1}\int_{t-T}^t \left(\underline{u}_m(k) - \underline{v}_s(k)\right) dk \tag{3.45}$$

and theoretical steady-state coordination error will be zero in the free motion case (for which $\underline{u}_m$ and $\underline{v}_s$ approach $\underline{0}$). Thus, although the classical scheme is intrinsically susceptible to coordination error, such error would be expected to accumulate

only due to non-idealities such as the discrete and finite-precision nature of digital implementation, data loss in the communication channel, and coordination error in the initial conditions.

Unfortunately, even executing an impedance change simultaneously (e.g., scheduling the change at least T seconds in advance) does not eliminate this error:

$$\Delta q = \sqrt{2} \int_0^t \left[\mathbf{B}_{1/2}^{-1}(k) \left(\underline{u}_m(k) + \underline{v}_s(k-T) \right) \right. $$
$$\left. - \mathbf{B}_{1/2}^{-1}(k) \left(\underline{u}_m(k-T) + \underline{v}_s(k) \right) \right] dk \qquad (3.46)$$

Thus, the only error-free way to effect an impedance change would be to do so in a period during which $\underline{u}_m = \underline{v}_m = \underline{u}_s = \underline{v}_s = 0$.

Because, however, the tendency to accumulate coordination error is already such a widely recognized phenomenon in wave-based control, a variety of techniques already exist for mitigating its effect. Among the most generically applicable techniques are those of Niemeyer and Slotine [36] and Chopra et al. [33]. The former selectively reshapes the wave variables to compensate for position errors; and the latter applies an outer proportional control loop, the added energy due to which is compensated by damping at the master and slave sites. The feedback passivation scheme of Chopra et al. [34] instead corrects for position drift through a substantial reformulation of the teleoperation scheme. A detailed discussion of this reformulation is beyond the scope of the present dissertation; however, a preliminary investigation into the associated impedance selection problem is presented in Appendix A.

In addition to the foregoing means of correcting for error that has accumulated, measures can be taken to reduce the amount of error that accumulates in the first place. Tanner and Niemeyer [67] proposed a modification of the wave variable teleoperator in which different impedance values ($B_{\dot{x}}$ and B_F, respectively) are used for each of the velocity and force/torque signals. This enables an operational paradigm in which the force impedance parameter may be varied online without introducing coordination error (so long as the velocity impedance remains constant). Whereas the analysis of the preceding section showed that impedance changes within the classical approach do not affect the energy of the system, however, impedance increases within this modified scheme always increase the total system energy. The authors propose a corrective scheme that involves waiting for sufficient dissipation to occur before allowing another impedance change. This allows for only discrete updates to the impedance value. Repeating the analysis of Subsection 2.3.1 demonstrates that the effective mechanical parameters displayed to the operator are identical to those given in Subsection 2.3.1 for the classical scheme, replacing B with the equivalent channel impedance $B_{eff} = \sqrt{B_{\dot{x}} B_F}$. Thus, the advice contained in this dissertation regarding impedance selection is equally applicable to the equivalent channel impedance in this dual-impedance scheme.[2] The capacity for online variation of that choice will simply be constrained within the considerations presented in that original work (namely, nonpassive behavior permitting only discrete updates to the

---

[2]The advice in this chapter would be used to select $\mathbf{B}_{eff}$. The simplest implementation would choose $\mathbf{B}_{\dot{x}}$ as a constant scalar multiple of the identity matrix, thus avoiding any issues of non-commutativity. The force impedance would then be chosen as $\mathbf{B}_F = \left(\mathbf{B}_{\dot{x}}^{-1} \mathbf{B}_{eff}\right)^2$.

wave impedance with mandatory timeouts in between).

Discussion in the present work, however, is couched in terms of the classical, single-impedance approach, which retains passivity (the central tenet upon which this teleoperation scheme is founded) despite variations in wave impedance. Subsection 3.6.2 presents a scheme for limiting the rate of impedance change, since it is the magnitude of change across the interval T that drives the coordination error discussed here. What coordination error results after this mitigating measure is then assumed to be corrected by one of the existing passive solutions in prior work.

3.4   Effective Mechanical Parameters

Subsection 2.3.1 summarized the effective mechanical parameters displayed to the operator at low frequency in the single-input-single-output (SISO) case. That analysis, based upon manipulation of the system's transfer function, becomes considerably less tractable in the multivariable case. The SISO analysis of Niemeyer and Slotine [58], however, which was observed in Subsection 2.3.1 to yield identical results for inertia and stiffness, is repeated here in matrix-vector form.

The communication channel is viewed here as a "virtual tool" having some effective inertia and stiffness with regard to its effort variables ($\underline{\tau}_{mc}$ and $\underline{\tau}_{sc}$) and flow variables ($\underline{\dot{q}}_{md}$ and $\underline{\dot{q}}_{sd}$). These properties then combine with those of the remainder of the teleoperation system in the usual way for components in series.[3]

The sums and differences of the wave variables (2.3)-(2.6) may be written in

---

[3]i.e., inertias add directly ($m_{1+2} = m_1 + m_2$) and stiffnesses add inversely ($k_{1+2}^{-1} = k_1^{-1} + k_2^{-1}$).

the following forms, which will be used in the ensuing derivations.

$$\sqrt{2}\left(\underline{u}_m - \underline{v}_s\right) = \mathbf{B}_{1/2}\left(\underline{\dot{q}}_{md} - \underline{\dot{q}}_{sd}\right) + \mathbf{B}_{1/2}^{-T}\left(\underline{\tau}_{mc} + \underline{\tau}_{sc}\right) \qquad (3.47)$$

$$\sqrt{2}\left(\underline{u}_m + \underline{v}_s\right) = \mathbf{B}_{1/2}\left(\underline{\dot{q}}_{md} + \underline{\dot{q}}_{sd}\right) + \mathbf{B}_{1/2}^{-T}\left(\underline{\tau}_{mc} - \underline{\tau}_{sc}\right) \qquad (3.48)$$

$$\sqrt{2}\left(\underline{v}_m - \underline{u}_s\right) = \mathbf{B}_{1/2}\left(\underline{\dot{q}}_{md} - \underline{\dot{q}}_{sd}\right) - \mathbf{B}_{1/2}^{-T}\left(\underline{\tau}_{mc} + \underline{\tau}_{sc}\right) \qquad (3.49)$$

$$\sqrt{2}\left(\underline{v}_m + \underline{u}_s\right) = \mathbf{B}_{1/2}\left(\underline{\dot{q}}_{md} + \underline{\dot{q}}_{sd}\right) - \mathbf{B}_{1/2}^{-T}\left(\underline{\tau}_{mc} - \underline{\tau}_{sc}\right) \qquad (3.50)$$

Effective stiffness is identified by examining the steady-state efforts $\underline{\tau}_{mc}$ and $\underline{\tau}_{sc}$ associated with a constant displacement $\underline{q}_{md} - \underline{q}_{sd} = \int_0^t \left(\underline{\dot{q}}_{md}(k) - \underline{\dot{q}}_{sd}(k)\right) dk$. Combining (3.47) and (3.49) yields

$$\sqrt{2}\mathbf{B}_{1/2}^{-1}\left(\underline{u}_m - \underline{v}_s + \underline{v}_m - \underline{u}_s\right) = 2\left(\underline{\dot{q}}_{md} - \underline{\dot{q}}_{sd}\right) \qquad (3.51)$$

Thus, the displacement between the two ends of the communication channel is given by

$$\begin{aligned}
\Delta\underline{q} &= \int_0^t \left(\underline{\dot{q}}_{md}(k) - \underline{\dot{q}}_{sd}(k)\right) dk \\
&= \sqrt{2}^{-1}\mathbf{B}_{1/2}^{-1}\int_0^t \left(\underline{u}_m(k) - \underline{v}_s(k) + \underline{v}_m(k) - \underline{u}_s(k)\right) dk \\
&= \sqrt{2}^{-1}\mathbf{B}_{1/2}^{-1}\int_{t-T}^t \left(\underline{u}_m(k) - \underline{v}_s(k)\right) dk \qquad (3.52)
\end{aligned}$$

where the relations $\underline{v}_m(k) = \underline{v}_s(k-T)$ and $\underline{u}_s(k) = \underline{u}_m(k-T)$ have been applied.

74

At steady state (i.e., when $\underline{u}_m$ and $\underline{v}_s$ are constant) this becomes:

$$\Delta \underline{q} = \frac{T}{\sqrt{2}} \mathbf{B}_{1/2}^{-1} \left(\underline{u}_m - \underline{v}_s \right) \tag{3.53}$$

The corresponding steady state master and slave control torques may be identified by combining (3.47) and (3.49), recognizing that $\underline{\dot{q}}_{md} = \underline{\dot{q}}_{sd} = \underline{0}$ at steady state:

$$\underline{\tau}_{mc,steady} = \underline{\tau}_{sc,steady} = \sqrt{2} \mathbf{B}_{1/2}^T \underline{u}_m = -\sqrt{2} \mathbf{B}_{1/2}^T \underline{v}_s \tag{3.54}$$

Thus, combining (3.53) and (3.54), the steady-state behavior of the communication channel may be written in the form $\underline{\tau}_{mc} = \underline{\tau}_{sc} = \mathbf{K}_{comm} \Delta \underline{q}$ with the stiffness given by

$$\mathbf{K}_{comm} = \frac{1}{T} \mathbf{B} \tag{3.55}$$

Effective inertia is identified as the $\mathbf{M}_{comm}$ such that

$$\mathbf{M}_{comm} \underline{\dot{q}}_{md} = \mathbf{M}_{comm} \underline{\dot{q}}_{sd} = \int_0^t \left(\underline{\tau}_{mc} - \underline{\tau}_{sc} \right) dk \tag{3.56}$$

where the two ends of the communication channel are assumed to move in unison in order to avoid stiffness effects. Subtracting (3.50) from (3.48),

$$\underline{u}_m + \underline{v}_s - \underline{u}_s - \underline{v}_m = \sqrt{2} \mathbf{B}_{1/2}^{-T} \left(\underline{\tau}_{mc} - \underline{\tau}_{sc} \right)$$

$$\rightarrow \left(\underline{\tau}_{mc} - \underline{\tau}_{sc} \right) = \frac{\sqrt{2}}{2} \mathbf{B}_{1/2}^T \left(\underline{u}_m + \underline{v}_s - \underline{u}_s - \underline{v}_m \right) \tag{3.57}$$

Thus, (3.56) becomes

$$\mathbf{M}_{comm}\dot{\underline{q}}_{md} = \mathbf{M}_{comm}\dot{\underline{q}}_{sd} = \int_0^t \left(\underline{\tau}_{mc} - \underline{\tau}_{sc}\right) dk$$

$$= \frac{\sqrt{2}}{2}\mathbf{B}_{1/2}^T \int_0^t \left(\underline{u}_m + \underline{v}_s - \underline{u}_s - \underline{v}_m\right) dk \tag{3.58}$$

$$= \frac{\sqrt{2}}{2}\mathbf{B}_{1/2}^T \int_{t-T}^t \left(\underline{u}_m + \underline{v}_s\right) dk \tag{3.59}$$

Assuming identical steady-state acceleration and torque conditions on both sides of the communication channel (i.e., $\dot{\underline{q}}_{md} = \dot{\underline{q}}_{sd} = \underline{a}t$, where $\underline{a} =$ const, and $\underline{\tau}_{mc} = \underline{\tau}_{sc} = \underline{\tau}_c =$ const), it follows from (3.48) and (3.50) that

$$\dot{\underline{q}}_d = \frac{\sqrt{2}}{2}\mathbf{B}_{1/2}^{-1}\left(\underline{u}_m + \underline{v}_s\right) = \frac{\sqrt{2}}{2}\mathbf{B}_{1/2}^{-1}\left(\underline{u}_s + \underline{v}_m\right) \tag{3.60}$$

$$\rightarrow \underline{u}_m + \underline{v}_s = \sqrt{2}\mathbf{B}_{1/2}\dot{\underline{q}}_d = \sqrt{2}\mathbf{B}_{1/2}\underline{a}t \tag{3.61}$$

Thus, (3.59) becomes

$$\mathbf{M}_{comm}\underline{a}t = \frac{\sqrt{2}}{2}\mathbf{B}_{1/2}^T \int_{t-T}^t \left(\sqrt{2}\mathbf{B}_{1/2}\underline{a}k\right) dk \tag{3.62}$$

$$= \mathbf{B}\int_{t-T}^t \left(\underline{a}k\right) dk = \frac{1}{2}\mathbf{B}\underline{a}k^2|_{t-T}^t \tag{3.63}$$

$$= \frac{1}{2}\mathbf{B}\underline{a}\left(2tT - T^2\right) \tag{3.64}$$

And one can see that (taking $t \rightarrow \infty$ so as to identify the steady-state response),

$$\mathbf{M}_{comm} = \mathbf{B}T \tag{3.65}$$

76

3.5 Directional Impedance Selection

While the results of the previous chapter are promising, the environmental stiffness will almost always be naturally defined in the Cartesian space rather than the joint space for any realistic manipulation task. It is therefore necessary to represent the robot's inertia with respect to the Cartesian motion of its end effector rather than the individual angular motions of its joints. Assuming the manipulator Jacobian is square and invertible, this change of variables is possible via [79]:

$$\mathbf{M}_{\text{cart}} = \mathbf{J}^{-T}\mathbf{M}_{\text{joint}}\mathbf{J}^{-1} \tag{3.66}$$

(Generalization to redundant manipulators, for which $\mathbf{J}$ is nonsquare, is discussed in Subsection 3.6.1.) The elements on the main diagonal of $\mathbf{M}_{\text{cart}}$ represent the inertia associated with pure motion along each Cartesian axis; and a decoupled treatment of these axes is considered presently. Appendix B presents some considerations regarding the challenge of moving beyond this limitation, presenting a numerical rather than analytical approach.

Following from (2.34), a suitable[4] wave impedance choice for each Cartesian degree of freedom is taken to be

$$B_{\text{cart},jj} = K_{e,jj}\sqrt{\frac{M_{cart,jj}}{k_{ref}}} \tag{3.67}$$

---

[4]Several other optimal results from the linear SISO analysis of Chapter 2 were summarized in Table 2.1; and one could readily substitute any of those expressions for (2.34) if desired.

These values are collected in the diagonal matrix $\mathbf{B}_{\text{cart}}$. (In principle, k_{ref} could take on a different value in each Cartesian dimension; however, providing the user with different stiffness sensitivities on different axes may have undesirable implications with regard to transparency.) Because $\mathbf{K}_e$ and $\mathbf{M}$ are positive definite matrices, their diagonal elements are necessarily positive. $\mathbf{B}_{\text{cart}}$ will therefore be a diagonal matrix of positive values (and hence positive definite). It is noted that the calculation of the quasi-optimal Cartesian impedance requires knowledge of the manipulator's inertia matrix; however, because this information is used only to facilitate optimality (not stability), even a crude approximation may be useful. Communication latency will necessitate that the master and slave each evaluate this expression on the basis of their own state, which will in general have some coordination error with respect to the other. A mismatch in impedance does not, however, pose a risk of destabilizing the system; it will merely degrade performance (See Section 3.3).

Because only the diagonal elements of the environmental stiffness matrix $\mathbf{K}_e$ are employed, this approach confines impedance selection to the principal axes. Using a rotation matrix, however, the principal axes of the work space may be realigned in any desired manner—in this case, perpendicular to the manipulated surface. Consider the manipulator Jacobian and environmental stiffness matrix originally represented in frame A as ${}^{A}\mathbf{J}$ and ${}^{A}\mathbf{K}_e$, respectively. If ${}^{B}_{A}\mathbf{R}$ represents the rotation matrix from frame A coordinates to the coordinates of an impedance selection frame B, which has an axis aligned with the contact axis, then the quantities

transform according to:

$$^{B}\mathbf{J} = {}_{A}^{B}\mathbf{R}^{A}\mathbf{J} \tag{3.68}$$

$$^{B}\mathbf{K}_{e} = {}_{A}^{B}\mathbf{R}^{A}\mathbf{K}_{e}{}_{A}^{B}\mathbf{R}^{T} \tag{3.69}$$

It is assumed in the following discussion that $\mathbf{K}_e$ and the manipulator Jacobian have already been rotated to align with the contact frame. Note that the above is equivalent to a singular value decomposition of the stiffness matrix.

It is possible to implement this scheme directly in Cartesian space, performing the scattering transformation on Cartesian forces, torques, and velocities. Subsection 3.5.1 shows that a robotic manipulator is passive in the Cartesian space. By operating in joint space, however, one may employ equations that do not become undefined if the robot enters a singular pose, which may be more desirable[5]. Moreover, the inertias that play a significant role in impedance selection are more nearly constant in the joint space. It is true that the above calculation of $\mathbf{M}_{\text{cart}}$ in (3.66) will still fail in such a scenario; but if a singular (or nearly singular) pose is encountered then any positive definite impedance matrix may be employed to maintain stability (temporarily sacrificing any attempt at optimality) until that condition is corrected. (See Subsection 3.6.2 for discussion of the switching scheme.) For this reason, the Cartesian-space wave impedance is transformed into joint space for implementation in Subsection 3.5.2.

───────────────────

[5]Additionally, an implementation following in the footsteps of Diolaiti et al. [42] might realize advantages in achievable stiffness rendering via a joint space implementation.

It is noted that the chosen treatment of the directional wave impedance confines itself to the selection of scalar impedances along each of a set of orthogonal axes. Although the use of a rotation matrix as described above enables the selection of an impedance coordinate frame that does not need to align with the principal axes in which the robot's kinematics were originally expressed, it is natural at this point to consider whether non-orthogonal axes can be used advantageously. One might imagine, for example, simultaneous contact with two nonparallel springs and the desire to construct an impedance matrix having eigenvectors aligned with these spring axes. The requirement of a symmetric matrix, however, is again limiting in this scenario. A symmetric matrix with nonrepeated eigenvalues necessarily has orthogonal eigenvectors. Indeed, the eigendecomposition is equivalent to the Singular Value Decomposition (SVD) in this case.[6] Moreover, this implies that any positive definite stiffness matrix will become diagonal under the appropriate choice of rotation, thus eliminating such motivation for considering a non-orthogonal basis in the first place.

---

[6]Although the final results are mathematically equivalent (differing, possibly, in the ordering of values or in the signs of the directional vectors), this dissertation couches discussion of the structure of $\mathbf{B}$ in terms of the SVD because it intrinsically yields orthogonal component matrices, which may increase robustness to any numerical errors that might otherwise detract from the positive definiteness of $\mathbf{B}$. However, any discussion of the singular values of $\mathbf{B}$ contained herein applies equally to the eigenvalues; and, similarly, anything said of the singular directions applies equally to the eigenvectors. Both the SVD and eigendecomposition have computational complexity $O(n^3)$ for an $n \times n$ matrix [80].

3.5.1 Manipulator Passivity with Cartesian Variables

As discussed in Subsubsection 3.2.1.1, it is well-known that manipulators are passive in the joint space under direct drive in the absence of delay. It has been shown by Vance [79] from analysis of the Cartesian-space dynamical model that a nonredundant manipulator[7] in a nonsingular pose will behave passively in the task space as well[8]. It follows from the principle of virtual work, however, that a manipulator that is passive in the joint space will also be passive in the Cartesian space regardless of redundancy or singularity. Consider the work done by an operator applying a force $\underline{F}$ at the end-effector, moving it through a displacment $\delta\underline{x}$. Using $\delta\underline{x} = \mathbf{J}\delta\underline{q}$,

$$\underline{F}^T\delta\underline{x} = \underline{F}^T\mathbf{J}\delta\underline{q} \tag{3.70}$$

Now consider the work done by an equivalent set of joint torques $\underline{\tau} = \mathbf{J}^T\underline{F}$. This can be written as

$$\underline{\tau}^T\delta\underline{q} = \underline{F}^T\mathbf{J}\delta\underline{q} \tag{3.71}$$

The right hand sides of both of the above equations are identical, and one can therefore conclude that

$$\underline{F}^T\delta\underline{x} = \underline{\tau}^T\delta\underline{q} \tag{3.72}$$

In other words, the work done by a set of joint torques $\underline{\tau}$ acting across a joint

---

[7]A kinematically redundant manipulator has more joints than the dimension of its task space.

[8]The author shows that $\dot{\mathbf{M}}_{\text{cart}} - 2\mathbf{C}_{\text{cart}}$ is skew symmetric. The remainder of the proof of passivity is therefore identical to that presented in Subsubsection 3.2.1.1.

displacement $\delta \underline{q}$ is (consistent with intuition) the same as that done by the equivalent force $\underline{F}$ acting across the resulting Cartesian displacement $\delta \underline{x}$. Thus, if there exists a storage function $V(\underline{q}, \dot{\underline{q}})$ such that the passivity condition (2.1) is satisfied in the joint space with $\underline{\tau}$ as input and $\dot{\underline{q}}$ as output:

$$\underline{\tau}^T(t)\dot{\underline{q}}(t) \geq \dot{V}(\underline{q}, \dot{\underline{q}}, \ddot{\underline{q}}) \tag{3.73}$$

then it immediately follows that the system modeled by (3.2) will remain passive if treated in the Cartesian space with $\underline{F}$ as input and $\dot{\underline{x}}$ as output, using the exact same storage function V:

$$\underline{\tau}^T\dot{\underline{q}} \geq \dot{V}(\underline{q}, \dot{\underline{q}}, \ddot{\underline{q}}) \quad \Longrightarrow \quad \underline{F}^T\dot{\underline{x}} \geq \dot{V}(\underline{q}, \dot{\underline{q}}, \ddot{\underline{q}}) \tag{3.74}$$

The foregoing argument does not assume that the Jacobian is square or invertible, and applies to both kinematically redundant and nonredundant manipulators even in singular poses. This is simply a mathematical statement of what is obvious from physical intuition: whether the work done on the manipulator (modeled as a chain of rigid bodies) is described in the Cartesian space or the joint space, its total mechanical energy cannot increase at a rate exceeding the work done on the system.

3.5.2 Transformation Between the Joint and Cartesian Spaces

It was shown that the energy stored in the communication channel (3.28) can be expressed in terms of $\underline{u}_m^T\underline{u}_m$ and $\underline{v}_s^T\underline{v}_s$. Consider the expression (3.20) and the

corresponding representation of $\underline{v}_s^T\underline{v}_s$, rewritten for an implementation directly in Cartesian space (i.e., using Cartesian flow $\underline{\dot{x}}$ and force $\underline{F}$):

$$\underline{u}_{m,cart}^T\underline{u}_{m,cart} = \frac{1}{2}\left(\underline{\dot{x}}_{md}^T\mathbf{B}_{m,cart}\underline{\dot{x}}_{md} + 2\underline{F}_{mc}^T\underline{\dot{x}}_{md} + \underline{F}_{mc}^T\mathbf{B}_{m,cart}^{-1}\underline{F}_{mc}\right) \qquad (3.75)$$

$$\underline{v}_{s,cart}^T\underline{v}_{s,cart} = \frac{1}{2}\left(\underline{\dot{x}}_{sd}^T\mathbf{B}_{s,cart}\underline{\dot{x}}_{sd} - 2\underline{F}_{sc}^T\underline{\dot{x}}_{sd} + \underline{F}_{sc}^T\mathbf{B}_{s,cart}^{-1}\underline{F}_{sc}\right) \qquad (3.76)$$

It is a property of the manipulator Jacobian that a force $\underline{F}$ at the end effector resolves to joint torques

$$\underline{\tau} = \mathbf{J}^T\underline{F} \qquad (3.77)$$

and Cartesian velocity of the end effector relates to joint rates via

$$\underline{\dot{x}} = \mathbf{J}\underline{\dot{q}} \qquad (3.78)$$

Using these relations, (3.75) and (3.76) can be rewritten in terms of the joint space power variables $\underline{\dot{q}}_m$, $\underline{\dot{q}}_s$, $\underline{\tau}_{mc}$, and $\underline{\tau}_{sc}$:

$$\underline{u}_{m,cart}^T\underline{u}_{m,cart} = \frac{1}{2}\left(\underline{\dot{q}}_{md}^T\mathbf{J}_m^T\mathbf{B}_{m,cart}\mathbf{J}_m\underline{\dot{q}}_{md} + 2\underline{\tau}_{mc}^T\mathbf{J}_m^{-1}\mathbf{J}_m\underline{\dot{q}}_{md} + \underline{\tau}_{mc}^T\mathbf{J}_m^{-1}\mathbf{B}_{m,cart}^{-1}\mathbf{J}_m^{-T}\underline{\tau}_{mc}\right)$$

$$= \frac{1}{2}\left(\underline{\dot{q}}_{md}^T\mathbf{J}_m^T\mathbf{B}_{m,cart}\mathbf{J}_m\underline{\dot{q}}_{md} + 2\underline{\tau}_{mc}^T\underline{\dot{q}}_{md} + \underline{\tau}_{mc}^T\mathbf{J}_m^{-1}\mathbf{B}_{m,cart}^{-1}\mathbf{J}_m^{-T}\underline{\tau}_{mc}\right)$$

$$\qquad (3.79)$$

$$\underline{v}_{s,cart}^T\underline{v}_{s,cart} = \frac{1}{2}\left(\underline{\dot{q}}_{sd}^T\mathbf{J}_s^T\mathbf{B}_{s,cart}\mathbf{J}_s\underline{\dot{q}}_{sd} - 2\underline{\tau}_{sc}^T\mathbf{J}_s^{-1}\mathbf{J}_s\underline{\dot{q}}_{sd} + \underline{\tau}_{sc}^T\mathbf{J}_s^{-1}\mathbf{B}_{s,cart}^{-1}\mathbf{J}_s^{-T}\underline{\tau}_{sc}\right)$$

$$= \frac{1}{2}\left(\underline{\dot{q}}_{sd}^T\mathbf{J}_s^T\mathbf{B}_{s,cart}\mathbf{J}_s\underline{\dot{q}}_{sd} - 2\underline{\tau}_{sc}^T\underline{\dot{q}}_{sd} + \underline{\tau}_{sc}^T\mathbf{J}_s^{-1}\mathbf{B}_{s,cart}^{-1}\mathbf{J}_s^{-T}\underline{\tau}_{sc}\right) \qquad (3.80)$$

The corresponding equations for an implementation directly in joint space are:

$$u_{m,joint}^T \underline{u}_{m,joint} = \frac{1}{2} \left(\dot{\underline{q}}_{md}^T \mathbf{B}_{m,joint} \dot{\underline{q}}_{md} + 2\underline{\tau}_{mc}^T \dot{\underline{q}}_{md} + \underline{\tau}_{mc}^T \mathbf{B}_{m,joint}^{-1} \underline{\tau}_{mc} \right) \qquad (3.81)$$

$$v_{s,joint}^T \underline{v}_{s,joint} = \frac{1}{2} \left(\dot{\underline{q}}_{sd}^T \mathbf{B}_{s,joint} \dot{\underline{q}}_{sd} - 2\underline{\tau}_{sc}^T \dot{\underline{q}}_{sd} + \underline{\tau}_{sc}^T \mathbf{B}_{s,joint}^{-1} \underline{\tau}_{sc} \right) \qquad (3.82)$$

Comparing (3.81) with (3.79) and (3.82) with (3.80), one can see that the two systems are energetically equivalent when (dropping the m and s subscripts):

$$\boxed{\mathbf{B}_{joint} = \mathbf{J}^T \mathbf{B}_{cart} \mathbf{J}} \qquad (3.83)$$

When implementation in the joint space is desired, the master and slave manipulators in the proposed scheme therefore each evaluate the choice of wave impedance according to this transformation (where $i = m, s$ again indicates master or slave):

$$\mathbf{B}_{joint,i}(\underline{q}_i, \mathbf{K}_e) = \mathbf{J}^T(\underline{q}_i) \mathbf{B}_{cart}(\underline{q}_i, \mathbf{K}_e) \mathbf{J}(\underline{q}_i) \qquad (3.84)$$

This is a congruence transform [81]; and it is shown in Subsection 3.5.3 that $\mathbf{B}_{joint}$ will be positive definite as long as $\mathbf{B}_{cart}$ is positive definite and $\mathbf{J}$ is of full rank.

The master and slave systems may either independently select the wave impedance parameter on the basis of their own respective states, or either system may publish an impedance choice, which the other will implement with delay. One could even have the publishing system delay implementation of the new impedance value for a time T so that both systems may transition to it simultaneously. All but the final of

these options results in a slight mismatch of impedance choice between the two ends of the communication channel. As was seen in the analysis of Section 3.2, however, an impedance mismatch cannot destabilize the system.

It is also interesting to note that the transform (3.83) is identical to that used in other compliant control contexts to transform stiffness matrices [63]. Consider a Cartesian stiffness of the form $\underline{F} = \mathbf{K}\underline{x}$. The change in force due to a small displacement $\delta\underline{x}$ is given by:

$$\delta\underline{F} = \mathbf{K}\delta\underline{x} = \mathbf{K}\mathbf{J}\delta\underline{q} \tag{3.85}$$

Multiplying both sides of this equation by $\mathbf{J}^T$,

$$\mathbf{J}^T\delta\underline{F} = \mathbf{J}^T\mathbf{K}\mathbf{J}\delta\underline{q} \tag{3.86}$$

$$\delta\underline{\tau} = \mathbf{J}^T\mathbf{K}\mathbf{J}\delta\underline{q} \tag{3.87}$$

This same derivation may be repeated with a Cartesian damping of the form $\underline{F} = \mathbf{D}\underline{\dot{x}}$, making use of the fact that $\delta\underline{x} = \mathbf{J}\delta\underline{q}$:

$$\underline{F} = \mathbf{D}\frac{\delta\underline{x}}{dt} \tag{3.88}$$

$$\underline{F} = \mathbf{D}\mathbf{J}\frac{\delta\underline{q}}{dt} \tag{3.89}$$

$$\underline{\tau} = \mathbf{J}^T\underline{F} = \mathbf{J}^T\mathbf{D}\mathbf{J}\frac{\delta\underline{q}}{dt} \tag{3.90}$$

3.5.3 Positive Definiteness of Choice of Impedance

The inertia [81] of a matrix $\mathbf{A}$ is defined to be the ordered triple $(e^+(\mathbf{A})$, $e^-(\mathbf{A}), e^0(\mathbf{A}))$ where $e^+(\mathbf{A})$ is the number of positive eigenvalues of $\mathbf{A}$, $e^-(\mathbf{A})$ is the number of negative eigenvalues of $\mathbf{A}$, and $e^0(\mathbf{A})$ is the number of zero eigenvalues.

Sylvester's Law of Inertia [81] states that, for a symmetric matrix $\mathbf{A}$ and nonsingular matrix $\mathbf{S}$, the matrices $\mathbf{A}$ and $\mathbf{SAS}^T$ will have the same inertia. If $\mathbf{J}_i$ is assumed invertible, Sylvester's Law therefore guarantees that $\mathbf{B}_{\text{joint},i}$ as given above will have the same number of positive eigenvalues as $\mathbf{B}_{\text{cart}}$. Positive definiteness of $\mathbf{B}_{\text{cart}}$ therefore implies positive definiteness of $\mathbf{B}_{\text{joint},i}$ in the case of a nonredundant manipulator in a nonsingular pose.

In the case of a redundant manipulator, for which the manipulator Jacobian matrix $\mathbf{J}_i$ is not square, it can readily be shown that the resulting choice of wave impedance will be merely positive *semi*-definite. The proof, adapted from [82] (which presents it in a more general sense), is given below; and handling of this situation is discussed in subsection 3.6.1.

For a manipulator Jacobian $\mathbf{J} \in \mathbb{R}^{m \times n}$, $m < n$, consider its singular value decomposition $\mathbf{J} = \mathbf{U \Sigma V}^T$. Then the joint space wave impedance can be expressed

as:

$$\mathbf{B}_{\text{joint}} = \mathbf{J}^T \mathbf{B}_{\text{cart}} \mathbf{J} \tag{3.91}$$

$$= \mathbf{V}\boldsymbol{\Sigma}\mathbf{U}^T \mathbf{B}_{\text{cart}} \mathbf{U}\boldsymbol{\Sigma}\mathbf{V}^T \tag{3.92}$$

$$= \mathbf{V}\left[\boldsymbol{\Sigma}\mathbf{U}^T \mathbf{B}_{\text{cart}} \mathbf{U}\boldsymbol{\Sigma}\right]\mathbf{V}^T \tag{3.93}$$

$$= \mathbf{V}\mathbf{X}\mathbf{V}^T \tag{3.94}$$

where $\mathbf{X} = \boldsymbol{\Sigma}\mathbf{U}^T \mathbf{B}_{\text{cart}} \mathbf{U}\boldsymbol{\Sigma}$. By Sylvester's Law of Inertia, assuming $\mathbf{J}$ to be of full rank,

$$\text{inertia}(\mathbf{X}) = \text{inertia}(\mathbf{V}\mathbf{X}\mathbf{V}^T) = \text{inertia}(\mathbf{B}_{\text{joint}}) \tag{3.95}$$

because $\mathbf{V}$ is an orthogonal matrix and thus guaranteed to be invertible.

$\mathbf{X}$ itself would be expected to have some number of zero singular values, because $m < n$. Collecting the nonzero singular values together, $\boldsymbol{\Sigma}$ can be written as

$$\mathbf{X} = \begin{pmatrix} \tilde{\boldsymbol{\Sigma}}^T \mathbf{U}^T \mathbf{B}_{\text{cart}} \mathbf{U}\tilde{\boldsymbol{\Sigma}} & \mathbf{0} \\ \mathbf{0} & \mathbf{0} \end{pmatrix} \tag{3.96}$$

where $\tilde{\boldsymbol{\Sigma}} \in \mathbb{R}^{m \times m}$. The eigenvalues of the nonzero submatrix will also be eigenvalues of $\mathbf{X}$ itself, with the additional zero entries contributing $m-n$ zero eigenvalues. $\mathbf{B}_{\text{cart}}$ becomes positive *semi*-definite due to these zero eigenvalues.

3.6 Bounding the Wave Impedance

3.6.1 Magnitude

As mentioned in Subsection 2.4.2, it will be necessary in practice to bound the choice of impedance within some reasonable range of values. This becomes less straightforward in the present application, in which the impedance is a matrix rather than a scalar. A simple technique for applying suitable bounds is to perform a Singular Value Decomposition (SVD) of the impedance matrix.[9] Decomposing $\mathbf{B}_{\mathrm{joint}} = \mathbf{U}\boldsymbol{\Sigma}\mathbf{V}^T$ (where, for a positive definite matrix, $\mathbf{U} = \mathbf{V}$), the singular values σ_j appear as the diagonal values of $\boldsymbol{\Sigma}$. Any σ_j that exceed some chosen bounds (denoted here as σ_{min} and σ_{max}) for implementation may be replaced with the corresponding maximum or minimum acceptable value:

$$\sigma'_j = \begin{cases} \sigma_j & \sigma_{min} \leq \sigma_j \leq \sigma_{max} \\[2mm] \sigma_{max} & \sigma_j > \sigma_{max} \\[2mm] \sigma_{min} & \sigma_j < \sigma_{min} \end{cases} \tag{3.97}$$

Then the bounded impedance choice $\mathbf{B}'_{\mathrm{joint}} = \mathbf{U}\boldsymbol{\Sigma}'\mathbf{V}^T$ may be used in place of $\mathbf{B}_{\mathrm{joint}}$. Due to the computational cost of the singular value decomposition, it may

---

[9]See, for example, [80] for discussion of the SVD. Another simple approach, allowing for different upper and lower impedance bounds for each joint individually (and potentially requiring less computation overall), might be implemented by bounding individual elements of the matrix using the Gershgorin circle theorem in order to enforce bounds on the eigenvalues. Such an approach would, however, necessarily be rather conservative.

be necessary in practice to update the wave impedance at a lower rate than the control rate.

In addition to mitigating numerical difficulties, bounding the singular values of the wave impedance in this way enables extension of this technique into two important application conditions that would not otherwise be possible: manipulators having one or more redundant degrees of freedom, and environments having one or more axes of zero stiffness. Each of these conditions has the effect of rendering the matrix dictated by (3.83) merely positive *semi*-definite, thus causing the wave transformation (which requires that $\mathbf{B}^{-1}$ exist) to become ill-defined. Enforcement of a σ_{min} as above, however, can be used to map this positive semidefinite matrix to a matrix that is strictly positive definite. Care must be exercised in the reconstruction of the bounded impedance matrix, since when $\sigma_j = 0$ the corresponding columns of $\mathbf{U}$ and $\mathbf{V}$ may have opposite signs. The bounded impedance choice is therefore taken to be

$$\mathbf{B}'_{\text{joint}} = \mathbf{U}\mathbf{\Sigma}'\mathbf{U}^T$$

In the case of a redundant manipulator, it is necessary to define a Cartesian inertia matrix in order to evaluate (3.67). Although, by definition of a redundant manipulator, a unique mapping does not exist between Cartesian end effector state and the system's kinetic energy, the Moore-Penrose pseudoinverse[10] $\mathbf{J}^\dagger$ can be used (as long as $\mathbf{J}$ remains of full rank) to generate a reasonable approximation $\mathbf{M}_{\text{cart}} \approx$

---

[10]Or any other pseudoinverse—the purpose is simply to estimate the inertia associated with a given Cartesian end effector motion.

$(\mathbf{J}^{\dagger})^{T}\mathbf{M}_{\text{joint}}\mathbf{J}^{\dagger}$ for systems having a small number of redundant degrees of freedom. Again, one may sacrifice optimality in favor of stability by selecting any positive definite impedance matrix if $\mathbf{J}$ becomes rank deficient; and, again, because this inertia value is used only to achieve quasi-optimality and not stability, it is not necessary for an exact and unique mapping to exist in order to achieve some benefit.

An alternative application to redundant manipulators would be to augment the Cartesian task space with as many additional coordinates as are necessary to achieve a square matrix. A shoulder-elbow-wrist angle [83] or a subset of the joint angles themselves could be used for this purpose. This has the effect of introducing additional singularities, however, and would not likely be of greater utility unless one had some task-specific need to separately specify impedance in the supplemental coordinate(s).

It is noted that, if the environment consists of a collection of rigid or highly stiff objects between which the manipulator may move freely, then in practice this scheme amounts to selecting the maximum allowable impedance in the contact direction and the minimum allowable impedance in the free motion directions. In such a scenario, estimation of the precise magnitude of the environmental stiffness is far less important than estimation of the direction of the contact axis. A useful feature of the present technique, however, is that (unlike most prior work [66] [67] with the exception of [59]) it does not restrict itself to a binary consideration of contact versus free motion. In the event of intermediate levels of stiffness due to the presence of highly deformable objects in the environment, the present technique will adjust the wave impedance to compromise between the simultaneous considerations of inertia

and stiffness perception.

3.6.2 Rate of change

Although it was shown in Section 3.3 that a time-varying choice of wave impedance doe not pose a threat to the stability of the system, it does degrade performance by introducing master-slave coordination error. Although mitigating solutions are cited therein, one would generally wish to enforce a limit on the rate of impedance change so as to keep the resulting coordination error small enough to be managed by those solutions. Suppose it is desired to constrain the impedance matrix such that no element varies by an amount greater than $\delta_{max} > 0$ from one update cycle to the next.[11] The permissible δ_{max} will depend largely on the maximum acceptable coordination error. However, as shown in (3.42), the magnitude of that error will depend on the magnitude of the wave signals in the communication channel at the time of the communication change as well as on the impedance inverse; and, in general, some amount of trial and error may be necessary in order to identify a reasonable δ_{max} for a given system and operating conditions. δ_{max} might be chosen as a fixed constant (e.g., 10% of σ_{min} per delay interval T), or relative to the actual impedance choice at time t_1 (e.g., 10% of the smallest singular value of $\mathbf{B}_{t1}$).

Consider a step from time t_0, at which the wave impedance is $\mathbf{B}''_{t0}$ (where the double prime denotes bounding of impedance rate in addition to magnitude), to

---

[11]The duration of this update cycle need not depend in any particular manner upon the delay interval T nor upon the update rate of the controller itself.

time t_1 at which the foregoing calculation yields a candidate impedance choice of $\mathbf{B}'_{t1}$, which may exceed rate-of-change limitations. The greatest element change is identified:

$$\delta = \max_{i,j} |\mathbf{B}'_{t1} - \mathbf{B}''_{t0}|_{i,j} \tag{3.98}$$

This quantity is then compared against δ_{max}. A scaling factor $0 < \zeta \leq 1$ is then identified as

$$\zeta = \begin{cases} \delta_{max}/\delta & \delta > \delta_{max} \\ \\ 1 & \delta \leq \delta_{max} \end{cases} \tag{3.99}$$

The impedance change is then rescaled accordingly:

$$\mathbf{B}''_{t1} = \mathbf{B}''_{t0} + \zeta(\mathbf{B}'_{t1} - \mathbf{B}''_{t0}) \tag{3.100}$$

$$= (1 - \zeta)\mathbf{B}''_{t0} + \zeta\mathbf{B}'_{t1} \tag{3.101}$$

Because both $\mathbf{B}''_{t0}$ and $\mathbf{B}'_{t1}$ are positive definite (and $0 < \zeta \leq 1$), $\mathbf{B}''_{t1}$ will retain positive definiteness as well.

This rate bounding scheme additionally presents a simple means of switching away from quasi-optimal impedance selection in singular poses. It was noted in Section 3.5 that the quasi-optimal choice (3.67), due to its dependency on $\mathbf{M}_{\text{cart}} = \mathbf{J}^{-T}\mathbf{M}_{\text{joint}}\mathbf{J}^{-1}$, becomes ill-defined when the manipulator Jacobian is not invertible. It was also stated in Section 3.5 that any positive definite matrix may be substituted in order to maintain stability (temporarily sacrificing any attempt at optimality) until the singular condition is resolved.

The measure of manipulability $w = \sqrt{\det(\mathbf{JJ}^{\mathrm{T}})}$ introduced by Yoshikawa [84] becomes zero when a robot enters a singular pose[12]. Candidate values of $\mathbf{B}_{\mathrm{cart}}$ may be rejected (holding the previous legal value [13]) when this measure drops below some w_{min}. Once the singularity is resolved and $w > w_{min}$, new choices of $\mathbf{B}_{\mathrm{cart}}$ may be accepted and the rate-bounding scheme presented above will ensure that the system returns to use of the quasi-optimal choice within specified rate limits.

It is further noted that the transformation (3.83) from the Cartesian space to the joint space does not become ill-defined in the event of a singularity. Although bounding of the singular values as described in Subsection 3.6.1 will be necessary in order to enforce positive definiteness, the special handling of singularities described above would not be necessary if, for example, a constant choice of $\mathbf{B}_{\mathrm{cart}}$ were employed.

3.7 Additional Stability Considerations

The analysis of Section 3.2 obviously assumes ideal behavior of the mechanisms, actuators, sensors, and processors employed in the implementation of the system. Although the dissipation provided by the PI controllers and the natural friction present in the master and slave manipulators may often, in practice, inject

---

[12]Togai [85] proposes the inverse of the condition number of $\mathbf{J}$ as a more appropriate measure of nearness to a singularity. In contrast to Yoshikawa's measure of manipulability [84], this unitless quantity does not scale in a manner dependent upon the number of degrees of freedom of the manipulator. This measure may be substituted for w without modification to the present discussion.

[13]Or replacing it with any desired positive definite fallback choice—the proposed rate bounding scheme will ensure that the transition to this fallback choice is made within allowable rate limits.

sufficient damping to avoid any issues, these unmodeled dynamics present the risk of destabilizing the system. Tanner and Niemeyer [86] analyze the problem of sensor and actuator dynamics, proposing wave filters to dissipate the injected energy. They find that the pulse width modulation amplifiers employed in their setup contribute much of the problematic dynamics that are unmodeled above, behaving in practice as low pass filters and additionally injecting a small amount of pure time delay.[14] Resonance in their cable drive system, although by itself a passive mechanical phenomenon, is also found to represent a risk of instability when coupled with this phase lag. Yasrebi and Constantinescu [87] additionally explore the effect of sampling rates and computational delay in the context of haptic interaction with a virtual environment.

3.7.1 Diverging Impedance

It was shown in the preceding subsection that the total energy of the teleoperation system will not increase regardless of variation in wave impedance. As a brief demonstration of this analytical result, consider a choice of impedance that diverges exponentially with time:

$$B_{joint} = 2 + e^t \tag{3.102}$$

This scenario is simulated on a two-degree-of-freedom planar manipulator having links of length 1 m, mass 10 kg, and rotational inertia 3.33 kg-m^2. Round-trip

---

[14]This time delay exists in the sensor-actuator loop of the PI controller, not within the communication channel that is wave-passivized against latency.

communication delay is taken to be 0.1 seconds. The controllers have integral gain $K_I = 10$; and to avoid wave reflections $K_P = B_{joint}$. Gravity is not present (or assumed canceled). The arm is initially at full extension. The operator is modeled as a (passive) PD controller with $K_p = 10$ and $K_d = 10$ attempting to drive both joints through a counterclockwise rotation of $\pi/2$. Environmental stiffness K_e is taken to be 10 N/m in both the x and y axes. Round-trip communication latency is 0.1 seconds.

Fig. 3.1 shows the behavior of the joint angles during this simulation. Naturally, due to the extreme choice of wave impedance, convergence to the $\pi/2$ goal is quite poor. Nonetheless, the system remains stable; and both master and slave slow to negligible velocity by $t = 10$ seconds.

3.7.2   On the passivity of the human operator

It must be noted that, although Hogan [88] found the human arm to behave indistinguishably from a passive system, the assumption of passivity of the human operator has been called into question more recently [89]. It stands to reason that a human who chooses to continually pump energy into the system could certainly do so (except in the rather extreme consideration that a human isolated from a source of nourishment could be said to possess only a finite number of calories of internal energy at $t = 0$). Indeed, Niemeyer [90] remarks that "Naturally the operator must produce energy to generate [an] input and interact with the system," but assumes the input energy to be bounded. This subsection therefore explores the validity of
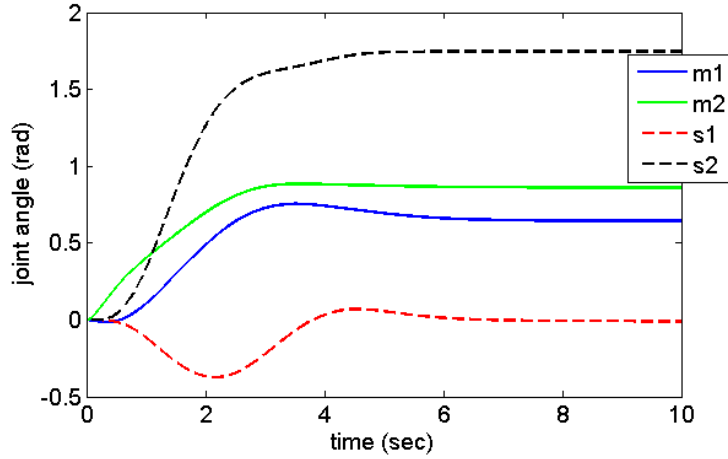
Figure 3.1: Joint angles during simulation with exponentially diverging wave impedance. Master joint angles are denoted m1 and m2. Slave joint angles are denoted s1 and s2.

this passivity assumption.

Any real manipulation task would almost necessarily require the operator to move the system toward a time-varying goal, which would likely require the input of an inherently unboundable amount of energy, except perhaps in the case of a finite list of discrete waypoints. Consider, for simplicity, a SISO scenario in which a human operator modeled as a PD controller with constant gains is tracking a time-varying desired position $x_{des}(t)$:

$$F_h = K_p(x_{des} - x) + K_d(\dot{x}_{des} - \dot{x}) \qquad (3.103)$$

The net work done on the operator by the teleoperation system is given by

$$P_h = -F_h\dot{x} = -K_p\dot{x}(x_{des} - x) - K_d\dot{x}(\dot{x}_{des} - \dot{x}) \qquad (3.104)$$

where a positive quantity indicates work done on the operator and a negative quantity indicates work done by the operator. If x_{des} is identically a constant, this model of the operator reduces to a spring-damper system and the net work performed (the time integral of P_h) can be readily bounded. Consider, without loss of generality, the case in which $x_{des} \equiv 0$:

$$\int_0^t P_h(t)dt = \int_0^t \left(K_p x \dot{x} + K_d \dot{x}^2 \right) dt \qquad (3.105)$$

$$= \frac{1}{2} K_p x^2 - \frac{1}{2} K_p x(0)^2 + \int_0^t K_d \dot{x}^2 dt \qquad (3.106)$$

$$\geq -\frac{1}{2} K_p x(0)^2 \qquad (3.107)$$

Consistent with the definition of passivity (2.2), the amount of work done by the operator can be bounded on the basis of an initial energy effectively stored by the operator at time $t = 0$.

If the operator wished to drive the system unstable, however, he or she could certainly make a time-varying choice of x_{des} to accomplish this. Consider, for example, the case in which $\dot{x}_{des} = \dot{x}$ but $x_{des}(0) \neq x(0)$. Under this choice, the integral of (3.104) becomes instead:

$$\int_0^t P_h(t)dt = -\int_0^t \left(K_p \dot{x}(x_{des} - x) + K_d \dot{x}(\dot{x}_{des} - \dot{x}) \right) dk \qquad (3.108)$$

$$= -\int_0^t \left(K_p \dot{x}(x + x_{des}(0) - x) + K_d \dot{x}(\dot{x} - \dot{x}) \right) dk \qquad (3.109)$$

$$= -x_{des}(0) \int_0^t K_p \dot{x} dk \qquad (3.110)$$

Because no particular relationship can be guaranteed in general between x_{des} and $\dot{x}$, neither the sign nor a maximum magnitude for this quantity can be guaranteed in general.

As an example which instead does not rely upon a deliberately unstable choice of x_{des}, consider the case of the foregoing human operator model (with $K_p = 10$ and, to achieve an energetically lossless response, $K_d = 0$) driving a robot modeled as a simple double integrator ($F_h = m\ddot{x}$, where $m = 10$). Fig. 3.2 shows the Bode plot of the resulting closed-loop system (with x_{des} as input and x as output). Although this is a marginally stable system (with poles at $\pm j\sqrt{K_p/m}$) and will not diverge in response to an impulse, the system is not bounded-input-bounded-output (BIBO) stable. It exhibits resonance at $\omega = 1$ rad/s. This scenario is simulated with a desired trajectory given by $x_{des}(t) = \sin(t)$. The resulting system trajectory $x(t)$ is as shown in Fig. 3.3a, and the kinetic energy of the robot $KE = \frac{1}{2}m\dot{x}^2$ is shown in Fig. 3.3b. In this particular case, because the system is linear, the resonant frequency can easily be identified and the nature of the instability is well understood. The point, however, is simply that the capacity for instability exists insofar as, from a pure passivity argument, stability can no longer be guaranteed.[15]

The divergent behavior of this system in response to a time-varying position goal underscores a significant contributing factor in the discussion of the passivity of human opreators. In [89] subjects were told to hold their hands at a *fixed location*; and it was the return motion after a perturbation that was responsible, at least in

---

[15]Naturally, this is in general not a guarantee of *instability*, but merely a failure of a particular analysis to guarantee stability.
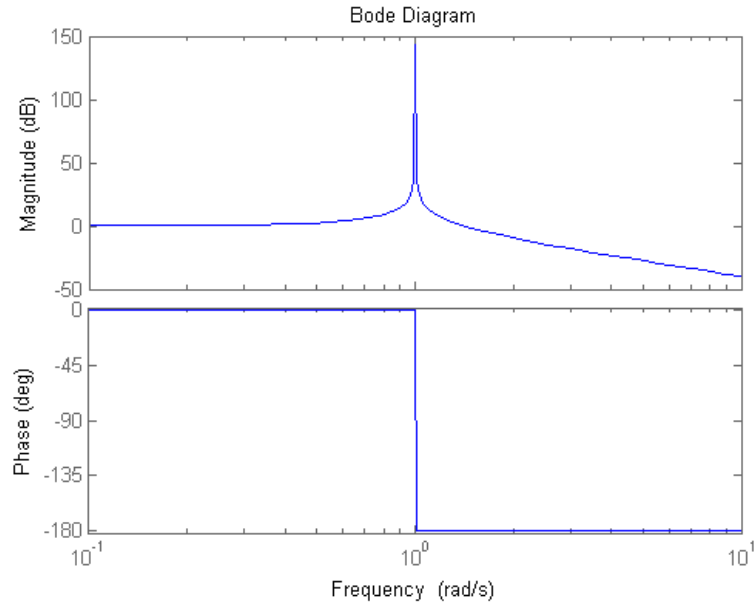
Figure 3.2: Bode plot of the closed-loop transfer function mapping desired position to actual system state

part, for the increase in total energy observed by the authors. In [88] it appears that the human operators were simply attempting to dampen oscillations rather than to correct for net movement.

The above is obviously a highly simplified scenario that fails to model the complexities of an actual human operator. The choice $K_d = 0$ in particular was made so as to contrive a situation in which the proportional control term may inject energy into a system that is otherwise energetically lossless. Such a choice makes possible the divergent behavior seen above which is clearly unstable. Passivity is, however, a more conservative condition than stability (i.e., a stable system is not necessarily passive, but a passive system is necessarily stable); and *nonpassivity* of the human operator would be expected to hold under any reasonable human dynamics model (which might, if more rigorous modeling were motivated, endeavor

99
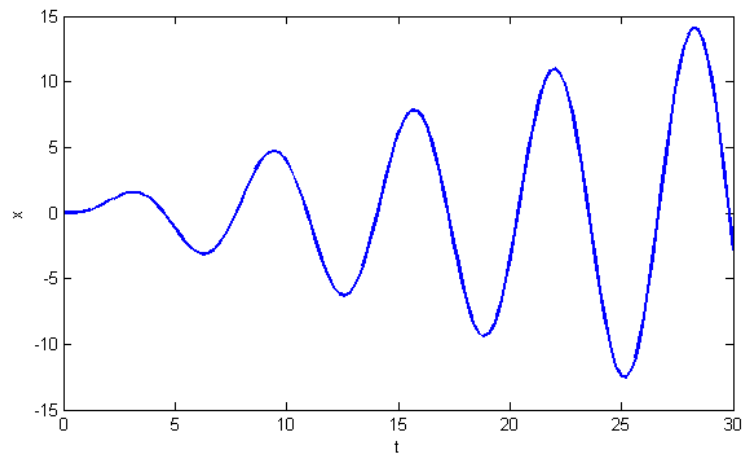
(a)
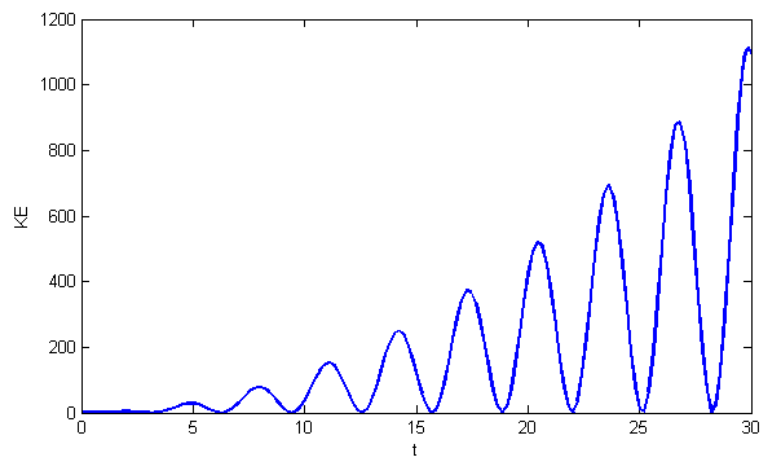
(b)

Figure 3.3: Simulation of a passive system being driven by an operator that is nonpassive due to a time-varying position goal

to take into account issues such as bandwidth limitations).

That a time-varying desired location is nonpassive may be seen most clearly by replacing the teleoperation system above with a pure linear damper $F = -D\dot{x}$, $D > 0$. Since the system force will always oppose motion here, any action on the part of the operator that continously causes motion will result in an unboundable amount of work being done on the system. Any reasonable model of human dynamics (i.e., any model that exerts a nonzero force F_h when $x_{des} \neq x$) will perform work on the system in response to, e.g., a sinusoidal x_{des} of finite amplitude. This is not to say that the human arm itself is nonpassive—indeed, as a biological manipulator it is likely as passive as any artificial one.[16] Rather, it is simply a statement that the human mind driving it cannot be expected to be universally passive. Just as a nonpassive control law can render a manipulator-controller system nonpassive in traditional control contexts, so too can it do so in the case of the human arm. A human operator has the free will to choose to cause motion at any time, and will never encounter a scenario in which he or she would like to cause motion but cannot due to depletion of a storage function.[17]

The work of Hogan more directly suggests that the human can stabilize the teleoperation system by stopping motion and maintaining a firm grasp in the event that excessive oscillations begin to develop. It therefore seems quite plausible that,

---

[16]Indeed, McIntyre and Slotine [91] have suggested that the human brain may interact with muscles in a manner resembling wave-based control.

[17]Again, with only the rather extreme exception that a human deprived of outside sustenance contains only a finite number of calories.

although a human operator is clearly an active system, he or she can at least choose to behave approximately passively when it becomes necessary. Employing what appears to be a similar line of thought, Hirche et al. [29] separate the force exerted by the operator into the sum of a force due to the (presumably passive) dynamics of the human arm itself and a "voluntarily applied force" generated deliberately. Training of human operators to be cognizant of passivity considerations may be a worthy avenue for future research. Dyck et al. [89] also suggest that the use of a passivity observer may enable a scheme in which a nonpassive human can be actively passivized. Moreover, Jazayeri and Tavakoli [92] take some initial steps toward relaxing the passivity requirement for (linear) teleoperation systems; and Matiakis et al. [93] have proposed a scheme for compensating a shortage of passivity.

In any event, the assumption that the human operator is passive is present in most state of the art work employing wave-based teleoperation; and moving beyond this assumption is a research problem extending far beyond the scope of the present study.[18] For the present work, it is simply observed that the Lyapunov-like analysis presented earlier in this chapter shows that the system's total energy cannot increase beyond that contained in the system at the start time $t = 0$ plus the work done on it by the operator and environment. Energy will not simply increase unprovoked due to the internal dynamics of the teleoperation system; and it is hoped that a human operator, behaving intelligently and perhaps under appropriate training, can refrain

[18]An active environment raises much the same stability concerns as an active operator. Consider, for example, surgery on a beating heart. That the environment is passive is similarly a standard assumption in the literature, and much of the same discussion applies.

from introducing unreasonably large amounts of energy into the system.

3.8   Chapter Summary

The idea of wave impedance selection (independent of whether or not the quasi-optimum (2.34) of the previous chapter is employed) has been extended to incorporate both joint space and Cartesian space considerations, treating **B** as a matrix quantity that need not yield an isotropic impedance distribution. This overcomes a significant limitation of prior work, which has typically relied in practice upon a scalar choice of impedance that is incapable of addressing the simultaneous and conflicting requirements associated with constrained motion.

The system designer can implement this impedance selection scheme as either a constant or time-varying choice. In the latter case, the considerations are much the same as those identified in prior work. It is shown explicitly that the passivity (and hence stability) of the standard wave-based teleoperator is unaffected by arbitrary time variations in impedance, although performance suffers in the form of master-slave coordination error. This error can be avoided through the dual-impedance approach of Tanner and Niemeyer [67]; however, doing so involves a nonpassive behavior that must be corrected by enforcing mandatory timeouts between discrete wave impedance changes. Rather than trading one problem (coordination error) for another (nonpassivity), the system designer may also choose to accept the introduction of coordination error. Subsection 3.6.2 presents a scheme for limiting the impedance rate in order to slow the accumulation of such error; and mitigating

schemes exist in the literature for dealing with the remaining error [36] [33].

Chapter 4: Simulation Results

4.1 Overview

This chapter presents a collection of simulation results validating the proposed scheme. Consideration is given both to the mechanical impedance displayed to the operator in a chosen reference pose and to the behavior of the system under simple operator behaviors.

4.2 Impedance Displayed to the Operator

The transparency of a telemanipulation system is often discussed in the context of the impedance displayed to the operator, where impedance is defined as the ratio of force (effort) to velocity (flow). This behavior is typically frequency dependent, and the impedance Z_t of a linear teleoperator is customarily described as a transfer function[1]:

$$Z_t(s) = \frac{F(s)}{V(s)} = \frac{F(s)}{sX(s)} \tag{4.1}$$

---

[1] Some researchers instead employ a generalized impedance having displacement rather than velocity in the denominator, more akin to stiffness than to damping.

where F is the output force displayed to the operator ($\underline{\tau}_{mc}$ in the joint space, or $\underline{F}_{mc} = \mathbf{J}^{-T}\underline{\tau}_{mc}$ in the Cartesian space) and V is the velocity of the master device ($\underline{\dot{q}}$ or $\underline{\dot{x}}_m$). A statement of the ideal transparency condition [75] is that the impedance displayed to the operator precisely match that of the remote environment:

$$Z_t(s) = Z_e(s) \tag{4.2}$$

While it may be possible in principle (and under sufficiently small communication delays) to approach this ideal condition in schemes that actively cancel the dynamics of the master and slave, this is not a reasonable standard for passivity-based schemes that make no such attempt. Thus, although Bode diagrams of the system impedance are presented in this chapter, the reader must bear in mind that these plots necessarily represent a combination of dynamics due to the environment, the master and slave manipulators, the associated passive controllers, and the wave-based communication channel.

Because the system response is frequency dependent, it is necessary to identify the range of frequencies of interest. Typical closed-loop motions of the human arm contain frequencies no greater than 2 Hz (12 rad/sec), with open-loop motions due to learned muscles responses and the natural dynamics of the arm yielding frequency content as high as 4 to 6 Hz (25 to 38 rad/sec) [94]. This section therefore explores the behavior of the system between frequencies of 1 rad/sec and 40 rad/sec.

For this impedance characterization study, the master and slave manipulators are modeled as identical, two-degree-of-freedom planar elbow manipulators. Each

robot link has length 1 m, mass 10 kg, and rotational inertia 3.33 kg-m^2. The arms are positioned in the x-y plane as shown in Fig. 4.1, with $\underline{q} = \underline{0}$ corresponding to full extension along the x-axis. The test configuration is as shown in Fig. 4.2, centered about the arm pose $\underline{q} = [\pi/4 \quad -\pi/4]^T$, which corresponds to an end-effector location at the equilibrium point of the environmental spring.[2] An environment capable of both pushing and pulling (i.e., permanent contact) is modeled with a stiffness of 10 kN/m in the x-direction and 10 N/m in the y-direction. One-way communication delay is taken to be 0.05 seconds. The effect of gravity is neglected, assuming that these manipulators either lie in the horizontal plane or that gravity has been canceled by the control system. K_p is matched to the wave impedance; and K_I for each joint is taken to be one-fifth of the corresponding diagonal element of the wave impedance (with the PI-like control law of Subsubsection 3.2.1.2 employed to allow for a time-varying choice of integral gain). When the quasi-optimal result of (2.34) is employed, k_{ref} is chosen as 100 N/m, σ_{min} as 100 kg $\cdot$ m^2/s, and σ_{max} as 1,000 kg $\cdot$ m^2/s. These values were identified via trial and error as suitable bounds within which the numerical simulations were well behaved under Runge-Kutta integration at reasonable step sizes (on the order of 10^{-4} seconds).

To mitigate the possibility of wave reflections, low pass filters (as suggested by Niemeyer and Slotine [25]) were applied to the wave variables in both directions

---

[2]The resulting impedance plots therefore represent the approximate linearized behavior about this reference configuraiton.
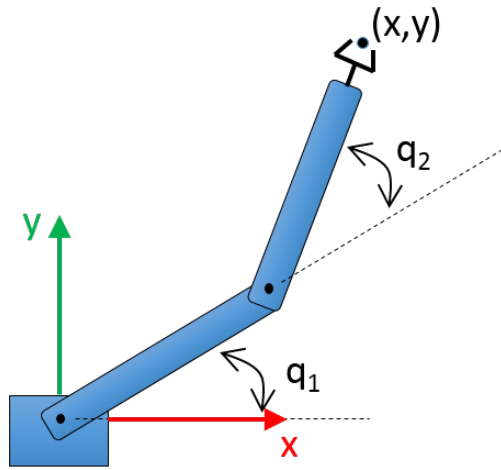
Figure 4.1: 2-degree-of-freedom planar elbow manipulator model
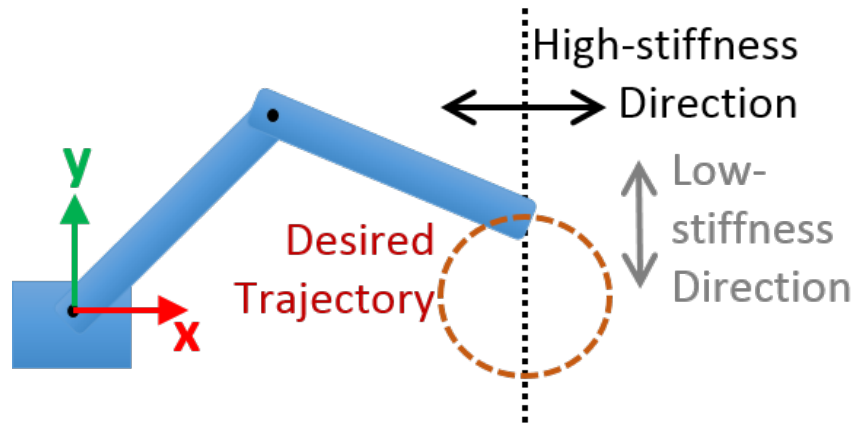
Figure 4.2: Overview of contact motion simulation

according to the following control laws:

$$\dot{\underline{u}}_s(t) = \lambda(\underline{u}_s(t) - \underline{u}_m(t - T))$$

$$\dot{\underline{v}}_m(t) = \lambda(\underline{v}_m(t) - \underline{v}_s(t - T))$$

where $\lambda = 250$.

4.2.1 Estimating Impedance in Simulation

Impedance transmitted to the operator was assessed using a method adapted from that of Hirche [95]. This technique consists of initializing the teleoperation system at a reference pose coinciding with the equilibrium position of the environment, exciting the master manipulator with a small-amplitude sinusoidal velocity signal in a chosen direction, and identifying the phase and gain relationship between this input velocity signal and the output force signal generated by the master controller[3]. In the present work, oscillations were 1 mm in half-amplitude. Impedance would obviously be expected to vary with robot pose; and the following characterization is only a single case study among the infinitely many possible choices of pose, chosen with $|q_2| = \pi/4$ so that the links would be neither fully parallel nor fully perpendicular. This was performed with scalar choices $B = \sigma_{min}$ and $B = \sigma_{max}$, as well as

---

[3]In the present work, three cycles of motion were simulated; and the latter two cycles (discarding the first so as to mitigate the effect of the transient response) of the resulting force signal $\underline{F}_{mc} = \mathbf{J}_m^{-T}\underline{\tau}_{mc}$ were fitted (via the MATLAB function `fminsearch`) with a sinusoid of the same frequency. The fitted sinusoid was then compared to the input velocity sinusoid in order to identify the gain and phase relationship between the two.

the presently-proposed directional scheme given by (3.67) and (3.83).

4.2.2   Results

Bode plots describing the estimated system impedance in the reference pose are presented in Figs 4.3 and 4.4 for the x- and y-directions, respectively. In Fig. 4.3, the blue magnitude curve associated with the presently proposed directional scheme lies visibly above the red curve of the low-impedance scalar choice $(B = 100 \text{ kg} \cdot \text{m}^2/\text{s})$, closing the gap between the high- and low-impedance curves by 25% on average, while in Fig. 4.4 these curves are nearly indistinguishable. This suggests that the proposed directional scheme has indeed succeeded in focusing the effects of the wave impedance in the x-direction without burdening the y-direction with substantially increased equivalent inertia or damping.[4] That the blue and green curves do not coincide with one another in the x-direction plots does, however, underscore the fact that this does not achieve the full equivalent of B = 1,000 $\text{kg} \cdot \text{m}^2/\text{s}$ in the x-direction. The phase curves in both cases remain within $\pm 1/3$ radian of zero across the frequencies of interest, suggesting that the force felt by the operator consists largely of damping (which is in phase with velocity) rather than stiffness (which is in phase with displacement).

---

[4]Recall that the goal here is to increase the resistance to motion in the high-stiffness x-direction as compared to the $B = 1,000$ case without burdening the low-stiffness y-direction with any greater motion penalty—thus treating the two axes according to their respective tuning considerations.
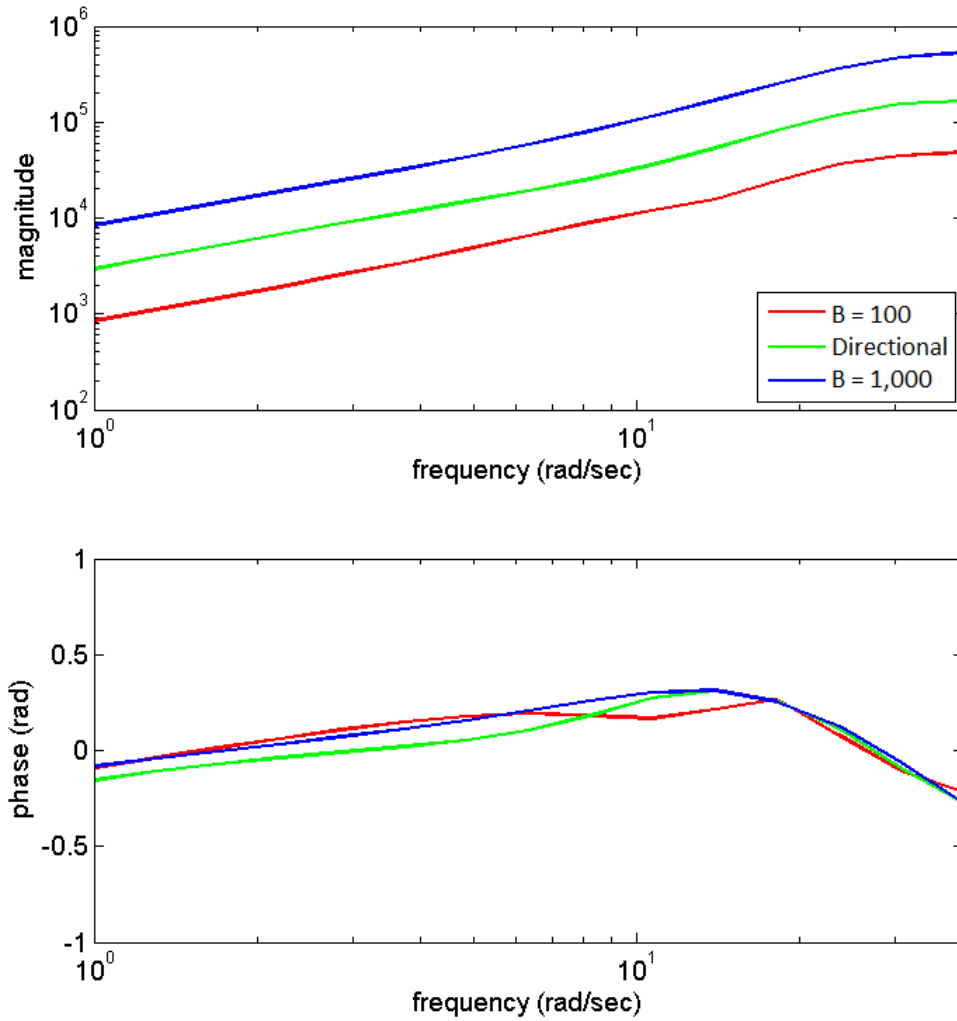
Figure 4.3: Magnitude gain and phase of the master controller force signal as compared to the input velocity signal about the chosen reference pose in the high-stiffness x-direction.
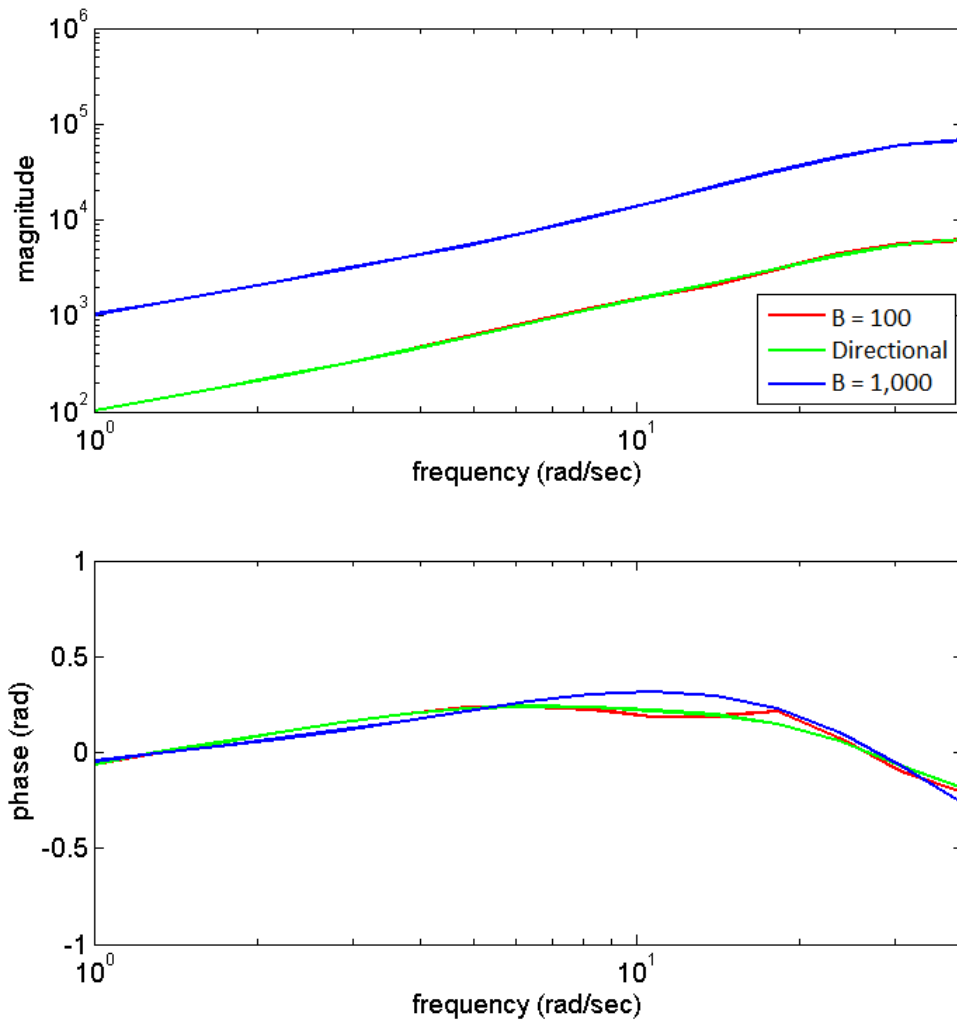
Figure 4.4: Magnitude gain and phase of the master controller force signal as compared to the input velocity signal about the chosen reference pose in the low-stiffness y-direction.

4.3   Contact Motion

Whereas the previous section looked at very small displacements about a reference position, the present section explores tracking of larger trajectory-based motion while still retaining the assumption of permanent contact with the same environment given above. The desired trajectory is given by a circle of diameter 50 cm, traversed at a nominal frequency of 1 rad/s. The starting point of the trajectory corresponds to the top of the circle and to the equilibrium point of the environmental spring, and is again given by $\underline{q}_0 = [\pi/4 \quad -\pi/4]^T$. The arrangement is shown in Fig. 4.2.

In contrast to the perfect tracking of the previous section, the human operator is modeled here as a PD controller with $K_p = K_d = 50$. Thus, the operator will attempt to drive the system along the desired circular path but, in the case of good transparency, will be unable to achieve large motions in the high-stiffness x-direction as compared to the low-stiffness y-direction. Good transparency will manifest in these simulations as small displacements (*poor* tracking of the desired trajectory) in the x-direction and large displacements (*good* tracking of the desired trajectory) in the y-direction.

4.3.1   Results

Fig. 4.5 shows the displacements experienced by the operator at the master site in the x- and y-directions as compared to the desired circular trajectory; and

Table 4.1 shows the corresponding peak-to-peak displacements along each axis:

$$\Delta x_{p-p} = \max_{0 \leq t \leq 10} (x(t)) - \min_{0 \leq t \leq 10} (x(t)) \qquad \Delta y_{p-p} = \max_{0 \leq t \leq 10} (y(t)) - \min_{0 \leq t \leq 10} (y(t)) \quad (4.3)$$

In the low-impedance case of Fig. 4.5a, the operator is able to track the desired trajectory quite well in the low-stiffness y-direction, with peak-to-peak displacements at 88% of the nominal trajectory diameter. Substantial displacements occur, however, in the high-stiffness x-direction, suggesting that transmission of contact forces to the operator is lacking. These nuisance displacements are reduced by 55% in the high-impedance case of Fig. 4.5b; however, motion in the low-stiffness y-direction (in which the operator would ideally be able to move with very little resistance) is burdened by nearly the same fraction (53%). The ratio of y-direction to x-direction displacement improves only slightly (less than 5%) across these two cases. In the directional case of Fig. 4.5c, however, the system is able to achieve both goals simultaneously: impeding motion along the x-axis while permitting it along the y-axis. Due to the off-diagonal impedance terms, motion in the x-direction is permitted at less than half the amplitude of even the high-impedance case, while motion in the y-direction is intermediate to the low- and high-impedance scenarios. Fig. 4.6 additionally shows the displacements at the slave site for reference. Some master-slave coordination error is evident in all three plots, as was expected in the uncorrected implementation.[5]

_____

[5]Corrective schemes from the literature are discussed briefly in Section 3.3. The effect of these schemes on transparency, however, is not well studied. Such measures are therefore avoided in the present chapter so as to explore the pure effect of the presently proposed impedance selection
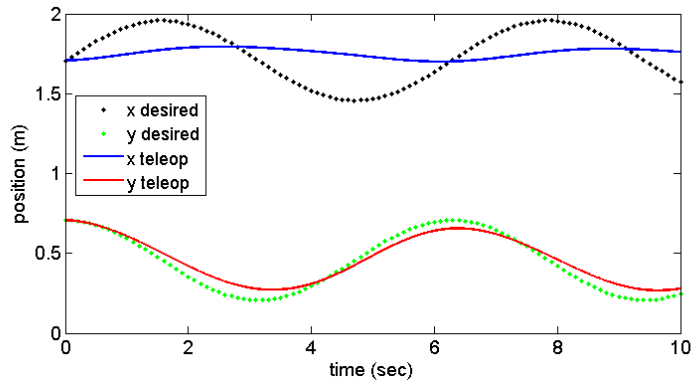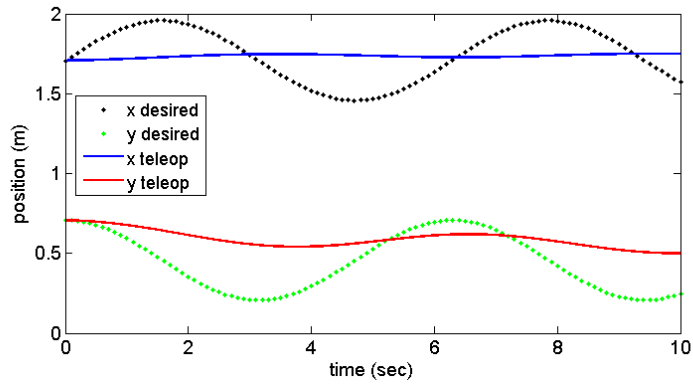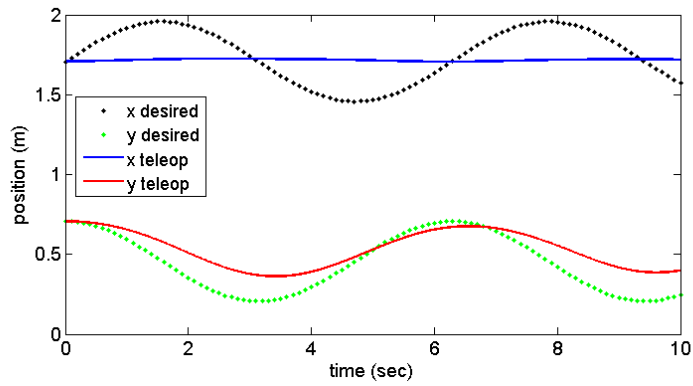
Figure 4.5: Desired and actual trajectories at the master (2-DOF) site for (a) $B = 100$, (b) $B = 1,000$, and (c) the presently-proposed directional impedance selection scheme.
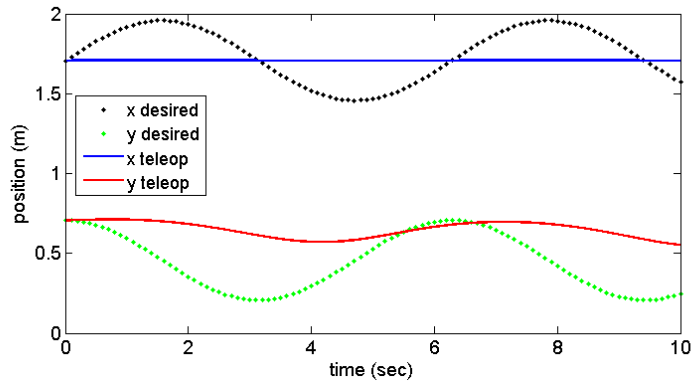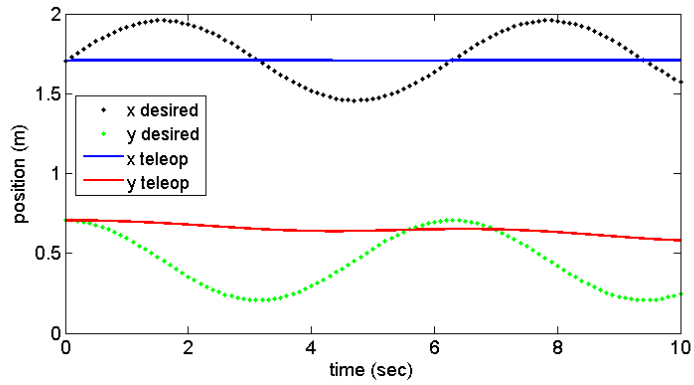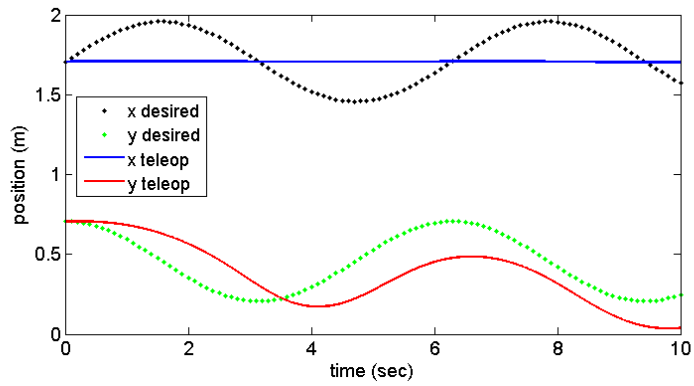
Figure 4.6: Desired and actual trajectories at the slave (2-DOF) site for (a) $B = 100$, (b) $B = 1,000$, and (c) the presently-proposed directional impedance selection scheme.

Table 4.1: Peak-to-peak master displacement (2-DOF)

	$B = 100 \ \frac{\text{kg} \cdot \text{m}^2}{\text{s}}$	$B = 1{,}000 \ \frac{\text{kg} \cdot \text{m}^2}{\text{s}}$	Directional
Δx_{p-p} (m)	0.0940	0.0423	0.0180
Δy_{p-p} (m)	0.4399	0.2070	0.3453
$\Delta y_{p-p}/x_{p-p}$	4.68	4.89	19.2

The ratio $\Delta y_{p-p}/x_{p-p}$ given in Table 4.1 underscores this, increasing by nearly a factor of four. This suggests that the proposed directional treatment more successfully manages the simultaneous and conflicting considerations of the high- and low-stiffness axes. Motion is restricted in the x-direction (for which motion should be difficult due to high stiffness) and permitted in the y-direction (for which motion should be comparatively easy due to low stiffness).

4.4 Redundant Manipulator

The scenario of the previous section is repeated here with a three-degree-of-freedom planar manipulator formed by adding an additional link (having identical properties to the others) to the two-link manipulator used above. This results in a system that is redundant in the two-dimensional (x,y) translational task space. It was noted in Subsection 3.6.1 that application to redundant manipulators becomes possible because the impedance bounding scheme introduced therein enforces a positive definiteness condition on what would otherwise be a merely semidefinite matrix. The initial pose is given by $\underline{q}_0 = [\pi/4 \quad -\pi/4 \quad \pi/4]^T$, with the equilibrium of the environmental spring translated to the end-effector location in that new pose. The

scheme.

conditions and parameters are otherwise identical to the previous section.

4.4.1 Results

Fig. 4.7 shows the resulting master trajectories, with peak-to-peak displacements given in Table 4.2. Once again, y-direction motion is successfully inhibited to a slightly greater degree than even in the high-scalar-impedance scenario while resulting in only a modest (22%) decrease in y-direction motion. As one would expect from the addition of a third joint (with stiffness rendering necessarily below actual environmental values), stiffness perception has suffered somewhat versus the 2-DOF case, resulting in more than double the x-direction displacement of that original scenario. Increasing σ_{max} could improve this somewhat, although one would expect to encounter numerical difficulties (and, in actual implementation, instability due to unmodeled dynamics) at excessively large values. Thus, effective implementation on robots having many degrees of freedom would be expected to be challenging.

4.5 Pure Cartesian Implementation

Simulation results presented to this point have been implemented in the joint space, as is customary in the teleoperation literature. It was shown in Subsection

Table 4.2: Peak-to-peak master displacement (3-DOF)

	$B = 100 \ \frac{\text{kg·m}^2}{\text{s}}$	$B = 1,000 \ \frac{\text{kg·m}^2}{\text{s}}$	Directional
Δx_{p-p} (m)	0.2317	0.1251	0.1005
Δy_{p-p} (m)	0.4451	0.2730	0.3476
$\Delta y_{p-p}/x_{p-p}$	1.92	2.18	3.46
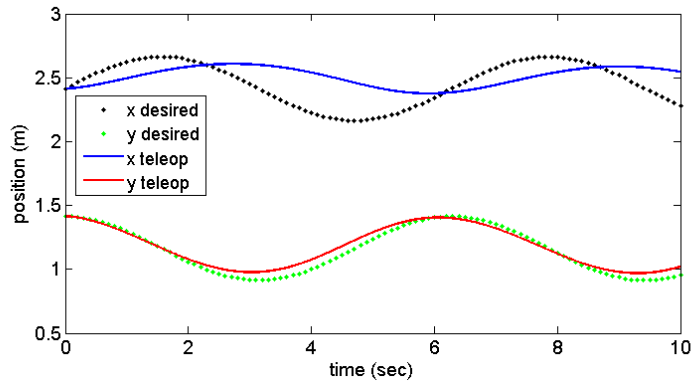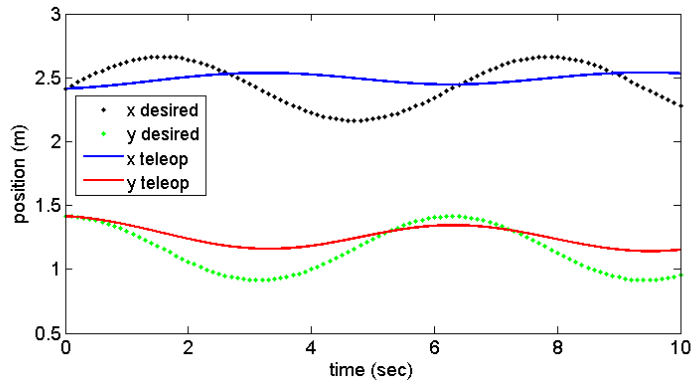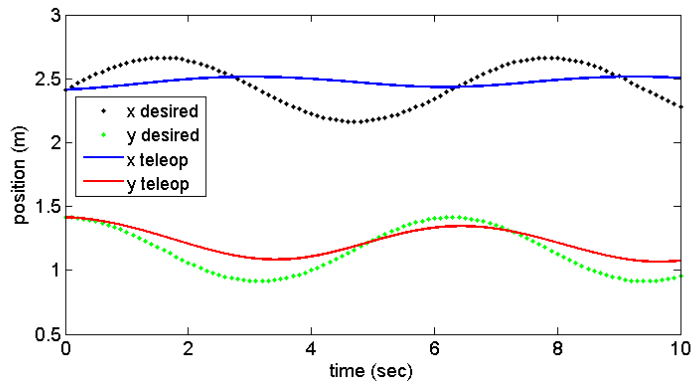
Figure 4.7: Desired and actual trajectories at the master (3-DOF) site for (a) $B = 100$, (b) $B = 1,000$, and (c) the presently-proposed directional impedance selection scheme.
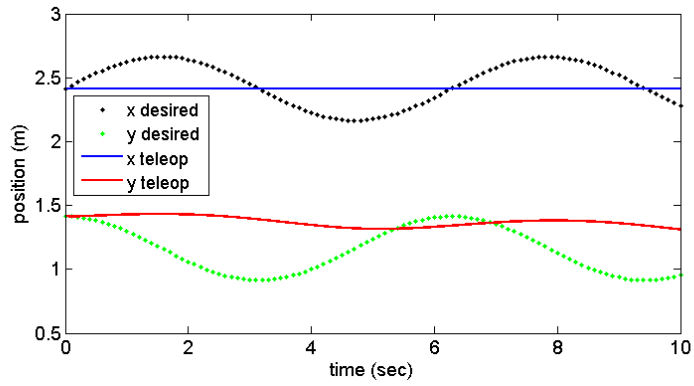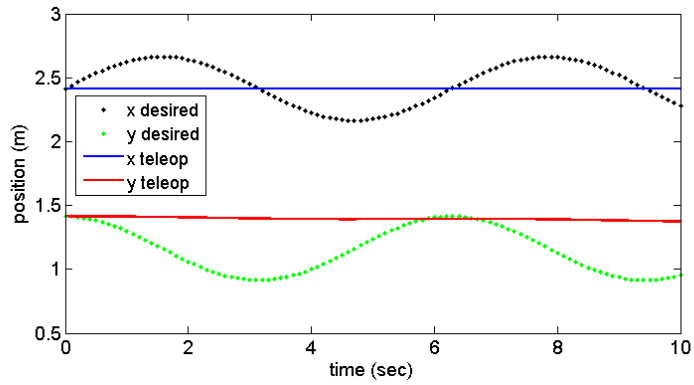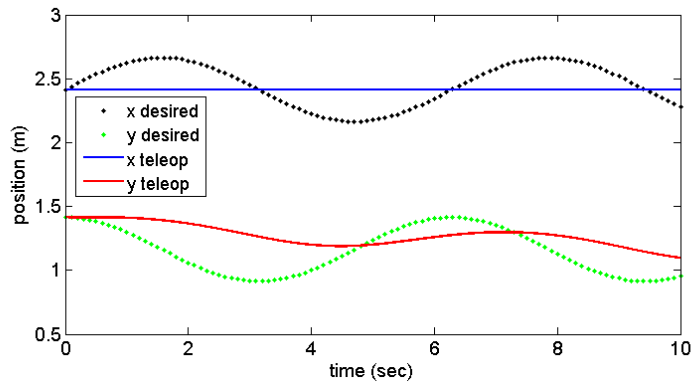
Figure 4.8: Desired and actual trajectories at the slave (3-DOF) site for (a) $B = 100$, (b) $B = 1,000$, and (c) the presently-proposed directional impedance selection scheme.

3.5.1, however, that this scheme may be implemented directly in the Cartesian space as well. This has been the custom in the case of haptic interaction with virtual environments [41] [38], wherein no slave manipulator exists and thus no meaningful joint space can be defined at the remote end of the system. In the wave transformation equations (2.3)-(2.6), joint rates $\dot{\underline{q}}$ and joint torques $\underline{\tau}$ are replaced with Cartesian end-effector velocities $\dot{\underline{x}}$ and forces $\underline{F}$, respectively. The corresponding forces are then applied to their respective manipulators via $\underline{\tau} = \mathbf{J}^{\mathrm{T}}\underline{F}$.

Because the system inertia is more nearly constant in the joint space than in the Cartesian space, tuning of this implementation is particularly challenging. Consider, for example, the lower-limit impedance choice from the above joint-space examples:

$$\mathbf{B}_{\mathrm{joint}} = \begin{pmatrix} 100 & 0 \\ 0 & 100 \end{pmatrix} \mathrm{kg} \cdot \mathrm{m}^2/\mathrm{s} \tag{4.4}$$

In the reference pose used in the preceding examples, this corresponds via (3.83) to a Cartesian space wave impedance of

$$\begin{pmatrix} 341.4 & 170.7 \\ 170.7 & 100.0 \end{pmatrix} \mathrm{kg/s} \tag{4.5}$$

Thus, an isotropic choice of wave impedance in the Cartesian space maps to markedly different values for each of the two joints in the present example; and these values may in general differ even more greatly depending upon the entries of the manipulator Jacobian $\mathbf{J}$. Because in practice numerical difficulties arise for excessively large or small values of impedance on a given joint, a Cartesian implementation necessar-

ily requires more conservative choices of σ_{min} and σ_{max}. In this pose alone, in order to provide the equivalent of at least $\sigma_{min,joint} = 100 \text{ kg} \cdot \text{m}^2/\text{s}$ at each joint, one must choose $\sigma_{min,cart} = 341.4 \text{ kg/s}$. Similarly, one would be forced to employ a $\sigma_{max,cart}$ of no greater than $1,000 \text{ kg/s}$ in order to avoid exceeding $\sigma_{max,joint} = 1,000 \text{ kg} \cdot \text{m}^2/\text{s}$. Thus, whereas the joint space implementation was able to achieve an impedance ratio of $\sigma_{max}/\sigma_{min} = 10$, commensurate bounds in the Cartesian space allow for a ratio of only 2.93; and motion over a finite subset of the manipulator's configuration space would be expected to restrict these bounds further still. The following subsection presents results employing these bounds, considering (as previously) constant choices of impedance corresponding to σ_{min} and σ_{max} as well as the quasi-optimal result of (2.34) bounded between these limits.

4.5.1 Results

Master trajectories are shown in Fig. 4.9, with peak-to-peak displacements given in Table 4.3. The quasi-optimal scheme again successfully restricts x-direction motion in a manner comparable to the high-constant-impedance case. Additionally, y-direction motion is permitted at the full amplitude of the low-impedance case as well. Due to the large choice of σ_{min} required, however, this displacement is considerably restricted as compared to the nominal target motion shown by the green dotted line. Due to this limitation, a pure Cartesian implementation may be generally undesirable as compared to the joint space implementation explored throughout most of the present work. Nonetheless, it is clear from inspection of Ta-

ble 4.3 that the proposed quasi-optimal scheme succeeds in matching the x-direction displacement of the high-impedance case (which is tuned on the basis of contact considerations associated with that high-stiffness axis) and the y-direction displacement of the low-impedance case (which was tuned on the basis of contact considerations associated with that low-stiffness axis). The proposed scheme therefore succeeds again in managing the simultaneous considerations of these two axes with much less compromise than in a typical scalar-wave-impedance arrangement. Corresponding slave trajectories are shown in Fig. 4.10.

4.6 Transition

Returning to a joint space implementation, this section explores the effect of discontinuous changes in desired wave impedance associated with transition between contact and free motion (i.e., between finite and zero values of environmental stiffness $\mathbf{K}_e$). Rodriguez-Seda [68] observed in simulation that rapid or abrupt changes in wave impedance could cause undesirable (but stable) oscillations; however, this occurred under a feedback-passivized, position-transmission scheme in the manner of Chopra et al. [34]. The following simulations implement discontinous impedance changes (both low-to-high and high-to-low) to assess whether this phenomenon oc-

Table 4.3: Peak-to-peak master displacement (Pure Cartesian implementation)

|	$B = 341.4 \frac{\text{kg}}{\text{s}}$	$B = 1,000 \frac{\text{kg}}{\text{s}}$	Directional
Δx_{p-p} (m)	0.0803	0.0300	0.0299
Δy_{p-p} (m)	0.1822	0.0887	0.1822
$\Delta y_{p-p}/x_{p-p}$	2.27	2.95	6.09
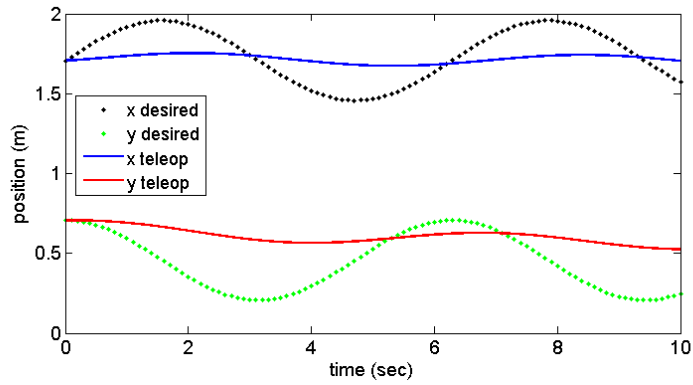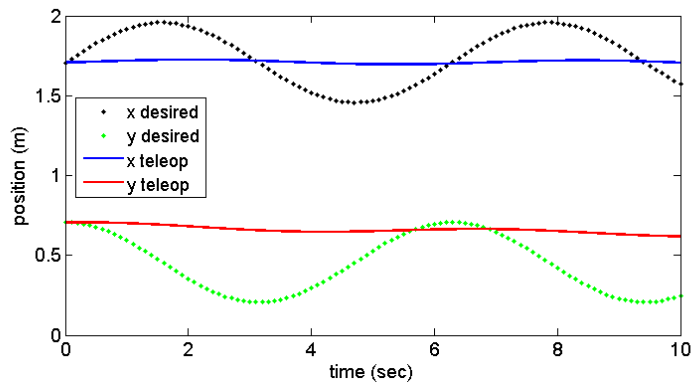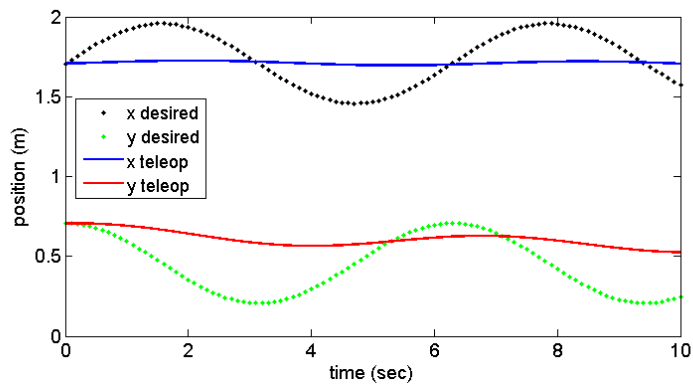
Figure 4.9: Desired and actual trajectories at the master site for a pure Cartesian implementation with (a) $B = 341.4$, (b) $B = 1,000$, and (c) the quasi-optimal result of (2.34) bounded between these same upper and lower limits.
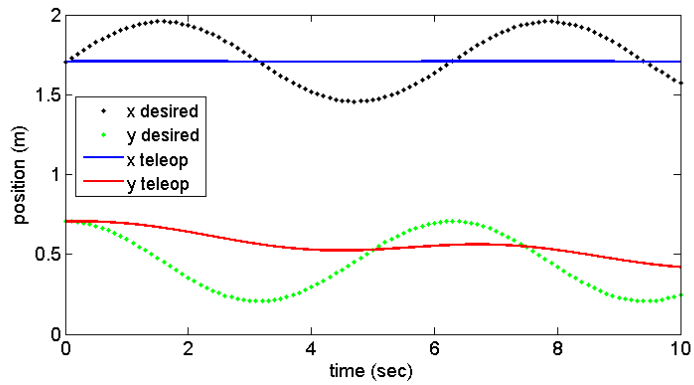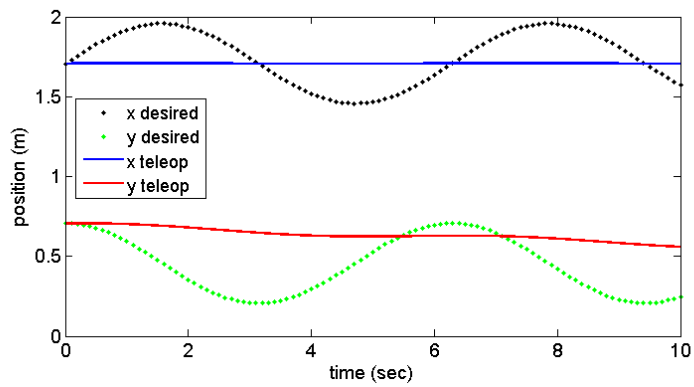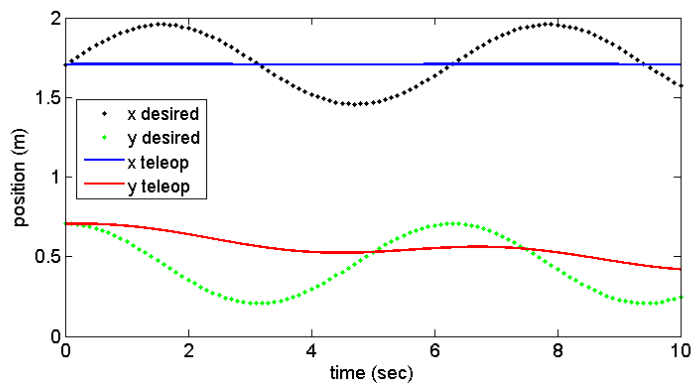
Figure 4.10: Desired and actual trajectories at the slave site for a pure Cartesian implementation with (a) $B = 341.4$, (b) $B = 1,000$, and (c) the presently proposed directional scheme bounded between these same upper and lower limits.

curs in the classical wave teleoperation scheme as well. In both of the following scenarios, the wall environment is modeled as a linear push-only spring having a stiffness of 10 kN/m in the x-direction and 0 in the y-direction. Impedance is chosen at both the master and slave sites using the value $K_{e,x} = 10$ kN/m when a contact force is experienced at the slave site, and $K_{e,x} = 0$ when no force is experienced. Information to the master regarding the contact state is delayed by the same amount as the wave signals (i.e., 0.05 seconds).

In the low-to-high transition scenario, the manipulator begins with its end-effector a distance of 10 cm (in the negative x-direction) from a stiff wall having its equilibrium point at the same location as in the preceding examples (i.e., at $x = 1.707$m). The operator pushes the master manipulator toward the wall (in the positive x-direction) with a constant force of 20N, sustaining that force even after contact occurs. Fig. 4.11 shows the resulting x-direction motion of both the master and slave, with the elements of the master's wave impedance matrix $\mathbf{B}_m \in \mathbb{R}^{2 \times 2}$ shown in Fig. 4.12. Due to the communication delay, the master's motion leads the slave's motion slightly, resulting in a slight overshoot of the wall location before the stiffness information can be relayed and further master motion thereby prevented. When contact occurs, slightly before $t = 2$ seconds, the diagonal elements of the wave impedance matrix transition from their minimal value of σ_{min} to larger values suitable for contact. No discernible oscillation is present as a result of this transition.

In the high-to-low transition scenario, the manipulators begin with a displacement of 5×10^{-4} m into the wall, in the positive x-direction. The operator pulls the master back from the wall with a constant force of 5N sustained for 1.5 seconds,

126
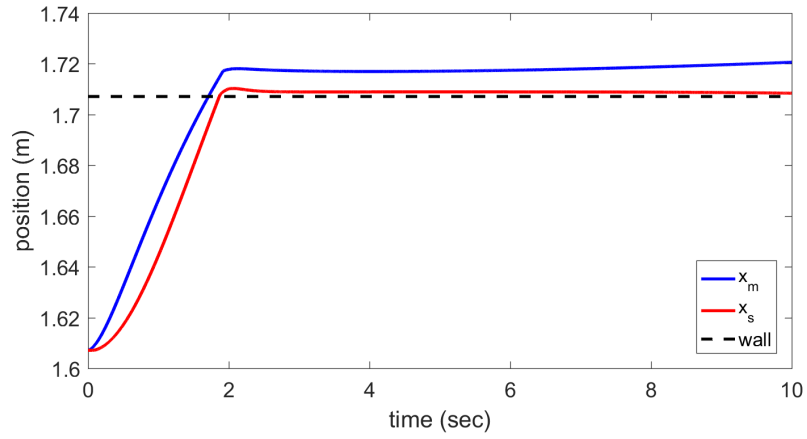
Figure 4.11: Master and slave end-effector x-coordinates during a transition from free motion to contact.
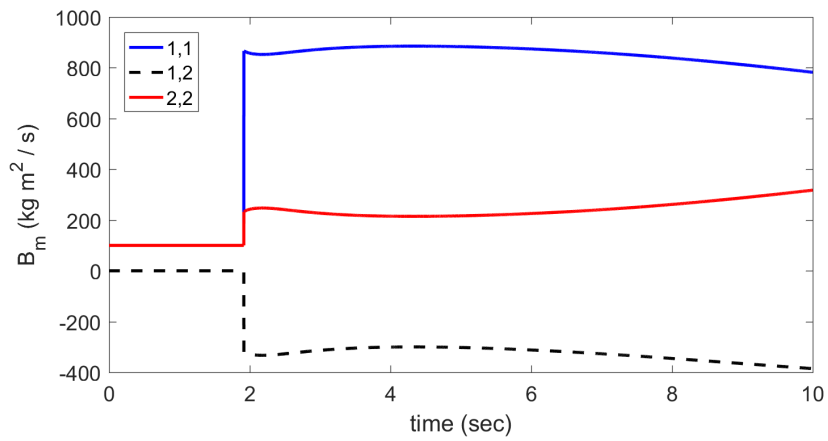
Figure 4.12: Elements of the master's wave impedance matrix (in the joint space) during a transition from free motion to contact.

after which time zero force is applied. Fig. 4.13 shows the resulting trajectories; and Fig. 4.14 shows the behavior of the elements of the wave impedance matrix at the master site. The (1,1) element of this matrix (corresponding to joint 1) transitions discontinuously from $\sigma_{max} = 1,000$ to $\sigma_{min} = 100$ without inducing discernible oscillations.

The results of these two maneuvers suggest that, in contrast to the experience of Rodríguez-Seda in the feedback passivation case, there may be no need to impose limits in the classical wave teleoperation case on the rate of change of the wave impedance. Taking no special measures beyond the impedance magnitude bounding implemented throughout this chapter, no discernible oscillations were observed. Rodríguez-Seda did not identify a theoretical cause of the oscillation observed in his feedback passivation scheme; and further consideration of this phenomenon is beyond the scope of the present study.

4.7 Repeated Transitions

Due to the tendency to accumulate substantial coordination error (See Section 3.3) during the larger impedance changes associated with transition between contact and free motion, tasks that involve repeated transitions within a short span of time present a particular challenge to any online impedance variation scheme. This section briefly explores possible solutions to this problem. First, such a task is simulated with constant scalar choices of impedance for comparison. Then, a continuously time-varying choice is implemented as above without any corrective
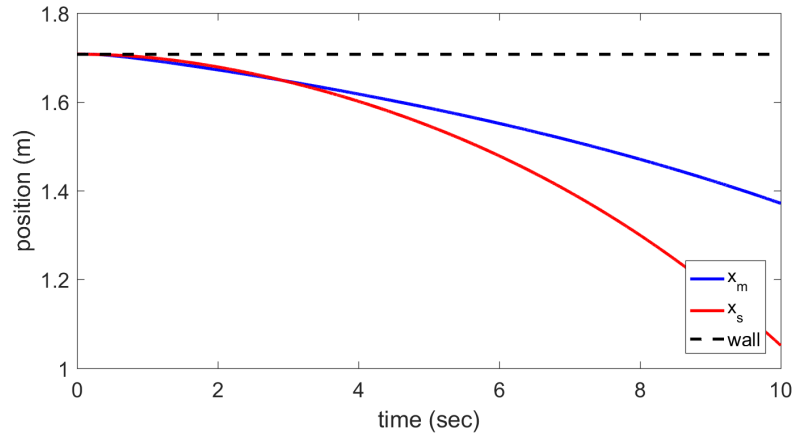
Figure 4.13: Master and slave end-effector x-coordinates during a transition from contact to free motion.
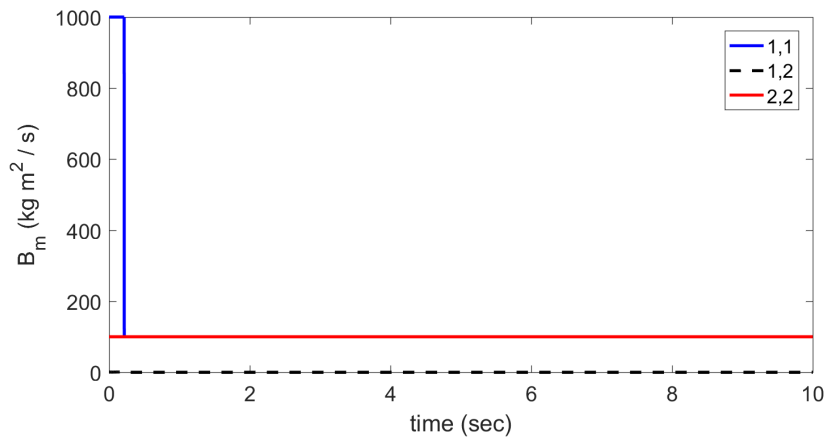
Figure 4.14: Elements of the master's wave impedance matrix (in the joint space) during a transition from contact to free motion.

scheme applied. Finally, the same time-varying scheme is implemented with an outer position loop as well as impedance rate limiting in order to explore the ability of these measures to mitigate the coordination error.

In these simulations, the manipulators begin in a pose 2 cm removed from the same 10 kN/m wall considered in the previous section. The desired trajectory consists again of a circle 50 cm in diameter (translated in the negative x-direction 2 cm as compared to Sections 4.3 - 4.5, such that the initial pose still represents the top of the circle).

4.7.1   Scalar Impedance

The scenario is simulated twice, with constant scalar imedances corresponding to $\sigma_{min} = 100$ kg $\cdot$ m^2/s and $\sigma_{max} = 1,000$ kg $\cdot$ m^2/s as above.

Fig. 4.15 shows the resulting trajectories. In the low-scalar-impedance case of Fig. 4.15a, stiffness information is not accurately transmitted to the operator and its travel into the wall appears completely unobstructed. The slave does, however, track with the master on both occasions that it pulls away from the wall. In the high impedance case of Fig. 4.15b, motion is generally more restricted. This restriction asserts itself both during travel in the +x and -x directions, however; and the slave fails to break contact the second time the master pulls away.
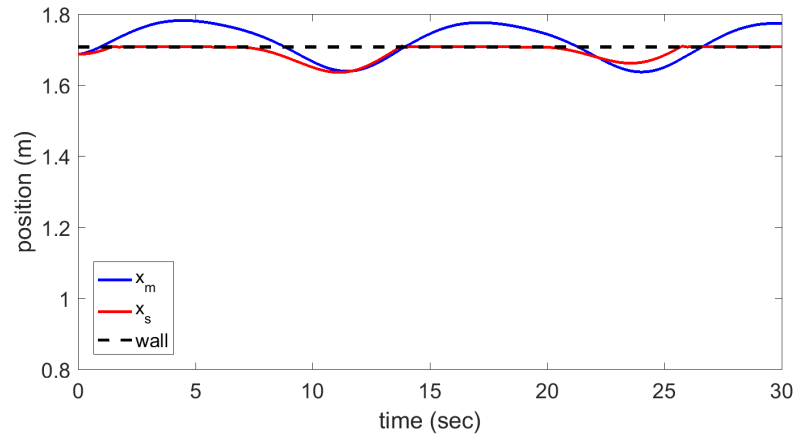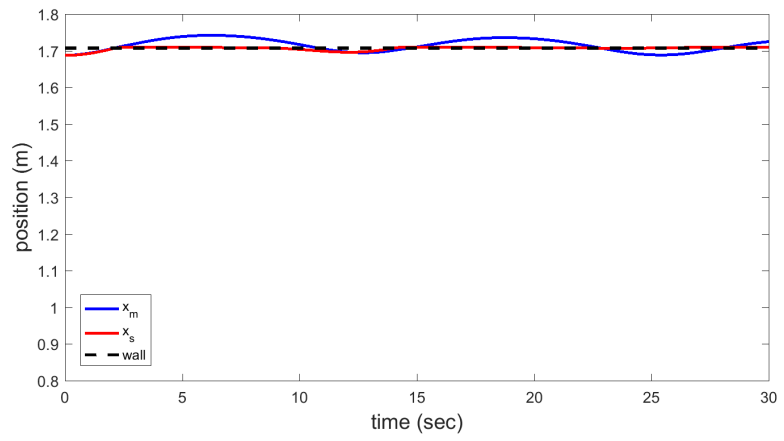
Figure 4.15: Master and slave x-coordinates during uncorrected motion relative to a stiff wall with (a) $B = 100$ and (b) $B = 1,000$.

4.7.2 The Uncorrected Scheme

In this arrangement, the slave reports to the master (with delay T) whether or not it is in contact. When in contact, each manipulator selects its wave impedance matrix on the basis of its current joint configuration. When not in contact, wave impedance becomes $\sigma_{min} = 100$ kg $\cdot$ m^2/s.

Fig. 4.16 shows the x coordinate of the master and slave manipulators when no corrective measures are employed and Fig. 4.17 shows the resulting variation in the master wave impedance. The system survives one transition into and out of contact before the coordination error becomes too large for the slave to regain contact.

4.7.3 Outer Position Loop with Impedance Rate Limit

This arrangement repeats the scenario of the previous subsection, but with impedance rate limitation as described in Subsection 3.6.2 (at 4,000 Hz with $\delta_{max} = 1.0$) and an outer position loop in the manner of Chopra et al. [33]. The outer position loop consists of the following forces, applied to the master and slave, respectively:

$$\underline{F}_{back} = K(\underline{q}_s(t-T) - \underline{q}_m(t)) \tag{4.6}$$

$$\underline{F}_{feed} = K(\underline{q}_m(t-T) - \underline{q}_s(t)) \tag{4.7}$$
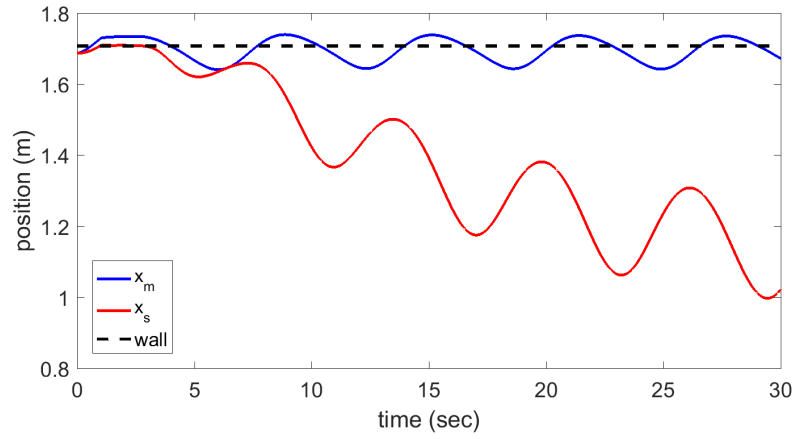
Figure 4.16: Master and slave x-coordinates during uncorrected motion relative to a stiff wall
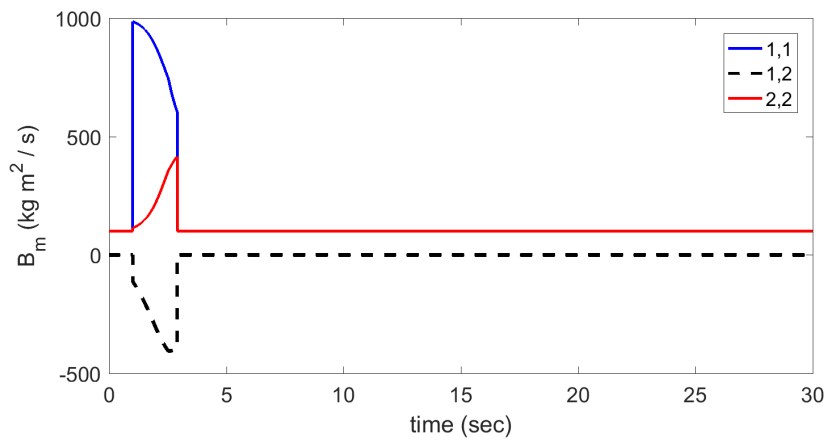
Figure 4.17: Elements of the master's joint-space impedance matrix during uncorrected motion

133

This behavior is, by itself, nonpassive and is compensated by damping $\underline{\tau} = -D\underline{\dot{q}}$ at the master and slave locations. If a certain level of joint friction of this form is known to exist naturally in the manipulators, then that may be used to satisfy the damping requirement. Otherwise, this damping must be artificially injected into the system through the addition of this term to the control laws. In the case that the master and slave have identical damping coefficients D, as is done here, the minimum dissipation level as a function of outer loop gain is KT (thus requiring knowledge of at least an upper bound on T). For the present simulation, these parameters were chosen as $D = 1.0$ and $K = 20$.

Fig. 4.18 shows the resulting motion; and Fig. 4.19 shows the master wave impedance. Master-slave coordination error is greatly reduced. There are now, however, sufficient coordinating and damping forces that the operator has considerable difficulty breaking contact with the wall. The slave does not drift increasingly away from the wall as in the uncorrected case; however, motion is generally distorted as compared to Subsection 4.7.1, with the basic sinusoidal waveform no longer clearly discernible. Of course, a smaller outer-loop gain could be used at the cost of a longer recovery time to the coordination error; and impedance changes may be scheduled to occur at appropriate discrete intervals rather than continuously.

4.8   Chapter Summary

Simulation results have been presented demonstrating that the proposed scheme does indeed result in greater mechanical impedance transmitted to the operator in
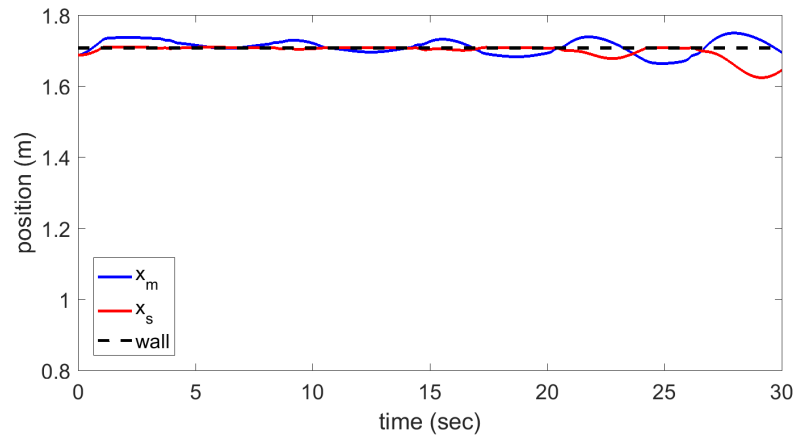
Figure 4.18: Master and slave x-coordinates during corrected motion relative to a stiff wall
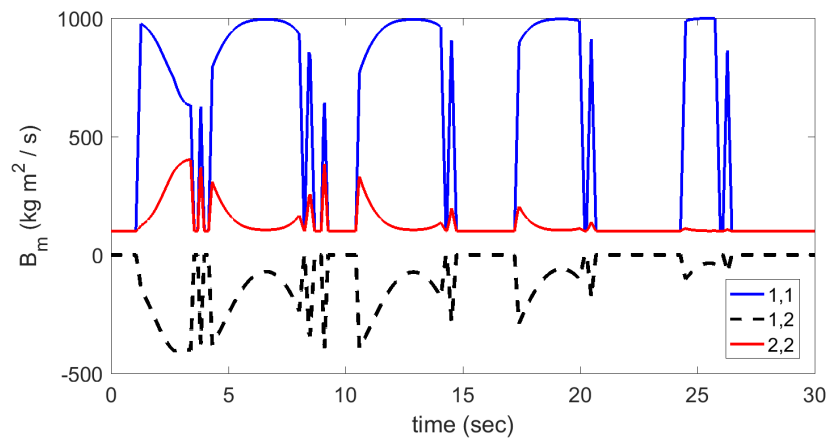
Figure 4.19: Elements of the master's joint-space wave impedance matrix during corrected motion

the chosen high-impedance direction. The discussion of Chapter 3 regarding time-varying impedance causing coordination error was confirmed. This presents a substantial challenge with regard to the applicability of such a scheme to tasks that involve repeatedly making and breaking contact—although, the wave impedance selection advice of Chapter 3 can still be used to select a constant choice of $\mathbf{B}$ that is appropriate for use in the neighborhood of a given reference pose. Table 4.4 summarizes these results.

Table 4.4: Summary of Simulation Conditions and Results

Section(s)	Conditions	Implementation Space	Results
4.2	Permanent Contact	Joint	Directional wave impedance choice affects mechanical impedance in the same directional fashion
4.3	Permanent Contact	Joint	Directional wave impedance choice affects achievable operator displacement in the same directional fashion
4.4	Permanent Contact; Redundant Manipulators	Joint	Successful handling of kinematic redundancy; Same qualitative results as 4.3 but less pronounced
4.5	Permanent Contact	Cartesian	Same qualitative results as 4.3 but less pronounced
4.6 and 4.7	Push-only Wall	Joint	Demonstrated abrupt wave impedance change; Confirmed prediction of Section 3.3 regarding coordination error

Chapter 5: Human Factors Study

5.1 Overview

Because the true test of a teleoperation scheme is its behavior under actual human operators, experimental trials were undertaken to evaluate the response of actual human subjects to the directional impedance choice of the proposed scheme.

5.2 Implementation

The SensAble Phantom Omni (now marketed as the Geomagic Touch) was used as the hardware platform for evaluation of the proposed impedance selection scheme. The Omni is a desktop device with three actuated degrees of freedom, and thus has a workspace corresponding to the three-dimensional translational Cartesian space. The API provided by the manufacturer provides access to the joint angle read by each of the three encoders and to the commanded joint torque to each of the corresponding three motors. (The stylus portion of the device is on an unactuated 3-degree-of-freedom gimbal for which coarser, potentiometer-based angle readings are available; however, stylus angles are not regarded as significant in the present study.) Communication with the Omni occurs via IEEE 1394 FireWire, and was

implemented at 1,000 Hz (the maximum rate supported by the Omni). Commanded torques were software-limited to the device's nominal values of 200 mN-m, 250 mN-m, and 200 mN-m for the first, second, and third joint, respectively.

Software access to the Omni device is provided via the OpenHaptics Toolkit, a closed-source set of software providing a C++ API. Interaction with the device is possible at three different levels of abstraction. The QuickHaptics micro API is intended for quick and easy setup of basic haptic simulations in which the user interacts with objects of geometrically simple shape and texture. The HLAPI provides more advanced access to the device while still focusing on interaction with a 3D environment simulated via their engine. The HDAPI, used in the present work, is the lowest level of access, giving the programmer the capacity to directly command the desired joint torques.

After initializing the device and starting the scheduler, system state information is available through `hdGetDoublev(HDenum pname, HDdouble *params)`. The first argument specifies the desired value (`HD_CURRENT_POSITION` for Cartesian tip position, `HD_CURRENT_JOINT_ANGLES` for the joint angles, and `HD_CURRENT_VELOCITY` for the Cartesian tip velocity); and the second argument provides a location to store that value. Unfortunately, joint rate data is not made available to the user. Joint rates were therefore estimated via finite differencing of the joint angle data.[1] A low pass filter having a 5% settling time of 19 milliseconds was used to mitigate the effect of noise.

---

[1]Because the device is kinematically nonredundant, one could instead identify the joint rate via $\underline{\dot{q}} = \mathbf{J}^{-1}\underline{\dot{x}}$ so long as the Jacobian remains well-conditioned.

Similarly, commands can be sent to the Omni device via `void hdSetDoublev( HDenum pname, const HDdouble *params)`. After enabling force output, joint torque commands are specified to set value `HD_CURRENT_JOINT_TORQUE`. Cartesian forces could be commanded in a similar way if desired, via `HD_CURRENT_FORCE`, although this capability was not required for the present application.

The simulation was implemented on a Lenovo Thinkpad T410 laptop computer with a 2.67 GHz Core i5 processor and 8 GB of RAM. This system was adequate to perform the necessary computations, including communication with the Phantom device (at 1,000 Hz), updating the master and slave impedance choices individually (at 500 Hz each), and numerically simulating the dynamic behavior of the slave (at 1,000 Hz). Manipulators having more than three degrees of freedom would naturally require greater computation than the present scenario. This experience would seem to suggest, however, that the necessary computations are within the capabilities of modern systems.

Although the Phantom Premium is well characterized [96], information in the literature regarding the Phantom Omni is somewhat sparse and stricken with occasional typographical errors, inconsistent parameter identification, and/or a faulty understanding of its internal mechanisms. Unlike the Premium, which employs a parallel-link mechanism to drive its elbow, the Omni pitch joints are cable driven. Additionally, an internal spring is used for gravity compensation. The model employed in the present work is given in Appendix C.

5.3   Experimental methodology

The Phantom Omni itself acted as the master manipulator, while a computer simulation of a second Omni device (according to the model of App. C) acted as the slave manipulator. The slave's environment consisted of a linear spring. Along an axis oriented at some angle in the horizontal plane, the stiffness was chosen to be 500 N/m. Along the two perpendicular axes, it was taken to be 1 N/m. Subjects were asked to move the tip of the Omni device radially outward and inward, from and to the spring equilibrium position, at various angles in order to identify the direction in which they perceived the greatest impedance to motion. A protractor was fixed below the workspace of the device as a reference. A gel wrist support was additionally provided, which subjects were permitted to move according to their comfort requirements. The test setup is shown in Fig 5.1. Between axis identification attempts, the simulation software pseudorandomly selected a new angle for the high-stiffness axis within the horizontal plane. Angles were chosen in ten-degree increments; and subjects were similarly instructed to identify angles to the nearest ten degrees. Subjects were given the opportunity to record written comments to the researcher during their trials.

The primary purpose of this experiment was to test two hypotheses intended to verify the basic advantages of implementing a directional impedance selection scheme (although not the specific quasi-optimization of that selection): (1) that subjects would exhibit a smaller mean absolute error in the case of the presently proposed directional scheme than in other (scalar impedance) wave-based schemes,

141

Figure 5.1: Setup of the Phantom Omni device with gel wrist support and reference protractor.

and (2) that a bias introduced by knowledge error in the impedance selection process would not completely eliminate subject perception of the true environment (i.e., that the directional choice of wave impedance serves to *reinforce*, not replace, sensation of the environment). To test the second hypothesis in particular, a test case (Configuration E, below) was introduced having faulty knowledge of the true environmental stiffness direction (in the form of a constant $+30°$ offset added to the correct value). Each subject participated in 6 sets of 20 axis identifications.

The scenarios associated with each set were as given in the list at the end of this paragraph, where task A utilizes the force reflection teleoperation scheme [10]:

$$\underline{\tau}_{mc}(t) = G_c \underline{\tau}_{sc}(t - T) \tag{5.1}$$

$$\underline{\tau}_{sc}(t) = K_c \left(\underline{q}_m(t - T) - \underline{q}_s(t) \right) \tag{5.2}$$

where G_c and K_c are controller gains. The remaining tasks are various configurations of wave-based schemes:

A. Force reflection

B. Large scalar impedance $(B = 4 \times 10^{-2} \text{ kg} \cdot \text{m/s}^2)$

C. Directional impedance selection (perfect knowledge, $\sigma_{max}/\sigma_{min} = 10$)

D. Directional impedance selection ($+30°$ bias error, $\sigma_{max}/\sigma_{min} = 10$)

E. Directional impedance selection ($+30°$ bias error, $\sigma_{max}/\sigma_{min} = 2$)

F. Small scalar impedance $(B = 4 \times 10^{-3} \text{ kg} \cdot \text{m/s}^2)$

All subjects performed tasks A, B, C, and D. Each subject performed only one of tasks E (4 subjects) and F (5 subjects). Configuration A was used as a baseline for comparison; and all subjects performed under Configuration A for their initial and final (sixth) tasks in order to help identify any changes in performance due to fatigue or learning. Tasks 2 through 5 were assigned from the wave-based configurations (Configurations B through F) in pseudorandom order with two exceptions: (1) Task F was constrained to not be the subject's first wave-based teleoperation scheme (because stiffness perception was expected to be quite poor), and (2) the knowledge error cases (Configuration D and E) were constrained to not occur before the perfect-knowledge case (Configuration C). These constraints were implemented to avoid unreasonably biasing subject familiarization with both wave-based teleoperation in general and the proposed directional approach specifically. Table 5.1 shows the ordering of tasks for each of the nine participants. Participants are identified

here via a pseudorandomly-assigned three-digit code that is not indicative of the order in which they participated. In the directional-impedance operating scenarios (Configurations C, D, and E), σ_{min} and σ_{max} were taken to be the same values used in the scalar-impedance scenarios—namely, 4×10^{-3} and 4×10^{-2} kg $\cdot$ m^2/s, respectively, in order to facilitate direct comparison. Similarly, because the force reflection scheme of Configuration A is not intrinsically stable in the presence of communication latency, all trials were performed with only 1 millisecond of latency. This test is therefore primarily an exploration of the effect of directional gain choice.

For the initial portion of each subject's first set of tasks (always Task A: Force Reflection), after the subject indicated the perceived high-impedance direction, the true environmental high-stiffness direction was revealed to the subject in order to ensure adequate familiarization with the task. The true direction was not known to either the subject or the researcher until after the subject's response was recorded. This familiarization portion consisted of the first 10 or 11 trials (depending on subject-indicated readiness to proceed) of Task #1.

Table 5.1: Sequence of tasks for each participant

Participant	Task #1	Task #2	Task #3	Task #4	Task #5	Task #6
157	A	C	D	B	F	A
329	A	C	B	E	D	A
386	A	B	F	C	D	A
450	A	B	C	D	E	A
688	A	B	C	F	D	A
733	A	C	F	B	D	A
812	A	C	E	B	D	A
918	A	C	E	D	B	A
925	A	B	C	D	E	A

In all wave-based scenarios, the integral gain $\mathbf{K}_\mathrm{I}$ was taken to be the identity matrix, the proportional gain $\mathbf{K}_\mathrm{p}$ was equal to $\mathbf{B}$ to avoid wave reflections, and the reference stiffness k_{ref} was 100 N/m. In the Force Reflection case of Task A, controller proportional gains were $G_c = K_c = 1$. No corrective measures were taken for the accumulation of master-slave coordination error during an axis identification trial. The slave state was, however, reset to correspond to the master state at the start of each new axis identification attempt.

Nine subjects participated in total (8 males and 1 female with a median age of 22 years, all of whom were right-handed).

This study was conducted under approval issued August 31, 2015, by the Institutional Review Board of the University of Maryland, College Park.

5.4   Results and Discussion

Subject estimation error was calculated as the shortest angle between the actual and subject-reported directions. Analysis of Variance (ANOVA) was performed to assess the effects on subject error (the output) of three input variables: the cumulative number of axis identifications performed by the subject across all tasks up to that time (X1), the identity of the subject performing the task (X2), and the configuration schemes A-F (X3). X2 and X3 were treated as categorical variables. X1 (introduced to assess subject learning/fatigue effects) was treated as a continuous variable. Two separate ANOVA were performed: one with absolute error (an unsigned quantity) as the output variable and one with the (signed) error as the

output variable, thus facilitating assessment of both the magnitude of axis identification errors and any overall bias in the subject answers. In the ensuing discussion, $\alpha = 0.05$ is used as the threshold for statistical significance.

Table 5.2 shows the results for the first case, in which absolute error is treated as the output variable. Of primary interest is the rightmost column, indicating that subject identity (X2) and control scheme (X3) were statistically significant variables in the present trials whereas task count (X1) was not. That the p value associated with X1 is so large suggests that neither learning nor fatigue effects likely contributed substantially to overall subject task performance. Figure 5.2 shows the 95% confidence intervals associated with mean absolute error for the different control schemes considered (X3). The ideal tuning (Configuration C) of the proposed directional-impedance scheme yielded performance comparable to the Force Reflection baseline (Configuration A), with an overall mean absolute error that was statistically significantly lower than with the scalar choices of wave impedence (Configurations B and F). This demonstrates clearly that the proposed technique successfully implements a choice of impedance that is directional in a Cartesian sense, focusing its effects in the desired Cartesian direction. The introduction of knowledge error in Configurations D and E drove subjects to larger absolute errors; however, subject performance remained better than in the traditional scalar impedance cases (although this difference fell well short of statistical significance).

Of greatest interest in the knowledge-error scenarios is the extent to which subjects were biased in the erroneous $+30°$ direction. Positive values indicate a clockwise overestimate by the subject. Table 5.3 shows the results of this second

Table 5.2: ANOVA #1: Absolute error

| Source	Sum Sq.	d.f.	Singular?	Mean Sq.	F	Prob>F
X1 = Count	7.2188	1	0	7.219	0.0198	0.8882
X2 = Subj ID	13,749	8	0	1,719	4.706	1.13×10^{-5}
X3 = Scheme	47,865	5	0	9,573	26.21	6.97×10^{-25}
Error	352,419	965	0	365.2		
Total	417,520	979	0			
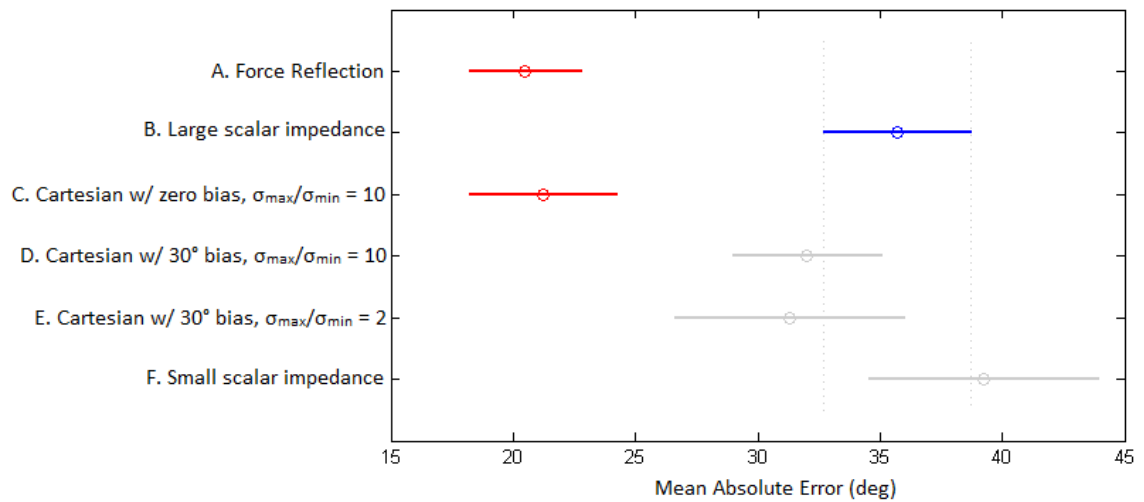
Figure 5.2: ANOVA #1: 95% confidence intervals for mean absolute error

ANOVA, in which signed error is treated as the output variable. Again, subject identity and control scheme were highly statistically significant variables while task count was not. Figure 5.3 shows the 95% confidence intervals associated with mean signed error for the different control schemes considered. Although the highly directionally tuned implementation of the proposed Cartesian scheme in the knowledge-error case (Configuration D) showed a strong subject bias toward the error direction, the less strongly tuned implementation (Configuration E) showed a clear and statistically significant reduction in the tendency toward that erroneous direction. This demonstrates that although a faulty choice of impedance directionality can certainly skew subject perception of the environment, perception of true environmental characteristics is far from completely destroyed.

Performance data for Subject 329, who had the median overall performance across those scenarios encountered by all subjects, are shown in Figs. 5.4 and 5.5. Consistent with the performance of the other subjects, all six of these plots exhibit a negative trend. Overall, subjects appeared to exhibit a bias toward the $+90°$ direction and toward positive (clockwise) offsets to the true angle. The former bias could be due to biases in the movement and force discriminating capabilities of

Table 5.3: ANOVA #2: Signed error

| Source	Sum Sq.	d.f.	Singular?	Mean Sq.	F	Prob>F
X1 = Count	357.9	1	0	357.9	0.3709	0.5427
X2 = Subj ID	28,050	8	0	3,506	3.633	3.54×10^{-4}
X3 = Scheme	100,667	5	0	20,133	20.86	7.75×10^{-20}
Error	931,197	965	0	965.0		
Total	1,061,095	979	0			
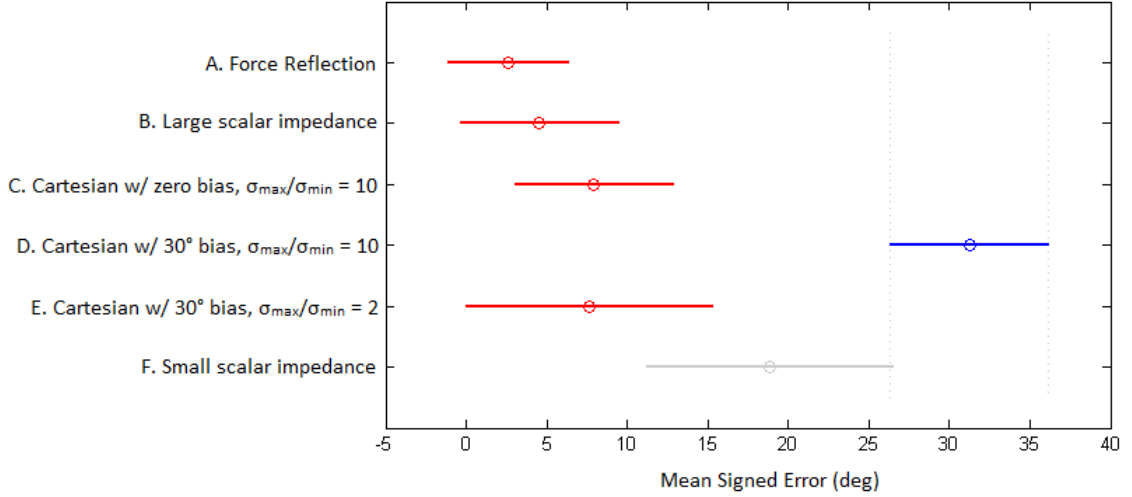
Figure 5.3: ANOVA #2: 95% confidence intervals for mean signed error

the human arm and/or to greater engagement of drive dynamics associated with the Omni's pitch joints. The latter bias may be attributable to biases associated with the right-handedness of the participants. Three subjects remarked in their comments that the task was more difficult when forces lay near the 0°/180° lateral direction. A fourth subject remarked that the system felt "lighter" in the vicinity of 90°.

Stiffness perception was quite lacking in the wave-based teleoperation schemes implemented here. Due to apparent limitations of the Omni device[2], the chosen wave impedance values were quite low across all test cases. Two subjects remarked in their comments that their Force Reflection task exhibited a greater restorative

---

[2]A pure joint-space implementation of damping $\underline{\tau} = -b\underline{\dot{q}}$, in the absence of any teleoperation scenario or wave transform, was found to induce substantial oscillations. These oscillations were clearly discernable for $b = 0.05 \frac{\text{kg}\cdot\text{m}^2}{\text{s}}$ and quite substantial for $b = 0.10 \frac{\text{kg}\cdot\text{m}^2}{\text{s}}$, especially in the cable-driven pitch joints (consistent with the observation of Tanner and Niemeyer [86] that oscillation in the cables becomes a nonpassive phenomenon when other components of the system introduce a phase lag). This suggests effects due to the dynamics of the Omni's sensor/actuator loop.

A: Force Reflection (first trial)
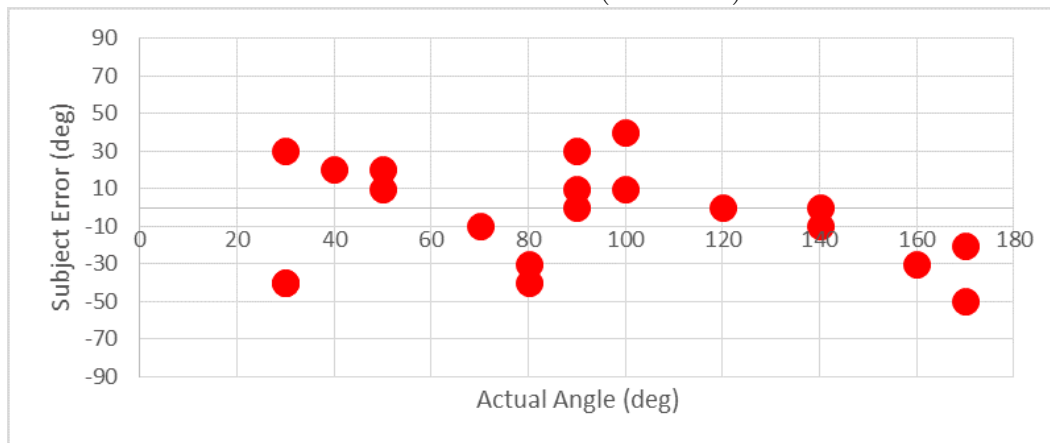
C: Directional (zero knowledge error)
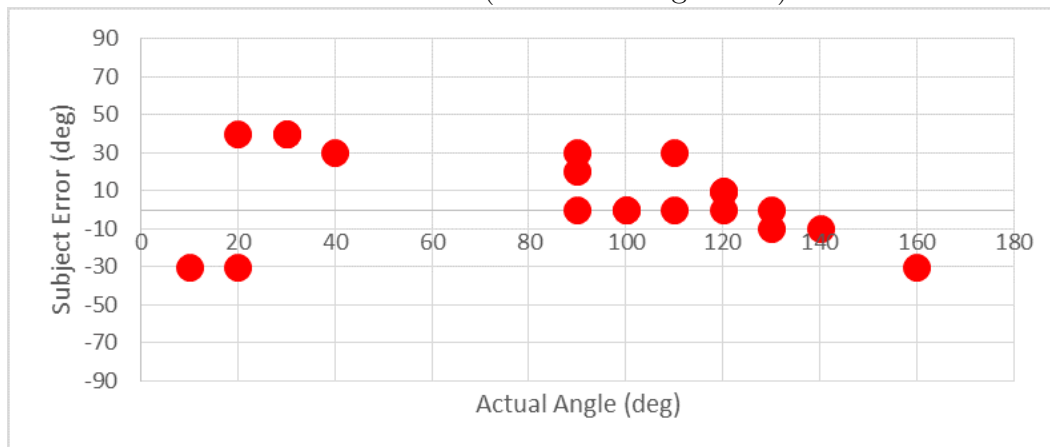
B: Large scalar impedance
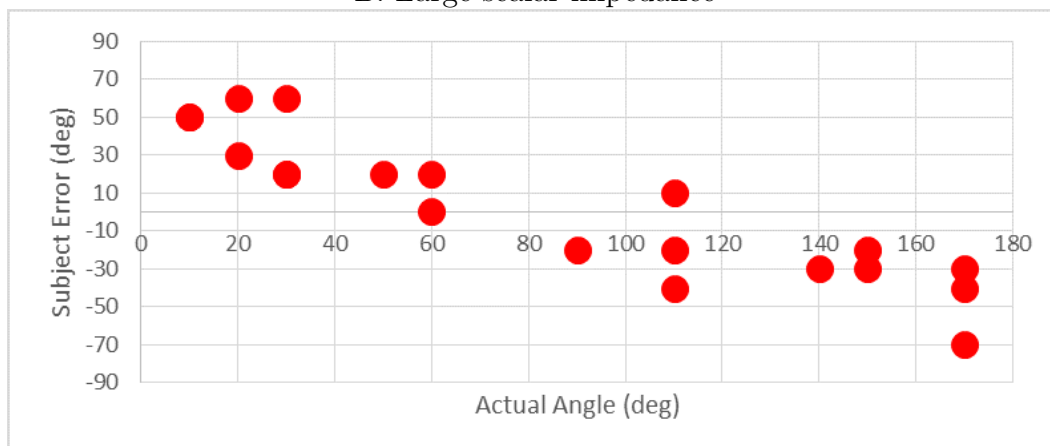
Figure 5.4: Estimation error of Subject 329 in the first three trials

150

E: Directional (30° knowledge error, $\sigma_{min}/\sigma_{max} = 2$)
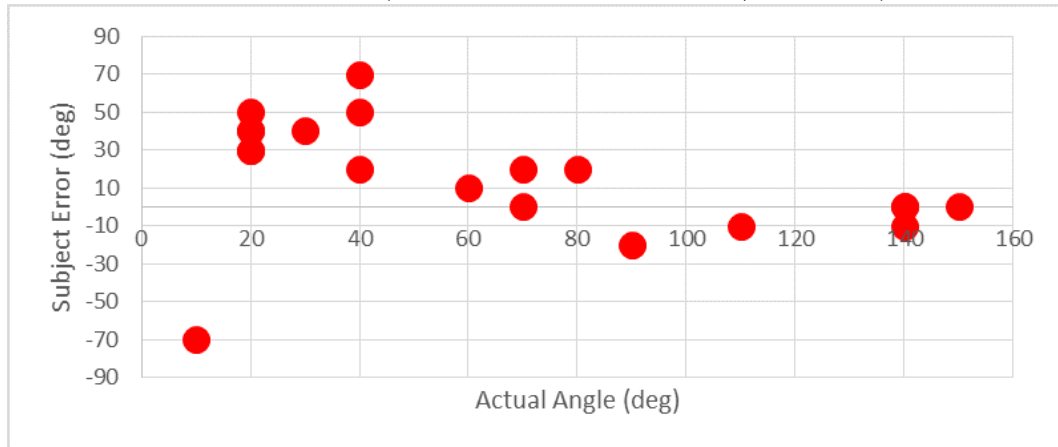
D: Directional (30° knowledge error, $\sigma_{min}/\sigma_{max} = 10$)
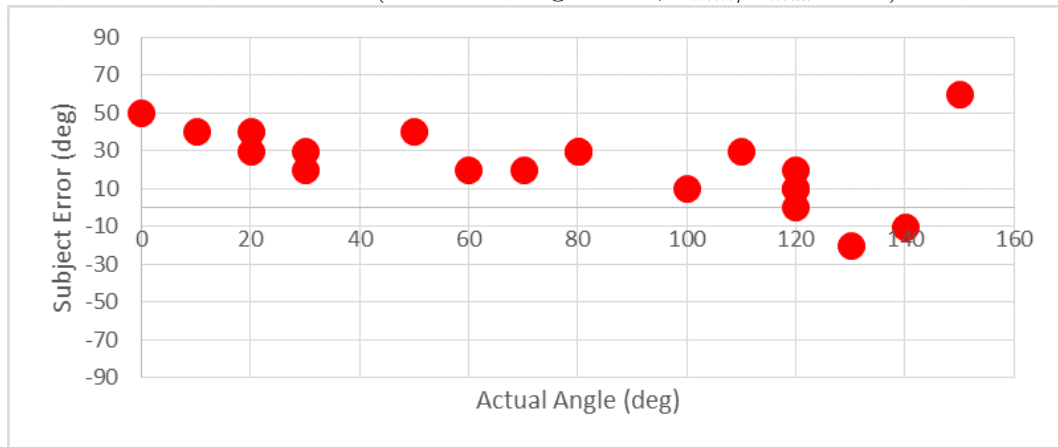
A: Force Reflection (final trial)
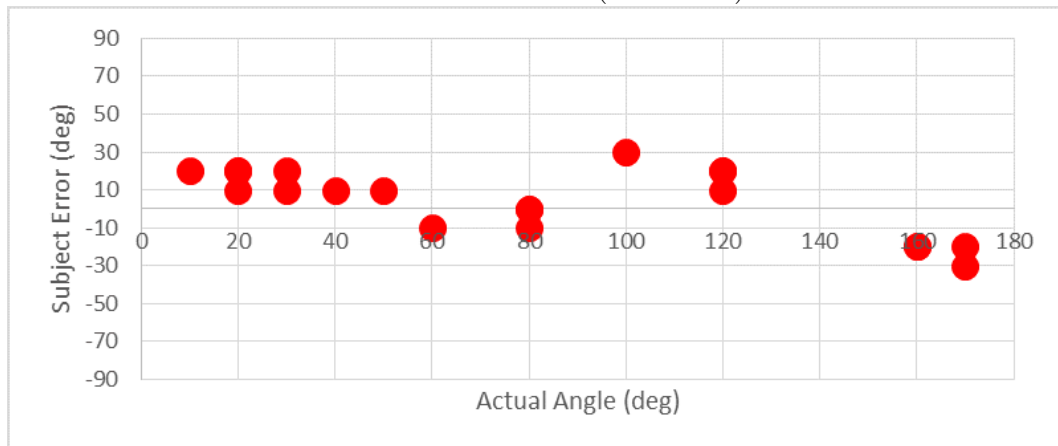
Figure 5.5: Estimation error of Subject 329 in the last three trials

force as compared to other tasks. Another subject commented with respect to one of the wave-based schemes that resistance felt "viscous" rather than "springy." This result is not unlike the experience of Lawn and Hannaford [57] at greater time delay, although those authors were able to achieve adequate stiffness perception at low time delays.

5.5   Chapter Summary

Experimental results have been presented demonstrating that subject ability to discriminate between free and contact directions is greatly improved by the proposed directional impedance selection scheme. Results also show that although bias can be introduced if (due to faulty knowledge of the environment) the high impedance direction does not align with the contact axis, this bias can be mitigated through parameter choice appropriate to the accuracy of environmental knowledge available.

Chapter 6: Adaptation

6.1 Overview

The performance degradation seen in the previous chapter in the presence of uncertainty in the environmental model points to a substantial hurdle to the usefulness of the proposed scheme. Teleoperation is generally motivated precisely when outright automation is not possible because the environment and/or task have not been modeled to a high degree of accuracy. For this reason, it is highly desirable to have an impedance selection scheme that does not require a priori knowledge of the environment. It is assumed for the purposes of this chapter that a force-torque sensor is available at the slave's end-effector in order to measure contact forces. Possible extensions in which, for example, contact forces might be estimated from joint torques are left for future work.

One could, of course, employ an environmental stiffness observer and use the resulting estimated stiffness matrix in the quasi-optimal result (2.34) employed in previous chapters. Erickson et al. [97] compare four schemes for doing so, including the use of linear regression as has been employed in many other areas of adaptive robot control. They find that linear regression is a viable approach, but only if the equilibrium position of the spring is known. In general, however, contact cannot be

expected to behave according to the linear spring model employed in that work; and excessive reliance on such a model may impair performance when the environment behaves in a nonlinear fashion.

Rodríguez-Seda [68] instead takes a simpler approach. When a given degree of freedom (treated in joint space) experiences a contact force, the wave impedance corresponding to that degree of freedom is gradually increased (at a designer-chosen rate) until it reaches some designer-chosen upper limit. Similarly, if contact force is not detected on a given degree of freedom, its wave impedance will decrease at the chosen rate until it reaches the chosen lower limit. Under such a system, however, even the smallest of contact forces on a given joint will (if persistent) eventually increase the wave impedance to its largest allowed value. This obviously poses a problem for joints that are nearly but not fully parallel to the motion constraint. The present work adopts a strategy that is similar to this scheme inasmuch as it relies on contact forces without attempting to estimate $\mathbf{K}_e$ explicitly, but differs in that it endeavors to increase wave impedance only along the axis of contact.

6.2   Adaptation Law

Consider the quantity $\mathbf{F}$ representing a filtered matrix transformation of the measured contact force $\underline{F}$ and updated (from time t_i to time t_{i+1}) according to the

following law:

$$
\mathbf{F}_{i+1} =
\begin{cases}
(1 - \gamma)\,\mathbf{F}_i & ||\underline{F}_{i+1}|| < F_{min} \\[2ex]
(1 - \gamma)\,\mathbf{F}_i + \frac{\gamma}{||\underline{F}_{i+1}||}\underline{F}_{i+1}\underline{F}_{i+1}^{T} & ||\underline{F}_{i+1}|| \geq F_{min}
\end{cases}
\tag{6.1}
$$

where $0 < \gamma < 1$ is a tuning parameter used to achieve a desired settling time (where smaller values represent a slower filter) and F_{min} is a force (larger than the noise floor of the force/torque sensor) below which force readings are neglected. In principle, the above law may be applied in either the Cartesian or joint space. Under ordinary circumstances, however, one might expect contact forces to remain more nearly constant in the Cartesian space, thus motivating use of (6.1) in that space. The vector norm in the denominator of (6.1) ensures that $\mathbf{F}$ behaves linearly (rather than quadratically) in the contact force. This matrix quantity (6.1) would in most cases be interpreted in the Cartesian space as $\mathbf{F}_{\text{cart}}$ and converted to joint space in the same manner (3.83) as was used for wave impedance:

$$
\mathbf{F}_{\text{joint}} = \mathbf{J}^{T}\mathbf{F}_{\text{cart}}\mathbf{J}
\tag{6.2}
$$

The remainder of this section adopts this interpretation notationally, although direct implementation in the Cartesian space is certainly possible.

The Singular Value Decomposition (SVD) of this matrix is considered:

$$
\mathbf{F} = \mathbf{U}\mathbf{\Sigma}_{\mathrm{F}}\mathbf{U}^{\mathrm{T}}
\tag{6.3}
$$

This may be interpreted in either the joint space or the Cartesian space, depending upon implementation. If one requires only to distinguish in a binary fashion between contact and free motion, one can specify a threshold filtered torque N_{thresh} above which magnitude the teleoperator will switch to high impedance σ_{max} and below which it will switch to low impedance σ_{min}. Defining $\mathbf{\Sigma}_{\mathrm{B}}$ to be the diagonal matrix of singular values of the wave impedance matrix, one populates it according to:

$$\Sigma_{B,j} = \begin{cases} \sigma_{min} & \Sigma_{F,j} < N_{thresh} \\[2mm] \sigma_{max} & \Sigma_{F,j} \geq N_{thresh} \end{cases} \tag{6.4}$$

The wave impedance choice is then constructed using the same orthogonal matrix $\mathbf{U}$ from (6.3):

$$\mathbf{B} = \mathbf{U}\mathbf{\Sigma}_{\mathrm{B}}\mathbf{U}^{\mathrm{T}} \tag{6.5}$$

If handling of intermediate levels of stiffness is required, one might instead choose to employ a wave impedance matrix that is proportional to $\mathbf{F}$ via some chosen positive scaling factor. Such an approach will, however, be sensitive to the variations in contact force experienced during the course of a typical manipulation task; and the use of a stiffness observer may be warranted in such scenarios.

The information encoded in the matrix $\mathbf{F}$ is measured at the slave site and thus necessarily transmitted with delay to the master. Because environmental contact would ordinarily be expected to behave in a Cartesian fashion, one would probably choose to transmit $\mathbf{F}_{\mathrm{cart}}$ (since it might remain more nearly constant) and to let the master and slave each transform this matrix separately on the basis of their own

respective Jacobians.

As previously, the wave impedance choice may be updated either discretely or continuously. A continuous update will, as described in Section 3.3, tend to induce master-slave coordination error that can be mitigated (but not completely eliminated) through existing techniques from the literature [33] [36]. This issue may be avoided through nonpassive discrete updates in the manner of Tanner and Niemeyer [67]. In such a scenario, **F** would typically still be updated continuously in order to keep track of contact behavior, but the choice of **B** would be updated at discrete times subject to the constraints described in [67]. The system might be configured to automatically update as often as is allowable within that constraint, or to update at scheduled times (either dictated in advance or determined by the operator) as appropriate to the given task.

6.3 Simulation

The following simulations employ the same 2-DOF planar elbow manipulator model used in Chapter 4. As in that chapter, two contact scenarios are considered— permanent contact with a spring capable of both pushing and pulling, and intermittent contact with a push-only wall. In both scenarios, the stiffness in the x-direction is 10 kN/m and (in contrast to the permanent contact scenario of Chapter 4[1]) the y-direction stiffness is zero. Again, $\sigma_{max} = 1,000 \mathrm{kg} \cdot \mathrm{m}^2/\mathrm{s}$, $\sigma_{min} = 100 \mathrm{kg} \cdot \mathrm{m}^2/\mathrm{s}$,

---

[1]This modification is necessary because the present scheme does not allow for intermediate-stiffness contact axes, although the choice of N_{thresh} does provide some capacity to reject low-stiffness information.

and $\mathbf{K}_I$ is taken to be the diagonal matrix corresponding to one-fifth of the diagonal elements of the corresponding wave impedance. Adaptation is performed with learning coefficient $\gamma = 0.001$ (at a rate of 4,000 Hz), $N_{thresh} = 1 \text{ N} \cdot \text{m}$, and $F_{min} = 0.5 \text{ N}$. To avoid excessive fluctuations in the wave impedance (especially in the permanent contact scenario, which employs a cyclical trajectory), the maximum change in impedance from one update to the next (also occuring at 4,000 Hz) is constrained in the manner of Subsection 3.6.2 to $\delta_{max} = 0.5 \text{ kg} \cdot \text{m}^2/\text{s}$.

6.3.1 Permanent Contact

As in the permanent contact scenario of Chapter 4, an operator modeled as a PD controller with gains $K_p = K_d = 50$ tracks the same 50-cm circular trajectory employed therein. Performance of the proposed adaptive scheme is compared against constant scalar choices of σ_{min} and σ_{max}. Fig. 6.1 shows the position of the master manipulator during the course of this maneuver for those three impedance choices. Table 6.1 summarizes the peak-to-peak master displacement in the x- and y-directions, discarding data from the first 5 seconds of simulation in order to assess the steady-state behavior. As in the non-adaptive directional case of Chapter 4, the adaptive directional scheme successfully transmits more impediment to motion to the operator in the x-direction than the high-impedance case, while permitting motion in the y-direction much more successfully (in this case, making up for 68% of the decrease in displacement amplitude of the high-impedance case as compared to the low-impedance case).
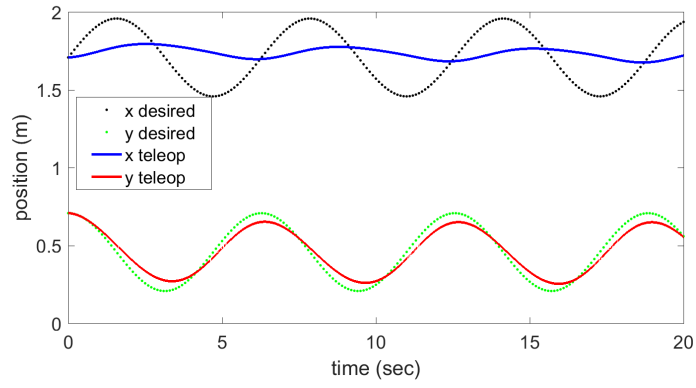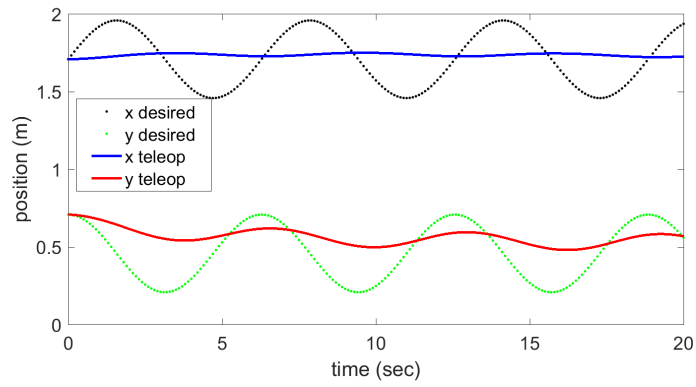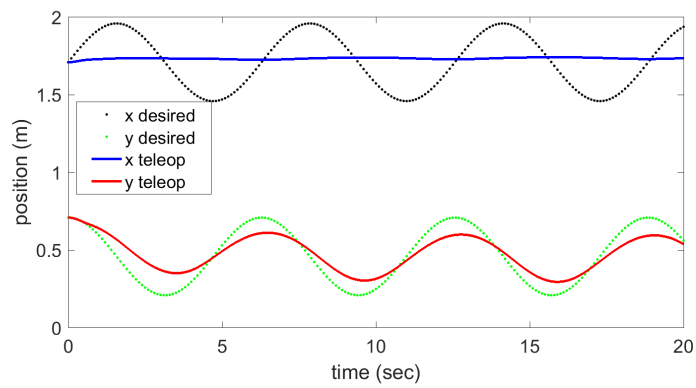
Figure 6.1: Position of the master manipulator during a permanent-contact manuever with (a) $B = 100$, (b) $B = 1,000$, and (c) the presently proposed adaptive scheme.
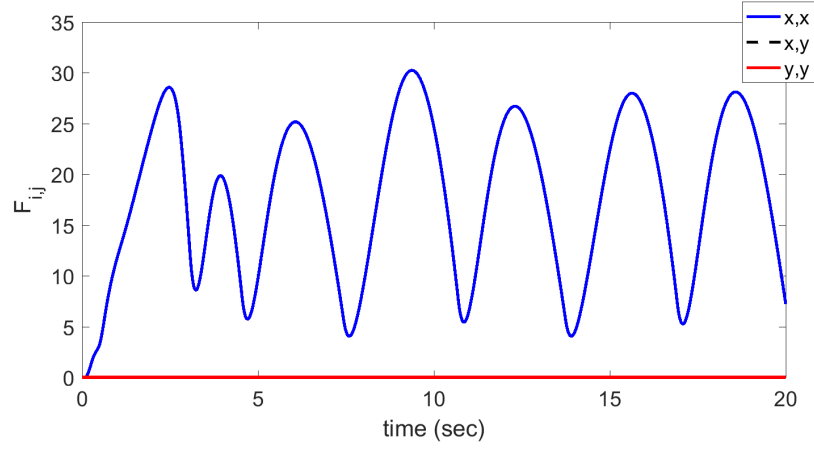
(a)
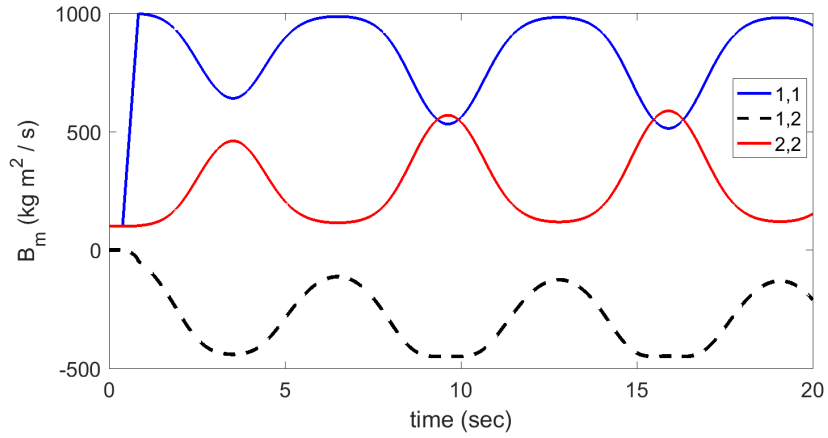
(b)

Figure 6.2: (a) Elements of $\mathbf{F}$ and (b) master wave impedance in the permanent contact scenario.

Table 6.1: Peak-to-peak master displacement during permanent-contact maneuver

	$B = 100 \ \frac{\text{kg} \cdot \text{m}^2}{\text{s}}$	$B = 1,000 \ \frac{\text{kg} \cdot \text{m}^2}{\text{s}}$	Adaptive
Δx_{p-p} (m)	0.100	0.029	0.016
Δy_{p-p} (m)	0.399	0.139	0.316

6.3.2 Transition

Low-to-high and high-to-low impedance choices are simulated under the same conditions as in Section 4.6.

6.3.2.1 Low to High

Fig. 6.3 shows the positions of the master and slave manipulators during and after the approach and contact to the wall, with contact occurring at approximately $t = 2$ seconds. As before, the operator applies a constant force of 20 Newtons throughout the simulation. There is again a delay before the increased impedance is successfully transmitted to the operator, allowing the master to penetrate approximately 2.1 cm beyond the wall location. Fig. 6.4 shows the variation in the master wave impedance during this time, ramping up to high values within half a second of contact.

6.3.2.2 High to Low

In the high-to-low impedance transition (withdrawing from the wall), $\mathbf{F}$ was initialized to the value obtained at the end of the preceding low-to-high simulation:

$$\mathbf{F}(t = 0) = \begin{pmatrix} 19.88 & 0 \\ 0 & 0 \end{pmatrix} \text{N} \tag{6.6}$$

As previously, the operator applies a force of 5 Newtons in the negative x-direction for the first 1.5 seconds of simulation.
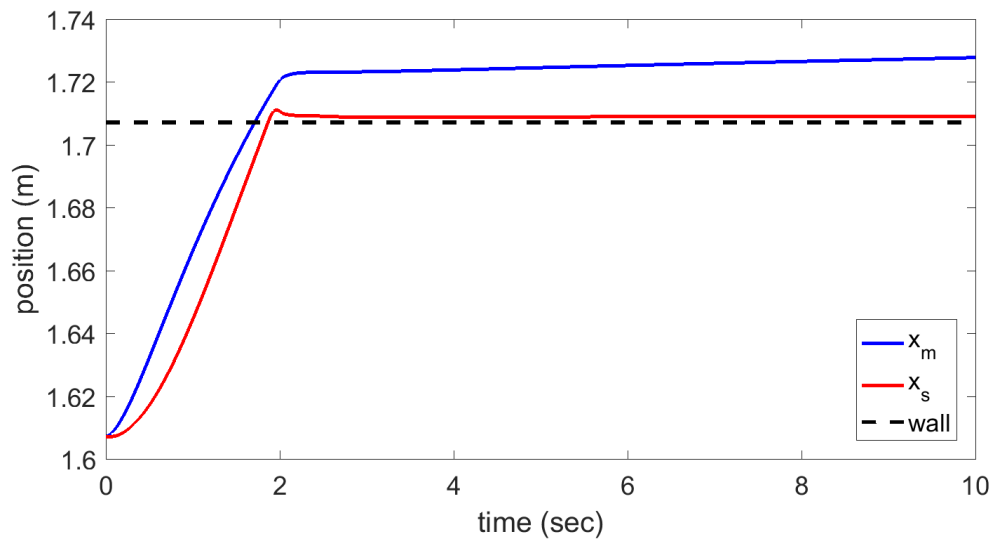
Figure 6.3: x-coordinate of the master and slave manipulators during a low-to-high impedance transition

Fig. 6.5 shows the x positions of the master and slave manipulators; and Fig. 6.6 shows the variation in the elements of the master wave impedance matrix. The system successfully ramps down from its maximal wave impedance values upon withdrawal from contact.

6.4   Chapter Summary

A scheme has been presented for choosing the wave impedance in real time when an environmental model is not available a priori. As with prior work, it resorts to a binary treatment of either a free or contact state along a given axis. In contrast to prior work, however, these axes are treated in the Cartesian space. This avoids excessive wave impedance on joint axes that are nearly but not quite parallel to the motion constraint. While not as effective as the ideal (perfect environmental
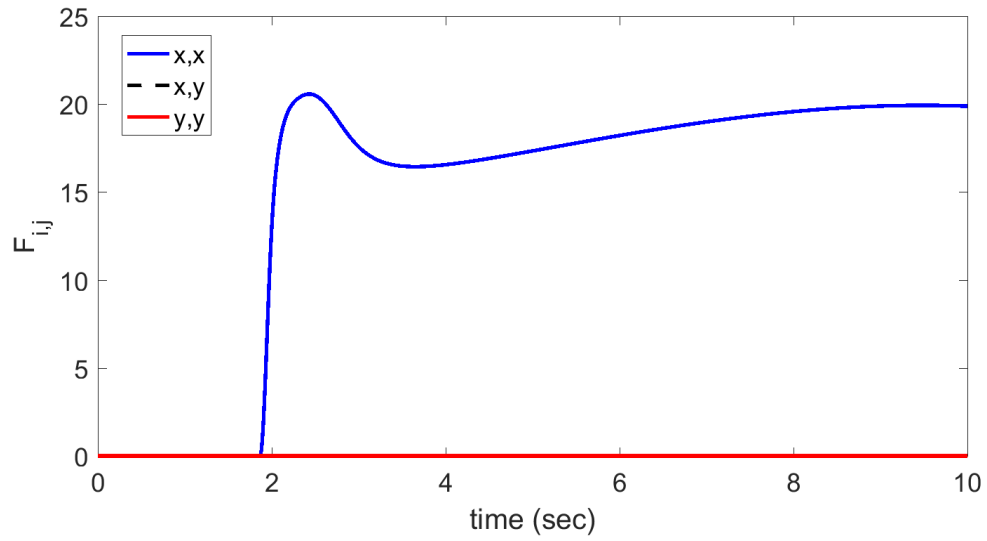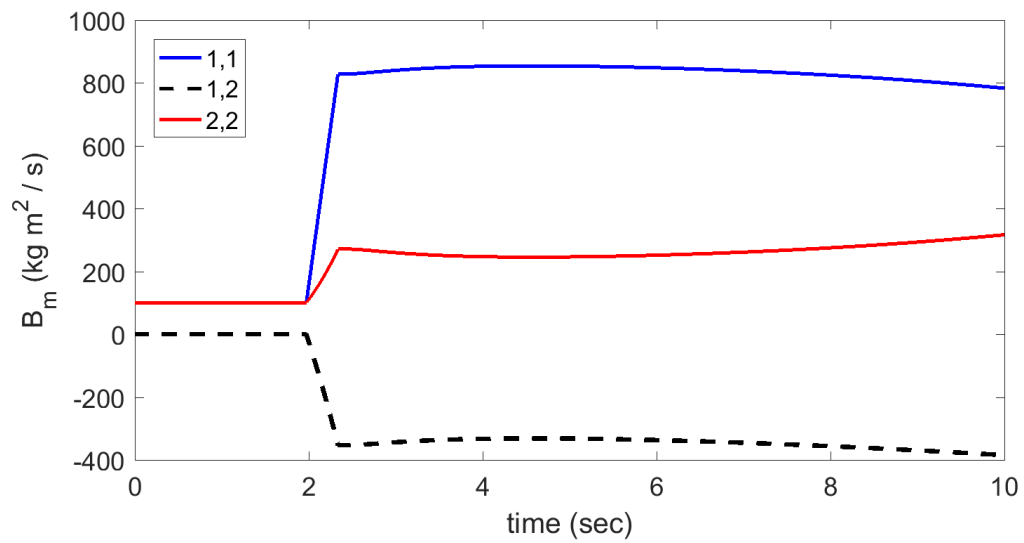
Figure 6.4: (a) Elements of **F** and (b) master wave impedance during a low-to-high impedance transition
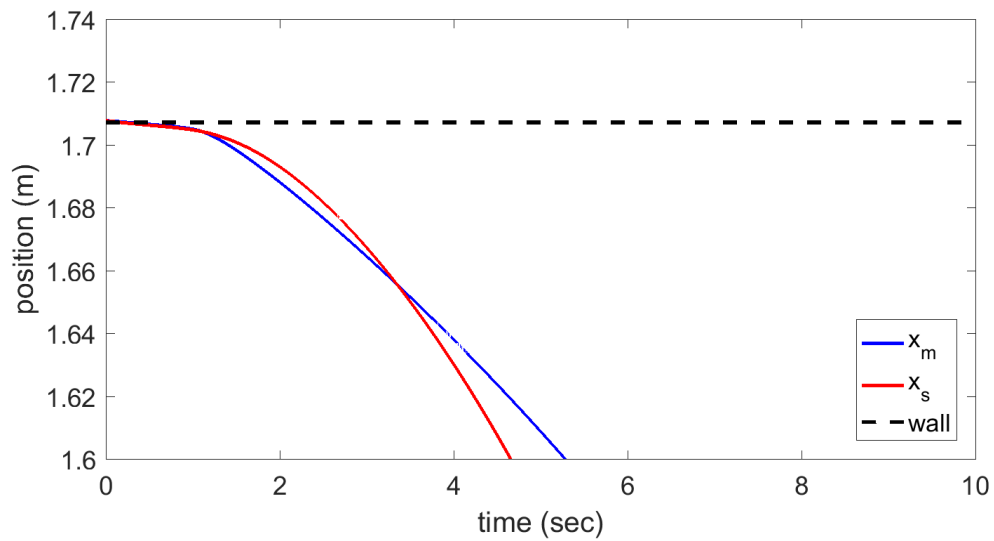
Figure 6.5: X-coordinate of the master and slave manipulators during a high-to-low impedance transition

knowledge) scenarios of Chapter 4, a substantive improvement in environmental stiffness transparency is obtained without requiring any knowledge of the remote environment.
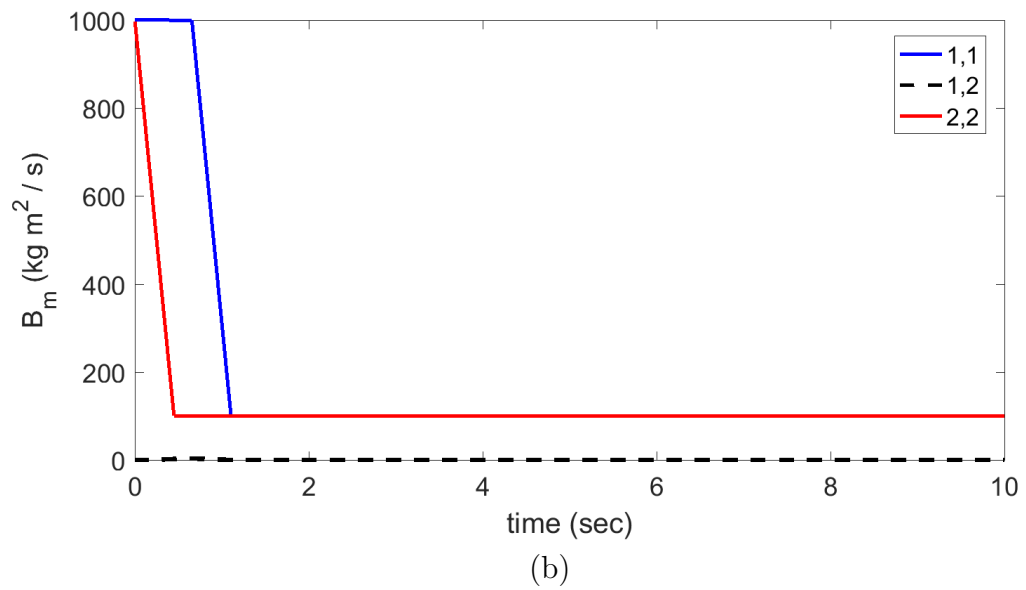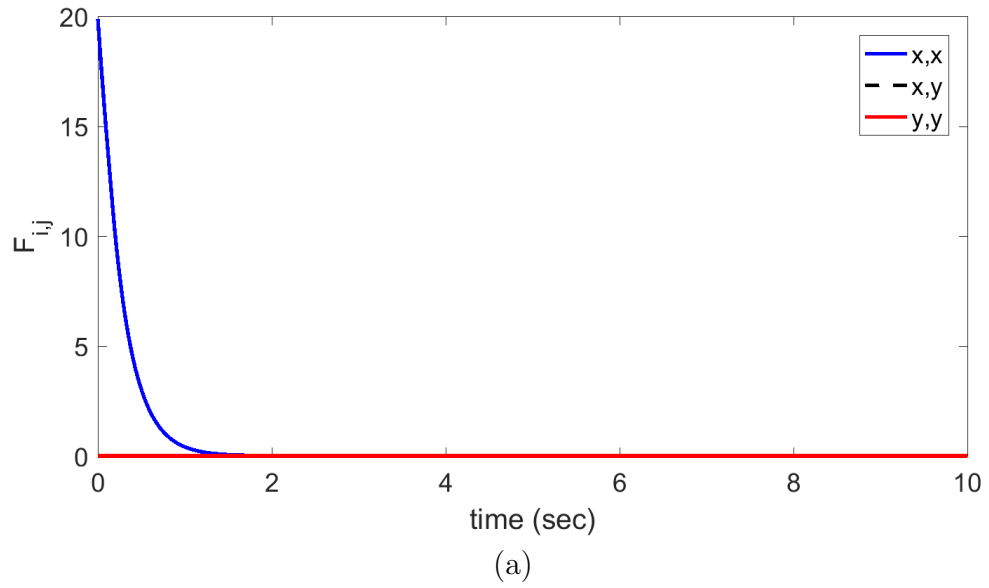
Figure 6.6: (a) Elements of **F** and (b) master wave impedance during a high-to-low impedance transition

Chapter 7: Conclusions and Future Work

7.1 Summary and Conclusions

A novel technique has been presented for selection of the wave impedance parameter employed in the passivity-based bilateral teleoperation scheme that has been popular in the literature in recent decades. This scheme both identifies a linearized optimum for the selection of this parameter and, most significantly, extends its treatment beyond the joint space considerations of prior work, taking into account the Cartesian nature of a realistic compliant contact task. This impedance can be allowed to vary at runtime in response to changing environmental stiffness conditions, although master-slave coordination error is found to be a substantial challenge to such an operational mode. For tasks that do not require traversal of a large region of the manipulator's workspace, a constant choice of wave impedance chosen about some central reference pose may be strongly motivated.

Simulation and experimental results validating the scheme have been presented, demonstrating a substantial improvement in transparency as compared to reasonable scalar choices. Human subjects demonstrated an ability to identify the high-stiffness environmental axis with an accuracy comparable to the ideal Force Reflection teleoperation scheme. Consideration has also been given to the case in

which environmental knowledge is not available *a priori* to inform the impedance selection process.

7.2   Future Work

A significant challenge to the present work is that of master-slave coordination error. While classical wave-based teleoperation has long been known to be vulnerable to accumulation of such error (and, as a result, several schemes already exist in the literature for mitigation of this error), unsynchronized variation in the wave impedance was shown in Section 3.3 to exacerbate this weakness. A particularly compelling avenue of future research, therefore, would be the extension of the proposed scheme into the feedback-passivized wave-based teleoperation scheme of Chopra et al. [34], which effectively solves the position drift problem. Most notably, it is not clear at this time how best to generalize (3.83) into this new arena, in which both position and velocity data are present in the communication channel. The experience of Rodríguez-Seda [68] suggests that oscillation rather than position drift would be the fundamental performance challenge of such a variable-impedance scheme. This feedback-passivized approach, as mentioned in Appendix A, represents a substantial departure from the robust simplicity of the classical wave teleoperation approach considered in the present work. Further research along the lines of Tanner and Niemeyer [67], Niemeyer and Slotine [36], and Chopra et al. [33] into coordination error mitigation strategies for the classical wave teleoperator are therefore still very much motivated. In particular, their effects on transparency are not well

studied.

The quasi-optimal result employed throughout this dissertation was shown to yield a substantial improvement as compared to scalar (isotropic) wave impedance choices. This result was derived, however, through the neglect of coupling between degrees of freedom as well as any nonlinear terms. The MIMO optimization of App. B begins to attempt to address the former, although a closed-form solution has not been identified. Such a numerical approach is amenable to offline tuning, but presents more substantial challenges when online wave impedance updates are desired.

Finally, the area of wave-based teleoperation in general is in need of further experimental work. The need for accurate velocity data presents a substantial implementation challenge, and may have been largely responsible (along with unmodeled dynamics in the actuation system) for the limited wave impedance attainable in the experimental trials of Chapter 5. Experimental results in the literature have generally depended on low-degree-of-freedom robotic systems that do not represent the full complexity of a typical 6+ DOF manipulator employed in realistic tasks. Moreover, the limitations of the haptic device employed in the present study prevented experimental exploration at realistic levels of latency. Revisiting this experiment with more capable hardware would be a worthwhile undertaking. Finally, the question of transparency extends far beyond the basic questions of apparent mass and stiffness considered in the present work. Stick/slip conditions and other more complex environmental phenomena merit attention; and human factors trials of tasks similar to those employed on the Engineering Test Satellite VII [24] would be a

worthwhile addition to the literature.

Appendix A: Results for Feedback Passivation

In addition to the classical wave-based scheme considered in the body of this dissertation, the feedback passivation scheme of Chopra et al. [34] has seen some attention in the literature. This scheme addresses the problem of position drift by transmitting an encoded combination of both position and velocity through the wave-based channel via control parameter $\lambda > 0$:

$$r = \dot{q} + \lambda q \tag{A.1}$$

where an adaptive scheme is employed in order to passivize the manipulator dynamics in this change of variable. In the ensuing analysis, perfect identification of the system parameters is assumed.

The Arcara and Melchiorri study [10] predates this scheme, but the analysis procedure of Subsection 2.3.1 is applied presently in order to arrive at the following equivalent low-frequency mechanical properties (neglecting joint friction for compactness of the ensuing expressions, and assuming $K_m = K_s = B$ for impedance

matching):

$$m_{eq} = m_m + m_s \left(1 - \frac{2\lambda m_s}{B} - 2\lambda T \right)$$

$$+ BT(1 - \lambda T) \tag{A.2}$$

$$b_{eq} = \lambda(m_s + BT) \tag{A.3}$$

$$k_{eq} = \frac{\lambda B K_e}{2K_e + \lambda B} \tag{A.4}$$

As in the classical wave-based scheme, stiffness perception will always be less than the true environmental stiffness. In contrast to the classical scheme, however, the perceived inertia is complicated considerably. Moreover, whereas the classical wave scheme reduces to an identity transformation as $T \to 0$, the scheme of Chopra et al. distorts the perception of all three of the parameters considered here, even in the zero-delay case:

$$m_{eq}|_{T\to0} = m_m + m_s \left(1 - \frac{2\lambda m_s}{B} \right) \tag{A.5}$$

$$b_{eq}|_{T\to0} = \lambda m_s \tag{A.6}$$

$$k_{eq}|_{T\to0} = \frac{\lambda B K_e}{2K_e + \lambda B} \tag{A.7}$$

The advantages, however, are considerable: In addition to the complete elimination of all steady-state coordination error $q_m - q_s$, the perceived stiffness is now *independent*[1] of delay time T. This is a substantial advantage over the classical scheme,

---

[1] This is, of course, at steady state. Information will still propagate through the system with a round-trip delay of $2T$.

which degrades quickly for increasing delays—motivating larger choices of B, which in turn increase the inertial penalty. The reader must bear in mind, however, that this scheme is founded upon an adaptive parameter estimation approach, which adds complexity and may present a risk of destabilization if those parameter estimates diverge due to unmodeled dynamics or other perturbations. This is a very substantial departure from the robust simplicity of the classical approach.

Any desired stiffness fidelity, $0 < \phi_k^{-1} = k_{eq}/K_e < 1$, may be achieved by rearranging (A.4) to solve for the product λB of the control parameters[2]:

$$\lambda B = \frac{2\phi_k^{-1}}{1 - \phi_k^{-1}} K_e \triangleq N K_e \tag{A.8}$$

And the desired inertia M_{des} to be displayed to the user may then dictate the values of λ and B separately. If time delay is negligible, (A.7) may be rearranged (substituting $B = NK_e/\lambda$) to solve for λ:

$$\lambda = \frac{\sqrt{K_e(m_m + m_s - M_{des})N}}{\sqrt{2}m_s} \tag{A.9}$$

where it is apparent from the above formulation that M_{des} must be chosen less than $m_m + m_s$, the native inertia of the system.

If instead time delay is not negligible, then a closed form solution is still

---

[2]Restraint is warranted in that the equivalent damping b_{eq} will grow proportionally to λB. This is not, however, a consideration completely unique to the feedback-passivized approach: The PI controllers in the classical wave approach will dissipate energy in a fashion proportional to both $K_p = B$ and the velocity tracking error. (The scatter-delay-scatter portion of Fig. 2.1 is, however, lossless; and this consideration vanishes if the controllers are omitted and the channel operated in a force-force configuration.)

possible. The result, however, is rather lengthy and yields no additional insight:

$$\lambda = \frac{1}{12m_s^2} \left[\frac{2 \cdot 2^{2/3} K_e m_s^2 N \left(K_e N T^2 + 3M_{des} - 3m_m - 3m_s \right)}{\sqrt[3]{A_4}} \right.$$
$$\left. - 2\sqrt[3]{2}\sqrt[3]{A_2} - 4K_e m_s N T \right] \tag{A.10}$$

$$A_1 = \left\{ K_e^3 m_s^6 N^3 \left[2 \left(K_e N T^2 + 3M_{des} - 3m_m - 3m_s \right)^3 \right.\right.$$
$$\left.\left. + K_e N T^2 \left(5K_e N T^2 + 9M_{des} - 9m_m + 18m_s \right)^2 \right] \right\}^{1/2} \tag{A.11}$$

$$A_2 = A_1 - 5K_e^3 m_s^3 N^3 T^3 - 9K_e^2 M_{des} m_s^3 N^2 T + 9K_e^2 m_m m_s^3 N^2 T - 18K_e^2 m_s^4 N^2 T$$
$$\tag{A.12}$$

$$A_3 = \left\{ K_e^3 m_s^6 N^3 \left[2 \left(K_e N T^2 + 3M_{des} - 3m_m - 3m_s \right)^3 \right.\right.$$
$$\left.\left. + K_e N T^2 \left(5K_e N T^2 + 9M_{des} - 9m_m + 18m_s \right)^2 \right] \right\}^{1/2} \tag{A.13}$$

$$A_4 = A_3 - 5K_e^3 m_s^3 N^3 T^3 - 9K_e^2 M_{des} m_s^3 N^2 T + 9K_e^2 m_m m_s^3 N^2 T - 18K_e^2 m_s^4 N^2 T$$
$$\tag{A.14}$$

Instead, an iterative solution may be more simply applied using (A.9) as the initial estimate. In this case, one wishes to find a root of the function

$$f(\lambda) = m_{eq} - M_{des} \tag{A.15}$$

where m_{eq} is given by (A.2) and again $B = NK_e/\lambda$. This function satisfies $\lim_{\lambda \to 0} f(\lambda) = +\infty$ and $\lim_{\lambda \to \infty} f(\lambda) = -\infty$. Additionally, its derivative is finite and negative ev-

erywhere in the design space $\lambda \in (0, \infty)$:

$$f'(\lambda) = \frac{df}{d\lambda} = -\frac{4\lambda m_s^2}{K_e N} - 2m_s T - \frac{K_e N T}{\lambda^2} \tag{A.16}$$

and the second derivative is continuous on this same interval. Precisely one real, positive solution will therefore exist; and the monotonic behavior of f makes it very well behaved for virtually any choice of numerical root-finding algorithm—e.g., the Newton-Raphson method:

$$\lambda_{j+1} = \lambda_j - \frac{f(\lambda_j)}{f'(\lambda_j)} \tag{A.17}$$

Note that in contrast to the zero-delay case above, any $M_{des} > 0$ may theoretically be achieved here with suitable choice of λ and B.

Appendix B: Discussion of MIMO Optimization

This appendix considers a possible extension of the optimization problem of Section 2.4 into the multiple-input-multiple-output (MIMO) case, presenting a candidate objective function for use in numerical optimization. Here, both the equivalent inertia and the equivalent stiffness are matrix quantities and cannot readily be expressed in terms of a Weber fraction. As a crude analogy to the scalar Φ defined in (2.52), however, consider the matrix quantity

$$\mathbf{\Phi} = \mathbf{W}_{\mathrm{M}} \left(\mathbf{M}_{\mathrm{m}} + \mathbf{M}_{\mathrm{s}}\right)^{-1} \mathbf{M}_{\mathrm{eq}} + \mathbf{W}_{\mathrm{K}}\mathbf{K}_{\mathrm{eq}}^{-1}\mathbf{K}_{\mathrm{e}} \qquad (\text{B.1})$$

where $\mathbf{W}_{\mathrm{M}}$ and $\mathbf{W}_{\mathrm{K}}$ represent matrix weights. In the case of perfect transparency, $\mathbf{\Phi}$ will reduce to the sum $\mathbf{W}_{\mathrm{M}} + \mathbf{W}_{\mathrm{K}}$. The equivalent stiffness and inertia of the teleoperation system are identified by combining expressions (3.65) and (3.55) in

the usual manner for physical elements in series[1]:

$$\mathbf{M}_{\text{eq}} = \mathbf{M}_{\text{m}} + \mathbf{M}_{\text{s}} + \mathbf{M}_{\text{comm}}$$

$$= \mathbf{M}_{\text{m}} + \mathbf{M}_{\text{s}} + \mathbf{B}T \tag{B.2}$$

$$\mathbf{K}_{\text{eq}}^{-1} = \mathbf{K}_{\text{e}}^{-1} + \mathbf{K}_{\text{comm}}^{-1}$$

$$= \mathbf{K}_{\text{e}}^{-1} + \mathbf{B}^{-1}T \tag{B.3}$$

Under ordinary circumstances, of course (unless the slave end effector is embedded in an environment having finite stiffness in all degrees of freedom), $\mathbf{K}_{\text{e}}^{-1}$ will not exist. The following discussion confines itself to the subspace of the task space in which finite stiffness occurs. In the case of simple contact with a surface, this will be along the axis perpendicular to that surface and the problem reduces to the scalar considerations of 2.4 along that axis. In more geometrically complicated scenarios, as in a peg-in-hole insertion task, stiffness may exist along multiple axes. It is this latter case that is considered presently, partitioning the singular value decomposition of the stiffness matrix as $\mathbf{K}_{\text{e}} = \mathbf{U}\mathbf{\Sigma}\mathbf{U}^T$. The nonzero singular values are collected in $\mathbf{\Sigma}_0$ and the corresponding singular vectors in $\mathbf{U}_0$. Inertias, stiffnesses, and impedances are projected into this subspace as $\mathbf{K}_0 = \mathbf{U}_0\mathbf{\Sigma}_0\mathbf{U}_0^T$, $\mathbf{M}_0 = \mathbf{U}_0^T\mathbf{M}\mathbf{U}_0$, and $\mathbf{B}_0 = \mathbf{U}_0^T\mathbf{B}\mathbf{U}_0$, respectively. Projected into the subspace on which the problem

---

[1]i.e., inertias add directly ($m_{1+2} = m_1 + m_2$) and stiffnesses add inversely ($k_{1+2}^{-1} = k_1^{-1} + k_2^{-1}$).

is meaningfully defined, then,

$$\boldsymbol{\Phi}_0 = \mathbf{W}_{\text{M},0} \left(\mathbf{M}_{\text{m},0} + \mathbf{M}_{\text{s},0}\right)^{-1} \mathbf{M}_{\text{eq},0} + \mathbf{W}_{\text{K},0}\mathbf{K}_{\text{eq},0}^{-1}\mathbf{K}_{\text{e},0}$$

$$= \mathbf{W}_{\text{M},0} \left(\mathbf{M}_{\text{m},0} + \mathbf{M}_{\text{s},0}\right)^{-1} \left(\mathbf{M}_{\text{m},0} + \mathbf{M}_{\text{s},0} + \mathbf{B}_0 T\right) + \mathbf{W}_{\text{K},0} \left(\mathbf{K}_{\text{e},0}^{-1} + \mathbf{B}_0^{-1}T\right) \mathbf{K}_{\text{e},0}$$

$$= \mathbf{W}_{\text{M},0} \left[\mathbf{I} + \left(\mathbf{M}_{\text{m},0} + \mathbf{M}_{\text{s},0}\right)^{-1} \mathbf{B}_0 T\right] + \mathbf{W}_{\text{K},0} \left[\mathbf{I} + T\mathbf{B}_0^{-1}\mathbf{K}_{\text{e},0}\right] \qquad \text{(B.4)}$$

Whereas $\boldsymbol{\Phi}$ would ideally become $\mathbf{W}_\text{M} + \mathbf{W}_\text{K}$ in the case of perfect transparency, this ideal quantity is subtracted from the above in order to arrive at an error measure representing a difference from the ideal (i.e., a measure that would become the zero matrix in the case of perfect transparency):

$$\boldsymbol{\Phi}_0' = \mathbf{W}_{\text{M},0} \left(\mathbf{M}_{\text{m},0} + \mathbf{M}_{\text{s},0}\right)^{-1} \mathbf{B}_0 T + \mathbf{W}_{\text{K},0}\mathbf{B}_0^{-1}\mathbf{K}_{\text{e},0}T \qquad \text{(B.5)}$$

The factor of T is eliminated because it does not affect the ideal choice of $\mathbf{B}_0$.

$$\boldsymbol{\Phi}_0'' = \mathbf{W}_{\text{M},0} \left(\mathbf{M}_{\text{m},0} + \mathbf{M}_{\text{s},0}\right)^{-1} \mathbf{B}_0 + \mathbf{W}_{\text{K},0}\mathbf{B}_0^{-1}\mathbf{K}_{\text{e},0} \qquad \text{(B.6)}$$

Minimization of a suitable choice of norm (e.g., the Frobenius norm), possibly squared, of this matrix is an obvious avenue for exploration, although no closed-form solution is identified at present. A sample objective function is presented in MATLAB code below for the 2×2 case, employing penalty functions in order to enforce positive definiteness. The input B is treated as a 3-vector corresponding to the unique elements of the symmetric matrix $\mathbf{B}$.

```
function out = mimophi( M,K,B )

eps = 1e-3;

Kpenalty = 1e6;

B = [B(1),B(2);B(2),B(3)];

out = norm(inv(M)*B + inv(B)*K,'fro')^2;

evals = eig(B);

for i=1:length(evals)

        if(evals(i) < eps)

                out = out + abs(evals(i)-eps)*Kpenalty;

        end

end

end
```

This is a different optimization problem from that treated in Chapter 3, and would be expected to yield a different optimum. Consider, for example, the case in which the inertia and stiffness matrices are given by

$$\mathbf{M} = \begin{pmatrix} 28.74 & 9.37 \\ 9.37 & 5.83 \end{pmatrix} \text{kg} \cdot \text{m}^2 \qquad \mathbf{K}_e = \begin{pmatrix} 100 & 0 \\ 0 & 1,000 \end{pmatrix} \text{Nm/rad}$$

Numerical optimization in the above manner with $\mathbf{W}_\mathrm{M} = \mathbf{W}_\mathrm{K} = \mathbb{I}$ yields the follow-

ing optima, employing the Frobenius norm and the induced 2-norm, respectively:

$$\mathbf{B}^*_{fro} = \begin{pmatrix} 12.29 & -2.52 \\ -2.52 & 164.67 \end{pmatrix} \text{kg} \cdot \text{m}^2/\text{s} \qquad \mathbf{B}^*_{2-norm} = \begin{pmatrix} 0.834 & -0.272 \\ -0.272 & 166.53 \end{pmatrix} \text{kg} \cdot \text{m}^2/\text{s}$$

By comparison, applying the scalar optimization result (2.53) in a quasi-optimal fashion to each axis separately would yield

$$\mathbf{B}^*_{quasi} = \begin{pmatrix} 53.61 & 0 \\ 0 & 241.5 \end{pmatrix} \text{kg} \cdot \text{m}^2/\text{s}$$

All of the above have the net effect of focusing greater impedance on those degrees of freedom that encounter greater stiffness; but each does so according to its own respective objective. The Frobenius norm is intuitively appealing because it applies equally to all elements of the matrix, thus representing a form of least squares match to the ideal inertia and stiffness matrices. Solving such an optimization problem numerically (especially if done in an online fashion), however, introduces considerable complications with regard to questions of convergence and global optimality.

Appendix C: Phantom Omni System Characteristics

This appendix presents the Omni model employed in the experimental trials of Chapter 5.

C.1   Forward kinematics

The Omni has no kinematically relevant joint offsets, and so behaves as a simple three-degree-of-freedom manipulator. A Cartesian offset is used to align with the Phantom coordinate convention, which places the origin near the center of the workspace. For consistency with the manufacturer's convention, the y axis is vertical and the z axis points toward the user. Also for consistency with the manufacturer's convention, q_3 is measured from the vertical (not from the preceding link, as is the usual convention in serial-link robotics). Fig. C.1a shows the Omni's joint angles; and Fig. C.1b shows the Cartesian coordinate frame. The quantity r is defined for convenience, representing the radius in the horizontal plane from the Phantom's shoulder to the stylus hinge point; and the resulting expressions for the

(x, y, z) position of the hinge point is given by:

$$r = L_1\cos(q_2) + L_2\sin(q_3) \tag{C.1}$$

$$x = r\sin(-q_1) \tag{C.2}$$

$$y = L_1\sin(q_2) - L_2\cos(q_3) + C_y \tag{C.3}$$

$$z = r\cos(q_1) - C_z \tag{C.4}$$

From analysis of the tip positions reported via `HD_CURRENT_POSITION`, it is clear that the manufacturer employs parameter values

$$L_1 = L_2 = 133.35 \text{ mm}$$

$$C_y = 23.35 \text{ mm}$$

$$C_z = 168.35 \text{ mm}$$

C.2 Jacobian matrix

The translational Jacobian matrix is identified via differentiation of the preceding forward kinematics model to obtain the matrix $\mathbf{J}$ such that $\dot{\underline{x}} = \mathbf{J}\dot{\underline{q}}$, where $\underline{x} = [x \ y \ z]^T$ as given by (C.2)-(C.4).

$$\mathbf{J}(\underline{q}) = \begin{pmatrix} -r\cos(q_1) & L_1\sin(q_1)\sin(q_2) & -L_2\cos(q_3)\sin(q_1) \\ 0 & L_1\cos(q_2) & L_2\sin(q_3) \\ -r\sin(q_1) & -L_1\cos(q_1)\sin(q_2) & L_2\cos(q_1)\cos(q_3) \end{pmatrix}$$

181
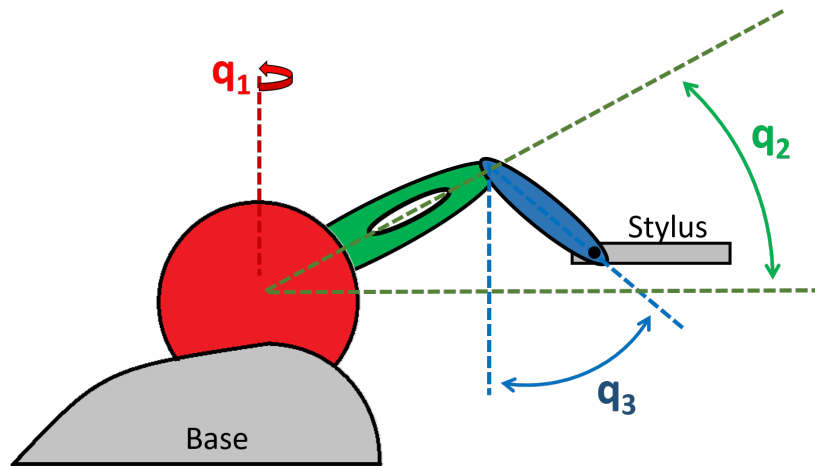
(a)
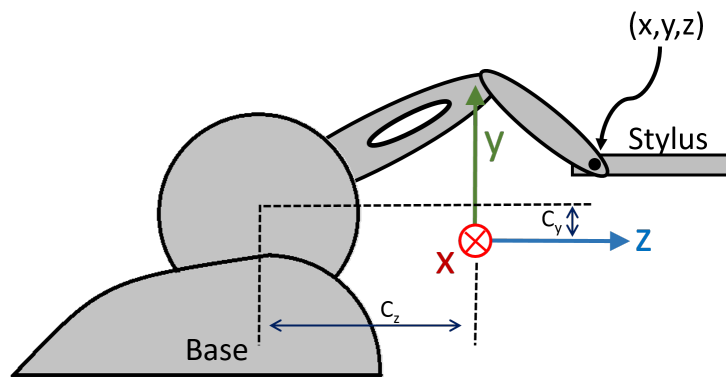
(b)

Figure C.1: (a) Joint angle conventions and (b) Cartesian coordinate frame for the Phantom Omni device

C.3 Dynamic equations of motion

The equations of motion of a serial link manipulator are given by the equation below.

$$\mathbf{M}(\underline{q})\ddot{\underline{q}} + \mathbf{C}(\underline{q}, \dot{\underline{q}})\dot{\underline{q}} + \underline{g}(\underline{q}) = \underline{\tau}$$

A Lagrangian derivation was used to identify the equations of motion, assuming the principal axes of each robot link aligned with that link's joint and longitudinal axes. Although small offsets exist between the joints, the effect on system dynamics is assumed to be negligible to within the precision to which the dynamics are characterized in the present study. Within these assumptions, the inertia matrix $\mathbf{M}$ has elements

$$M_{11} = I_{0ZZ} + \frac{1}{2}I_{1xx} + \frac{1}{2}I_{1yy} + \frac{1}{2}I_{2xx} + \frac{1}{2}I_{2yy} + \frac{1}{8}m_1 L_1^2$$
$$+ \frac{1}{2}m_2 L_1^2 + \frac{1}{8}m_2 L_2^2 + \frac{1}{2}m_3 L_1^2 + \frac{1}{2}m_3 L_2^2$$
$$+ \left[-\frac{1}{2}I_{xx1} + \frac{1}{2}I_{1yy} + L_1^2\left(\frac{1}{8}m_1 + \frac{1}{2}m_2 + \frac{1}{2}m_3\right)\right]\cos(2q_2)$$
$$+ m_2 L_1 L_2 \cos(q_2)\sin(q_3) + 2m_3 L_1 L_2 \cos(q_2)\sin(q_3)$$

$$M_{12} = M_{21} = 0$$

$$M_{13} = M_{31} = 0$$

$$M_{22} = I_{1zz} + L_1^2\left(\frac{1}{4}m_1 + m_2 + m_3\right)$$

$$M_{32} = M_{23} = L_1 L_2\left(-\frac{1}{2}m_2 - m_3\right)\sin(q_2 - q_3)$$

$$M_{33} = I_{2zz} + L_2^2\left(\frac{1}{4}m_2 + m_3\right)$$

The centripetal and Coriolis matrix $\mathbf{C}$ is given by

$$C_{11} = C_{22} = C_{33} = 0$$

$$C_{12} = \dot{q}_1 \left[\left(I_{1xx} - I_{1yy} + L_1^2(-\frac{1}{4}m_1 - m_2 - m_3) \right) \sin(2q_2) \right.$$
$$\left. + L_1 L_2(-m_2 - 2m_3)\sin(q_2)\sin(q_3) \right]$$

$$C_{13} = \dot{q}_1 \left[L_1 L_2(m_2 + 2m_3)\cos(q_2)\cos(q_3)+ \right.$$
$$\left. \left(-I_{2xx} + I_{2yy} + L_2^2(\frac{1}{4}m_2 + m_3)\sin(2q_3) \right) \right]$$

$$C_{21} = -\frac{1}{2}C_{12}$$

$$C_{23} = \dot{q}_3 \left[\frac{1}{2}m_2 L_1 L_2\cos(q_2 - q_3) + m_3 L_1 L_2\cos(q_2 - q_3) \right]$$

$$C_{31} = -\frac{1}{2}C_{31}$$

$$C_{32} = \dot{q}_2 \left[L_1 L_2(-\frac{1}{2}m_2 - m_3)\cos(q_2 - q_3) \right]$$

Although $\mathbf{C}$ is not skew symmetric, it can be readily verified that $\dot{\mathbf{M}} - 2\mathbf{C}$ is skew symmetric. The system therefore satisfies the passivity property.

For the purpose of the present work the following parameter values were assumed, deriving from a rough combination of cylindrincal approximations, measurements and adaptive control results presented in the literature, and the judgment of the author. Fortunately, for the present purposes it is not nearly so important that the master and slave have identical dynamics as it is that they have identical

184

kinematics.

$$m_1 = 0.035 \text{ kg} \qquad m_2 = 0.060 \text{ kg} \qquad m_3 = 0.040 \text{ kg}$$

$$I_{0zz} = 1 \times 10^{-4} \text{ kg} \cdot \text{m}^2$$

$$I_{1xx} = 4 \times 10^{-7} \text{ kg} \cdot \text{m}^2 \qquad I_{1yy} = 5.2 \times 10^{-5} \text{ kg} \cdot \text{m}^2 \qquad I_{1zz} = 5.2 \times 10^{-5} \text{ kg} \cdot \text{m}^2$$

$$I_{2xx} = 8 \times 10^{-7} \text{ kg} \cdot \text{m}^2 \qquad I_{2yy} = 9 \times 10^{-5} \text{ kg} \cdot \text{m}^2 \qquad I_{2zz} = 9 \times 10^{-5} \text{ kg} \cdot \text{m}^2$$

where the link frame z axis is taken to lie along the joint axis of rotation of its more proximal joint and the link frame x axis points along the link's longitudinal axis.

Finally, the gravity and spring terms are given by

$$g_1 = 0$$
$$g_2 = K_{sp}\left(q_2 - \frac{\pi}{2}\right) + \left(\frac{1}{2}m_1 + m_2 + m_3\right)gL_1\cos(q_2)$$
$$g_3 = \left(\frac{1}{2}m_2 + m_3\right)gL_2\sin(q_3)$$

where K_{sp} is the spring constant of the internal gravity-compensating spring. In the present experiments, neither gravity nor the compensating spring were simulated.

The cable drive system was assumed to differ negligibly from a direct drive system.[1] Thus, $\underline{\tau}$ was assumed to directly correspond to the joint torque commanded in software. Joint friction $\underline{\tau} = -D\underline{\dot{q}}$ was assumed with $D = 0.01$ kg/s.

---

[1] This assumption is consistent with the findings of Naerum et al. [98], who found the torque transformation due to the transmission system to be near identity during dynamic motion.

Appendix D: Computer Code

This appendix collects the computer code which formed the basis for the simulations and experiments presented throughout this dissertation.

D.1   Simulation

D.1.1   Impedance Estimation

The following MATLAB code was employed for the mechanical impedance estimation of Section 4.2. The first script is run by the user, uncommenting one of the script name choices. These scripts are presented after the main file below.

Main script:

```matlab
% Specify frequencies
w = logspace(0,log10(40),15);
tic;

% Specify simulation script
sigmin = 100; sigmax = 1000;
%scriptname = 'diss_sim_cartb';
%scriptname = 'diss_sim_constb'; bm = diag([100,100]); bs =
    bm; Ki = 20;

% Set up for simulations
magnitude = nan(1,length(w));
phase = nan(1,length(w));
close all;

% Initial conditions
```

```matlab
X0 = [ pi/4;−pi/4;0;0; pi/4;−pi/4;0;0]; % EQUILIBRIUM AND
    INITIAL GUESS POSE [ th1;th2;th1d;th2d ]m, [""]s
equilib = fwdkin_2dof(X0);
amplitude = [0.002;0.00];
startpos = equilib − amplitude;
for dummy = 1:3 % Solve for actual starting pose
    X0(1:2) = X0(1:2) + Jac_2dof(X0)\(startpos−fwdkin_2dof(
        X0));
end
X0(5:6) = X0(1:2);
if (1e−4 < norm(−amplitude − (fwdkin_2dof(X0)−equilib)) )
    error ('Could not solve for valid initial pose');
end

% Run simulations
for outerindex=1:length (w)
    % Clear the work space
    clearvars −except magnitude phase outerindex w
        scriptname bm bs X0 equilib amplitude Ki lambda
        sigmin sigmax ;
    params_2dof;

    % Set up parameters for this go
    Tend = 3*2*pi/w(outerindex);
    tstep = 0.001/w(outerindex); %0.0002; %0.00005;
    Kec = diag ([10e3,10]); %diag([1000,1]); % Cartesian
        space environmental stiffness, N/m
    lamfilt = 250;
    Kfilt = lamfilt*tstep; % Niemeyer's lam = Kfilt/tstep
    if (Kfilt >1)
        warning ('Filter parameter replaced with unity');
        Kfilt = 1;
    end
    crtinv = 1/sqrt (100);
    delaysec = 0.05;
    delay = floor (delaysec/tstep);

    % Trajectory
    xdes = @(t) equilib − amplitude*cos(w(outerindex)*t);
    xdesdot = @(t) +w(outerindex)*amplitude*sin (w(outerindex
        )*t);
    xdesddot = @(t) +w(outerindex)^2*amplitude*cos(w(
        outerindex)*t);

    % Run simulation
    eval (scriptname);
```

```matlab
        if( isnan(Forcemcarr(end,1)))
            Forcemcarr = Forcemcarr(1:end-1,:);
            T = T(1:end-1);
        end

    % Now we have to find the best fit sinusoid to the force
            response
        if( abs(amplitude(1)) > 0 )
            ampaxis = 1;
        else
            ampaxis = 2;
        end
        fc = Forcemcarr(floor(length(Forcemcarr)/3):end,ampaxis)
            ;
        tc = T(floor(length(Forcemcarr)/3):end);
        cost = @(B) sum( ( abs(B(1))*sin(w(outerindex)*tc+B(2))
            - fc' ).^2 );
        [B,fval] = fminsearch(cost, [5 0]);
        disp('w = ');
        disp(w(outerindex));
        disp('mag = ');
        disp(B(1)/amplitude(ampaxis));
        disp('phase = ');
        disp(B(2));

        magnitude(outerindex) = B(1)/amplitude(ampaxis);
        phase(outerindex) = B(2);

        save(['diss_sweep_',scriptname,'-ax',num2str(ampaxis),'-
            w=',num2str(w(outerindex)),'.mat']);

        figure(outerindex); clf;
        XD = xdesdot(T);
        plotyy(T,Forcemcarr(:,1),T,XD(ampaxis,:));
        title(num2str(outerindex));
        legend('F_{mc} (N)','velocity (m/s)');
        xlabel('time (sec)');
        toc

end
%%
save(['diss_sweep_',scriptname,'-ax',num2str(ampaxis),'-
    final.mat'],'w','magnitude','phase');
%%
figure(1+outerindex); clf;
loglog(w,abs(magnitude));
xlabel('frequency (rad/sec)');
```

```matlab
ylabel('magnitude');
%%
figure(2+outerindex); clf;
for j = 1:length(phase)
    if(phase(j)<-pi)
        phase(j) = phase(j) + 2*pi;
    end
end
loglog(w,phase);
xlabel('frequency (rad/sec)');
ylabel('phase (rad)');
%%
fh = figure(3+outerindex); clf;
subplot(2,1,1);
set(gca,'fontsize',14)
loglog(w,abs(magnitude),'LineWidth',2); hold on;
xlabel('frequency (rad/sec)');
ylabel('magnitude');
axis([0 w(end) 1e-7 1e-4]);
subplot(2,1,2);
set(gca,'fontsize',14)
semilogx(w,phase,'LineWidth',2); hold on;
axis([0 w(end) -1 1]);
xlabel('frequency (rad/sec)');
ylabel('phase (rad)');
set(fh, 'Position', [0 0 800 800]);
%%
Z = magnitude'.*exp(sqrt(-1)*phase');
Meq = nan(size(w));
Keq = nan(size(w));
Beq = real(Z);
for i = 1:length(w)-1
    A = [ w(i), -1/w(i); w(i+1), -1/w(i+1) ];
    c = imag([Z(i);Z(i+1)]);
    MK = A\c;
    Meq(i) = MK(1);
    Keq(i) = MK(2);
end
%%
disp('Done.');
toc
```

Supporting simulation scripts are given below.

diss_sim_cartb.m (Directional wave impedance choice):

```matlab
vm = [0;0]; us = [0;0]; eints = [0;0]; eintm = [0;0];
```

```matlab
es = [0;0]; esprev = [0;0]; em = [0;0]; emprev = [0;0];
T = 0:5*tstep:Tend;
X=X0;
Xhist = [X0',zeros(1,6); nan([length(T)-1,length(X0)+6])];
Ehist = [0 0 0 0; nan([length(T)-1,4])];
Fhist = [0 0; nan([length(T)-1,2])];
TIPs = [fwdkin_2dof(X(5:8))'; nan([length(T)-1,2])];
TIPm = [fwdkin_2dof(X(1:4))'; nan([length(T)-1,2])];
Bsarr = nan([ length(T)-1, 2, 2 ]);
Bmarr = nan([ length(T)-1, 2, 2 ]);
TAUhist = [0,0; nan([length(T)-1,2])];
Forcemcarr = [0,0; nan([length(T)-1,2])];
Zarr = []; Zave = [0 0];
Uarr = [0 0]; Varr = [0 0];
t = tstep;
count = 1;
Fe=[0;0];
dZarr = [];
i = 2;
xs = fwdkin_2dof(X(5:6));
once = 1;
while( t <= Tend)

    Mm = M_2dof(X(1:4)); Cm = Cmat_2dof(X(1:4));
    Ms = M_2dof(X(5:8)); Cs = Cmat_2dof(X(5:8));
    Jm = Jac_2dof(X(1:2));
    Js = Jac_2dof(X(5:6));

    % master
    xm = fwdkin_2dof(X(1:2));
    bcart = crtinv*Kec*sqrt(diag(diag( inv(Jm)'*Mm*inv(Jm) )
        ));
    bm = Jm'*bcart*Jm;
    [u,s,v] = svd(bm);
    for index = 1:size(s,2)
        if( s(index,index) > sigmax )
            s(index,index) = sigmax;
        elseif ( s(index,index) < sigmin )
            s(index,index) = sigmin;
        end
    end
    bm = u*s*u';
    Bmarr(count,:,:) = bm;
    if(once)
        Kim = diag(diag(bm/5));
        Kis = diag(diag(bm/5));
    end
```

190

```matlab
brt = sqrtm(bm); brtinv = inv(brt);
dotdes = -1/sqrt(2)*brtinv*vm - 0.5*X(3:4) - Kim*bm\
    eintm/2;
Fmc = -bm*(dotdes - X(3:4)) - Kim*eintm; % torque
um = 1/sqrt(2)*brt*dotdes+1/sqrt(2)*brtinv*Fmc;
%Fh = Kph * (xdes(t) - fwdkin_2dof(X(1:2))) + Kdh * (
    xdesdot(t) -
%Jac_2dof(X)*X(3:4) ); % operator force not computed
    here—it is
% (Master dynamics canceled to achieve perfect tracking)
emprev = em;
em = dotdes-X(3:4);
Kioldm = Kim;
Kim = diag(diag(bm/5));
Kideltam = (Kim-Kioldm);
%eintm = eintm + 0.5*(em+emprev)*tstep - 0.5*Kim\
    Kideltam*eintm;
eintm = sqrtm(Kim)\sqrtm(Kioldm)*eintm + 0.5*(em+emprev)
    *tstep;

% slave
Feprev = Fe;
xsprev = xs;
xs = fwdkin_2dof(X(5:6));
Fe = @(xs) -Kec*(xs - [1.7071;0.7071]); % linear spring
bcart = crtinv*Kec*sqrt(diag(diag( inv(Js)'*Ms*inv(Js) )
    ));
bs = Js'*bcart*Js;
[u,s,v] = svd(bs);
for index = 1:size(s,2)
    if( s(index,index) > sigmax )
        s(index,index) = sigmax;
    elseif ( s(index,index) < sigmin )
            s(index,index) = sigmin;
    end
end
bs = u*s*u';
Bsarr(count,:,:) = bs;
brt = sqrtm(bs); brtinv = inv(brt);
dotdes = 1/sqrt(2)*brtinv*us + 0.5*X(7:8) - Kis*bs\eints
    /2;
esprev = es;
es = (dotdes - X(7:8));
Fsc = bs*(dotdes - X(7:8)) + Kis*eints; % torque
vs = 1/sqrt(2)*brtinv*Fsc-us;
Kiolds = Kis;
```

```matlab
Kis = diag(diag(bs/5));
Kideltas = (Kis-Kiolds);
% eints = eints + 0.5*(es+esprev)*tstep - 0.5*Kis\
    Kideltas*eints;
eints = sqrtm(Kis)\sqrtm(Kiolds)*eints + 0.5*(es+esprev)
    *tstep;

xmdot = Jm*X(3:4);
Zarr(end+1,:) = transpose((Jm'\Fmc)./xmdot); % Recall
    Fmc is torque!
if( ~sum(isnan(Zarr(end,:))) )
    Zave = Zave + tstep*Zarr(end,:);
end

% integrate (with master dynamics canceled)
rhs = @(t,X) [ X(3:4) ; Jm\(xdesddot(t)-JacDot_2dof(X
    (1:4))*X(3:4)); X(7:8); M_2dof(X(5:8))\(Fsc+Jac_2dof(
    X(5:6))'*Fe(fwdkin_2dof(X(5:6)))-Cmat_2dof(X(5:8))*X
    (7:8)) ];
Xstep = ode5(rhs, [t t+tstep], X);
X = Xstep(end,:)';


% Communicate
Uarr(count,:) = um';
Varr(count,:) = vs';
if(count>delay)
    us = us + Kfilt*(Uarr(count-delay,:)'-us);
    vm = vm + Kfilt*(Varr(count-delay,:)'-vm);
else
    us = [0;0];
    vm = [0;0];
end

% Record history
if( 0 == mod(count,5) )
    Xhist(i,:) = [X', 0, 0, 0, bm(1,1), bm(1,2), bm(2,2)
        ];
    Ehist(i,:) = [ (X(1:4)-X(5:8))' ];
    TIPs(i,:) = fwdkin_2dof(X(5:6))';
    TIPm(i,:) = fwdkin_2dof(X(1:2))';
    Forcemcarr(i,:) = (Jm'\Fmc)';
    %TAUhist(i,:) = transpose( Jm'*Fh );
    %Fhist(i,:) = Fh';
    i = i + 1;
end
```

```
        t = t + tstep;
        count = count + 1;
end
```

diss_sim_constb.m (constant scalar wave impedance choice):

```
vm = [0;0]; us = [0;0]; eints = [0;0]; eintm = [0;0];
es = [0;0]; esprev = [0;0]; em = [0;0]; emprev = [0;0];
T = 0:5*tstep:Tend;
X=X0;
Xhist = [X0',zeros(1,6); nan([length(T)-1,length(X0)+6])];
Ehist = [0 0 0 0; nan([length(T)-1,4])];
Fhist = [0 0; nan([length(T)-1,2])];
TIPs = [fwdkin_2dof(X(5:8))'; nan([length(T)-1,2])];
TIPm = [fwdkin_2dof(X(1:4))'; nan([length(T)-1,2])];
Bsarr = nan([ length(T)-1, 2, 2 ]);
Bmarr = nan([ length(T)-1, 2, 2 ]);
TAUhist = [0,0; nan([length(T)-1,2])];
Forcemcarr = [0,0; nan([length(T)-1,2])];
Zarr = []; Zave = [0 0];
Uarr = [0 0]; Varr = [0 0];
t = tstep;
count = 1;
Fe=[0;0];
dZarr = [];
i = 2;
xs = fwdkin_2dof(X(5:6));
while( t <= Tend)

    Mm = M_2dof(X(1:4)); Cm = Cmat_2dof(X(1:4));
    Ms = M_2dof(X(5:8)); Cs = Cmat_2dof(X(5:8));
    Jm = Jac_2dof(X(1:2));
    Js = Jac_2dof(X(5:6));

    % master
    xm = fwdkin_2dof(X(1:2));
    Bmarr(count,:,:) = bm;

    brt = sqrtm(bm); brtinv = inv(brt);
    dotdes = -1/sqrt(2)*brtinv*vm - 0.5*X(3:4) - Ki*bm\eintm
        /2;
    Fmc = -bm*(dotdes - X(3:4)) - Ki*eintm; % torque
    um = 1/sqrt(2)*brt*dotdes+1/sqrt(2)*brtinv*Fmc;
    %Fh = Kph * (xdes(t) - fwdkin_2dof(X(1:2))) + Kdh * (
        xdesdot(t) -
    %Jac_2dof(X)*X(3:4) ); % operator force not computed
        here—it is
```

```matlab
%whatever it is to achieve perfect tracking
emprev = em;
em = dotdes-X(3:4);
eintm = eintm + 0.5*(em+emprev)*tstep;

% slave
xs = fwdkin_2dof(X(5:6));
Fe = @(xs) -Kec*(xs - [1.7071;0.7071]); % linear spring
Bsarr(count,:,:) = bs;
brt = sqrtm(bs); brtinv = inv(brt);
dotdes = 1/sqrt(2)*brtinv*us + 0.5*X(7:8) - Ki*bs\eints
    /2;
esprev = es;
es = (dotdes - X(7:8));
Fsc = bs*es + Ki*eints; % torque
vs = 1/sqrt(2)*brtinv*Fsc-us;
eints = eints + 0.5*(es+esprev)*tstep;

xmdot = Jm*X(3:4);
Zarr(end+1,:) = transpose((Jm'\Fmc)./xmdot); % Recall
    Fmc is torque!
if( ~sum(isnan(Zarr(end,:))) )
    Zave = Zave + tstep*Zarr(end,:);
end

% integrate (with master dynamics canceled)
rhs = @(t,X) [ X(3:4) ; Jm\(xdesddot(t)-JacDot_2dof(X
    (1:4))*X(3:4)); X(7:8); M_2dof(X(5:8))\(Fsc+Jac_2dof(
    X(5:6))'*Fe(fwdkin_2dof(X(5:6)))-Cmat_2dof(X(5:8))*X
    (7:8)) ];
Xstep = ode5(rhs, [t t+tstep], X);
X = Xstep(end,:)';

% Communicate
Uarr(count,:) = um';
Varr(count,:) = vs';
if(count>delay)
    us = us + Kfilt*(Uarr(count-delay,:)'-us);
    vm = vm + Kfilt*(Varr(count-delay,:)'-vm);
else
    us = [0;0];
    vm = [0;0];
end

% Record history
if( 0 == mod(count,5) )
    Xhist(i,:) = [X', 0, 0, 0, bm(1,1), bm(1,2), bm(2,2)
```

```matlab
                ];
            Ehist(i,:) = [ (X(1:4)-X(5:8))' ];
            TIPs(i,:) = fwdkin_2dof(X(5:6))';
            TIPm(i,:) = fwdkin_2dof(X(1:2))';
            Forcemcarr(i,:) = (Jm'\Fmc)';
            %TAUhist(i,:) = transpose( Jm'*Fh );
            %Fhist(i,:) = Fh';
            i = i + 1;
        end

        t = t + tstep;
        count = count + 1;
end
```

D.1.2   Circular Trajectory

This script produces the circular motion simulation of Section 4.3. This particular code implementations the joint space directional wave impedance scheme. Constant scalar choice can be effected by commenting out the appropriate update blocks and declaring fixed choices.

```matlab
params_2dof
%%
Tend = 10;
tstep = 0.00025;
Kph = 30;
Kdh = 15;
Kec = diag([1e4,1]); % Cartesian space environmental
    stiffness, N/m
crtinv = 1/sqrt(100);
sigmax = 500;
sigmin = 100;
delaysec = 0.050;
delay = floor(delaysec/tstep);
Bdotmax = 500;
%%
% Initial conditions and trajectory
X0 = [pi/4;-pi/4;0;0;pi/4;-pi/4;0;0]; % [th1;th2;th1d;th2d]m
    , [""]s
xdes = @(t) [1.7071+0.25*sin(t);0.4571+0.25*cos(t)];
xdesdot = @(t) [0.25*cos(t);-0.25*sin(t)];
```

```matlab
%%
vm = [0;0]; us = [0;0]; eints = [0;0]; eintm = [0;0];
es = [0;0]; esprev = [0;0]; em = [0;0]; emprev = [0;0];
T = 0:5*tstep:Tend;
X=X0;
Xhist = [X0',zeros(1,6); nan([length(T)-1,length(X0)+6])];
Ehist = [0 0 0 0; nan([length(T)-1,4])];
Fhist = [0 0; nan([length(T)-1,2])];
TIPs = [fwdkin_2dof(X(5:8))'; nan([length(T)-1,2])];
TIPm = [fwdkin_2dof(X(1:4))'; nan([length(T)-1,2])];
Bsarr = nan([ length(T)-1, 2, 2 ]);
Bmarr = nan([ length(T)-1, 2, 2 ]);
TAUhist = [0,0; nan([length(T)-1,2])];
Zave = [0;0]; Kave = [0;0];
Uarr = [0 0]; Varr = [0 0]; Fearr = [0 0];
t = tstep;
count = 1;
Fe=[0;0];
dZarr = [];
i = 2;
xs = fwdkin_2dof(X(5:6));
while( t <= Tend)

    Mm = M_2dof(X(1:4)); Cm = Cmat_2dof(X(1:4));
    Ms = M_2dof(X(5:8)); Cs = Cmat_2dof(X(5:8));
    Jm = Jac_2dof(X(1:2));
    Js = Jac_2dof(X(5:6));

    % master
    xm = fwdkin_2dof(X(1:2));
    if(count<=delay)
        bcart = crtinv*Kec*sqrt(diag(diag( inv(Jm)'*Mm*inv(
            Jm) )));
    else
        if(norm(Fearr(count-delay,:)) > 0 )
            bcart = crtinv*Kec*sqrt(diag(diag( inv(Jm)'*Mm*
                inv(Jm) )));
        else
            bcart = zeros([2 2]);
        end
    end
    bm = Jm'*bcart*Jm;
    if( t > tstep)
        soldm = sm;
    end
    [u,sm,v] = svd(bm);
    for index = 1:size(sm,2)
```

```matlab
            if ( sm(index,index) > sigmax )
                sm(index,index) = sigmax;
            elseif ( sm(index,index) < sigmin )
                    sm(index,index) = sigmin;
            end
            if ( t > tstep)
                n = sm(index,index) - soldm(index,index);
                if ( abs(n) > Bdotmax*tstep )
                    sm(index,index) = soldm(index,index) + sign(
                        n)*Bdotmax*tstep;
                end
            end
    end
    bm = u*sm*u';
    Bmarr(count,:,:) = bm;
    if(t <= tstep)
        Kim = diag(diag(bm/5));
        Kis = diag(diag(bm/5));
    end

    brt = sqrtm(bm); brtinv = inv(brt);
    dotdes = -1/sqrt(2)*brtinv*vm - 0.5*X(3:4) - Kim*bm\
        eintm/2;
    Fmc = -bm*(dotdes - X(3:4)) - Kim*eintm; % torque
    um = 1/sqrt(2)*brt*dotdes+1/sqrt(2)*brtinv*Fmc;
    Fh = Kph * (xdes(t) - fwdkin_2dof(X(1:2))) + Kdh * (
        xdesdot(t) - Jac_2dof(X)*X(3:4) );
    emprev = em;
    em = dotdes-X(3:4);
    Kioldm = Kim;
    Kim = diag(diag(bm/5));
    Kideltam = (Kim-Kioldm);
    eintm = sqrtm(Kim)\sqrtm(Kioldm)*eintm + 0.5*(em+emprev)
        *tstep;

    % slave
    Feprev = Fe;
    xsprev = xs;
    xs = fwdkin_2dof(X(5:6));
    if ( xs(1) > 1.7071 )
        Fe = -Kec*(xs - [1.7071;0.7071]); % linear spring
        bcart = crtinv*Kec*sqrt(diag(diag( inv(Js)'*Ms*inv(
            Js) )));
    else
        Fe = [0;0];
        bcart = zeros([2 2]);
    end
```

```matlab
        Fearr(end+1,:) = Fe';

        bs = Js'*bcart*Js;
        if(t > tstep)
            solds = ss;
        end
        [u,ss,v] = svd(bs);
        for index = 1:size(ss,2)
            if( ss(index,index) > sigmax )
                ss(index,index) = sigmax;
            elseif ( ss(index,index) < sigmin )
                ss(index,index) = sigmin;
            end
            if( t > tstep )
                n = ss(index,index)-solds(index,index);
                if( abs(n) > Bdotmax*tstep )
                    ss(index,index) = solds(index,index) + sign(
                        n)*Bdotmax*tstep;
                end
            end
        end
        bs = u*ss*u';
        Bsarr(count,:,:) = bs;
        brt = sqrtm(bs); brtinv = inv(brt);
        dotdes = 1/sqrt(2)*brtinv*us + 0.5*X(7:8) - Kis*bs\eints
            /2;
        Fsc = bs*(dotdes - X(7:8)) + Kis*eints; % torque
        vs = 1/sqrt(2)*brtinv*Fsc-us;
        eints = eints + (dotdes-X(7:8))*tstep;
        Kiolds = Kis;
        Kis = diag(diag(bs/5));
        Kideltas = (Kis-Kiolds);
        eints = sqrtm(Kis)\sqrtm(Kiolds)*eints + 0.5*(es+esprev)
            *tstep;

        % integrate
        rhs = @(t,X) [ X(3:4); M_2dof(X(1:2))\(Jac_2dof(X(1:2))
            '*Fh-Fmc-Cmat_2dof(X(1:4))*X(3:4)); X(7:8); M_2dof(X
            (5:8))\(Fsc+Jac_2dof(X(5:6))'*Fe-Cmat_2dof(X(5:8))*X
            (7:8)) ];
        Xstep = ode5(rhs, [0 tstep], X);
        X = Xstep(end,:)';

        dZ = 1/Tend*( (Jm'\Fmc)./(Jm*X(3:4)) )*tstep;
        dZarr(:,end+1) = dZ;
        if( dZ(1) == dZ(1) ) % if not NaN
            Zave(1) = Zave(1) + dZ(1);
```

```matlab
        end
        if(  dZ(2) == dZ(2)  )
            Zave(2) = Zave(2) + dZ(2);
        end
        dK = 1/Tend*(  (Jm'\Fmc)./(xm-xs)  )*tstep;
        if(  dK(1) == dK(1)  ) % if not NaN
            Kave(1) = Kave(1) + dK(1);
        end
        if(  dK(2) == dK(2)  )
            Kave(2) = Kave(2) + dK(2);
        end

        % Communicate
        Uarr(count,:) = um';
        Varr(count,:) = vs';
        if(count>delay)
            us = Uarr(count-delay,:)';
            vm = Varr(count-delay,:)';
        else
            us = [0;0];
            vm = [0;0];
        end

        % Record history
        if(  0 == mod(count,5)  )
            Xhist(i,:) = [X', 0, 0, 0, bm(1,1), bm(1,2), bm(2,2)
                ];
            Ehist(i,:) = [  (X(1:4)-X(5:8))'  ];
            TIPs(i,:) = fwdkin_2dof(X(5:6))';
            TIPm(i,:) = fwdkin_2dof(X(1:2))';
            TAUhist(i,:) = transpose( Jm'*Fh );
            Fhist(i,:) = Fh';
            i = i + 1;
        end

        t = t + tstep;
        count = count + 1;
end
Zave
%%
figure(1); clf;
plot(T(1:length(Ehist)),Ehist(:,1:2)); title('Joint position
    error');
legend('1','2');
xlabel('time (sec)'); ylabel('joint error (rad)');
%%
figure(2); clf;
```

```matlab
plot(T(1:length(Ehist)),Ehist(:,3:4)); title('Joint rate
    error');
legend('1','2');
%%
fh = figure(3); clf;
plot(T,Fhist(:,1),'b-','LineWidth',2); hold on;
plot(T,Fhist(:,2),'r-','LineWidth',2);
%title('Operator force');
lh = legend('F_x teleop','F_y teleop');
xlabel('time (sec)','FontSize',14); ylabel('force (N)','
    FontSize',14);
set(lh, 'FontSize', 13);
set(lh, 'Position', [0.8 0.77 0.15 0.13]);
set(gca,'fontsize',14)
set(fh, 'Position', [100 100 800 400]);
axis([0 10 -10 10]);
%%
figure(4); clf;
plot(T,Xhist(:,1),'b-','LineWidth',2); hold on;
plot(T,Xhist(:,2),'g-','LineWidth',2);
plot(T,Xhist(:,5),'r--','LineWidth',2);
plot(T,Xhist(:,6),'k--','LineWidth',2);
legend('m1','m2','s1','s2');
xlabel('time (sec)'); ylabel('joint angle (rad)');
%%
figure(5); clf;
plot(T(1:end),TIPm(:,1),'b-','LineWidth',2); hold on;
plot(T(1:end),TIPm(:,2),'g-','LineWidth',2);
plot(T(1:end),TIPs(:,1),'r--');
plot(T(1:end),TIPs(:,1),'k--');
legend('x_m','y_m','x_s','y_s');
axis equal;
%%
R = [];
for t=0:0.1:10
    R(end+1,:) = xdes(t);
end
%%
figure(5); clf;
plot(TIPm(:,1),TIPm(:,2),'b-','LineWidth',2); hold on;
plot(TIPs(:,1),TIPs(:,2),'g-','LineWidth',2);
plot(R(:,1),R(:,2),'k-.');
axis equal;
legend('master','slave','xdes');
xlabel('x'); ylabel('y');
%%
figure(6); clf;
```

```matlab
plot(T,TIPm(:,1),'b-','LineWidth',2); hold on;
plot(T,TIPm(:,2),'g-','LineWidth',2);
plot(T,TIPs(:,1),'b--','LineWidth',2);
plot(T,TIPs(:,2),'g--','LineWidth',2);
plot(0:0.1:10,R(:,1),'k-.');
plot(0:0.1:10,R(:,2),'k-');
axis equal;
legend('master','slave','xdes');
xlabel('x'); ylabel('y');
%%
fh = figure(7); clf;
plot(0:0.1:10,R(:,1),'k.'); hold on;
plot(0:0.1:10,R(:,2),'g.');
plot(T,TIPm(:,1),'b-','LineWidth',2);
plot(T,TIPm(:,2),'r-','LineWidth',2);
xlabel('time (sec)','FontSize',14);
ylabel('position (m)','FontSize',14);
lh = legend('x desired','y desired','x teleop','y teleop','
    Location','Best');
set(lh, 'FontSize', 13);
set(lh, 'Position', [0.14 0.5 0.17 0.19]);
set(gca,'fontsize',14)
set(fh, 'Position', [100 100 800 400]);
%%
figure(8); clf;
plot(T,Xhist(:,9),'b-'); hold on;
plot(T,Xhist(:,10),'k--');
plot(T,Xhist(:,11),'r-');
xlabel('time (sec)');
ylabel('estimated stiffness (N/m)');
legend('K11est','K12est','K22est');
%%
figure(9); clf;
plot(T,Xhist(:,12),'b-'); hold on;
plot(T,Xhist(:,14),'r-');
xlabel('time (sec)');
ylabel('b (N)');
legend('x','y');
%%
bsdot = diff(Bsarr)/tstep;
bmdot = diff(Bmarr)/tstep;
bsdotmax = zeros([2 2]);
bmdotmax = zeros([2 2]);
for i = 1:length(bsdot)
    for j = 1:2
        for k = 1:2
            if( abs(bsdot(i,j,k)) > bsdotmax(j,k) )
```

```
                        bsdotmax(j,k) = abs(bsdot(i,j,k));
                end
                if( abs(bmdot(i,j,k)) > bmdotmax(j,k) )
                        bmdotmax(j,k) = abs(bmdot(i,j,k));
                end
            end
        end
end
bsdotmax
bmdotmax
%%
fh = figure(10); clf;
T2 = 0:tstep:(Tend-2*tstep);
plot(T2,bmdot(:,1,1),'r-','LineWidth',2); hold on;
plot(T2,bmdot(:,2,2),'b--','LineWidth',2);
lh = legend('1,1','2,2','Location','NorthWest');
set(lh, 'FontSize', 13);
set(gca,'fontsize',14)
set(fh, 'Position', [100 100 800 400]);
xlabel('time (sec)');
ylabel('Bdot master');
%%
fh = figure(11); clf;
T2 = 0:tstep:(Tend-2*tstep);
plot(T2,bsdot(:,1,1),'r-','LineWidth',2); hold on;
plot(T2,bsdot(:,2,2),'b--','LineWidth',2);
lh = legend('1,1','2,2','Location','NorthWest');
set(lh, 'FontSize', 13);
set(gca,'fontsize',14)
set(fh, 'Position', [100 100 800 400]);
xlabel('time (sec)');
ylabel('Bdot slave');
```

D.2 Adaptive

The following MATLAB code was employed in the adaptive simulation of

Subsection 6.3.1

```
params_2dof
%%
Tend = 10;
tstep = 0.00025;
Kph = 30;
```

```matlab
Kdh = 15;
Kec = diag([1e4,1]); % Cartesian space environmental
    stiffness, N/m
crtinv = 1/sqrt(100);
sigmax = 500;
sigmin = 100;
delaysec = 0.050;
delay = floor(delaysec/tstep);
Bdotmax = 500;
%%
% Initial conditions and trajectory
X0 = [pi/4;-pi/4;0;0;pi/4;-pi/4;0;0]; % [th1;th2;th1d;th2d]m
    , [""]s
xdes = @(t) [1.7071+0.25*sin(t);0.4571+0.25*cos(t)];
xdesdot = @(t) [0.25*cos(t);-0.25*sin(t)];
%%
vm = [0;0]; us = [0;0]; eints = [0;0]; eintm = [0;0];
es = [0;0]; esprev = [0;0]; em = [0;0]; emprev = [0;0];
T = 0:5*tstep:Tend;
X=X0;
Xhist = [X0',zeros(1,6); nan([length(T)-1,length(X0)+6])];
Ehist = [0 0 0 0; nan([length(T)-1,4])];
Fhist = [0 0; nan([length(T)-1,2])];
TIPs = [fwdkin_2dof(X(5:8))'; nan([length(T)-1,2])];
TIPm = [fwdkin_2dof(X(1:4))'; nan([length(T)-1,2])];
Bsarr = nan([ length(T)-1, 2, 2 ]);
Bmarr = nan([ length(T)-1, 2, 2 ]);
TAUhist = [0,0; nan([length(T)-1,2])];
Zave = [0;0]; Kave = [0;0];
Uarr = [0 0]; Varr = [0 0]; Fearr = [0 0];
t = tstep;
count = 1;
Fe=[0;0];
dZarr = [];
i = 2;
xs = fwdkin_2dof(X(5:6));
while( t <= Tend)

    Mm = M_2dof(X(1:4)); Cm = Cmat_2dof(X(1:4));
    Ms = M_2dof(X(5:8)); Cs = Cmat_2dof(X(5:8));
    Jm = Jac_2dof(X(1:2));
    Js = Jac_2dof(X(5:6));

    % master
    xm = fwdkin_2dof(X(1:2));
    if(count<=delay)
        bcart = crtinv*Kec*sqrt(diag(diag( inv(Jm)'*Mm*inv(
```

```matlab
                Jm) )));
    else
        if (norm(Fearr(count-delay,:)) > 0 )
            bcart = crtinv*Kec*sqrt(diag(diag( inv(Jm)'*Mm*
                inv(Jm) )));
        else
            bcart = zeros([2 2]);
        end
    end
    bm = Jm'*bcart*Jm;
    if( t > tstep)
        soldm = sm;
    end
    [u,sm,v] = svd(bm);
    for index = 1:size(sm,2)
        if( sm(index,index) > sigmax )
            sm(index,index) = sigmax;
        elseif ( sm(index,index) < sigmin )
                sm(index,index) = sigmin;
        end
        if( t > tstep)
            n = sm(index,index) - soldm(index,index);
            if( abs(n) > Bdotmax*tstep )
                sm(index,index) = soldm(index,index) + sign(
                    n)*Bdotmax*tstep;
            end
        end
    end
    bm = u*sm*u';
    Bmarr(count,:,:) = bm;
    if(t <= tstep)
        Kim = diag(diag(bm/5));
        Kis = diag(diag(bm/5));
    end

    brt = sqrtm(bm); brtinv = inv(brt);
    dotdes = -1/sqrt(2)*brtinv*vm - 0.5*X(3:4) - Kim*bm\
        eintm/2;
    Fmc = -bm*(dotdes - X(3:4)) - Kim*eintm; % torque
    um = 1/sqrt(2)*brt*dotdes+1/sqrt(2)*brtinv*Fmc;
    Fh = Kph * (xdes(t) - fwdkin_2dof(X(1:2))) + Kdh * (
        xdesdot(t) - Jac_2dof(X)*X(3:4) );
    emprev = em;
    em = dotdes-X(3:4);
    Kioldm = Kim;
    Kim = diag(diag(bm/5));
    Kideltam = (Kim-Kioldm);
```

204

```matlab
eintm = sqrtm(Kim)\sqrtm(Kioldm)*eintm + 0.5*(em+emprev)
    *tstep;

% slave
Feprev = Fe;
xsprev = xs;
xs = fwdkin_2dof(X(5:6));
if( xs(1) > 1.7071 )
    Fe = -Kec*(xs - [1.7071;0.7071]); % linear spring
    bcart = crtinv*Kec*sqrt(diag(diag( inv(Js)'*Ms*inv(
        Js) )));
else
    Fe = [0;0];
    bcart = zeros([2 2]);
end
Fearr(end+1,:) = Fe';

bs = Js'*bcart*Js;
if(t > tstep)
    solds = ss;
end
[u,ss,v] = svd(bs);
for index = 1:size(ss,2)
    if( ss(index,index) > sigmax )
        ss(index,index) = sigmax;
    elseif ( ss(index,index) < sigmin )
            ss(index,index) = sigmin;
    end
    if( t > tstep )
        n = ss(index,index)-solds(index,index);
        if( abs(n) > Bdotmax*tstep )
            ss(index,index) = solds(index,index) + sign(
                n)*Bdotmax*tstep;
        end
    end
end
bs = u*ss*u';
Bsarr(count,:,:) = bs;
brt = sqrtm(bs); brtinv = inv(brt);
dotdes = 1/sqrt(2)*brtinv*us + 0.5*X(7:8) - Kis*bs\eints
    /2;
Fsc = bs*(dotdes - X(7:8)) + Kis*eints; % torque
vs = 1/sqrt(2)*brtinv*Fsc-us;
eints = eints + (dotdes-X(7:8))*tstep;
Kiolds = Kis;
Kis = diag(diag(bs/5));
Kideltas = (Kis-Kiolds);
```

```matlab
eints = sqrtm(Kis)\sqrtm(Kiolds)*eints + 0.5*(es+esprev)
    *tstep;

% integrate
rhs = @(t,X) [ X(3:4); M_2dof(X(1:2))\(Jac_2dof(X(1:2))
    '*Fh-Fmc-Cmat_2dof(X(1:4))*X(3:4)); X(7:8); M_2dof(X
    (5:8))\(Fsc+Jac_2dof(X(5:6))'*Fe-Cmat_2dof(X(5:8))*X
    (7:8)) ];
Xstep = ode5(rhs, [0 tstep], X);
X = Xstep(end,:)';

dZ = 1/Tend*( (Jm'\Fmc)./(Jm*X(3:4)) )*tstep;
dZarr(:,end+1) = dZ;
if( dZ(1) == dZ(1) ) % if not NaN
    Zave(1) = Zave(1) + dZ(1);
end
if( dZ(2) == dZ(2) )
    Zave(2) = Zave(2) + dZ(2);
end
dK = 1/Tend*( (Jm'\Fmc)./(xm-xs) )*tstep;
if( dK(1) == dK(1) ) % if not NaN
    Kave(1) = Kave(1) + dK(1);
end
if( dK(2) == dK(2) )
    Kave(2) = Kave(2) + dK(2);
end

% Communicate
Uarr(count,:) = um';
Varr(count,:) = vs';
if(count>delay)
    us = Uarr(count-delay,:)';
    vm = Varr(count-delay,:)';
else
    us = [0;0];
    vm = [0;0];
end

% Record history
if( 0 == mod(count,5) )
    Xhist(i,:) = [X', 0, 0, 0, bm(1,1), bm(1,2), bm(2,2)
        ];
    Ehist(i,:) = [ (X(1:4)-X(5:8))' ];
    TIPs(i,:) = fwdkin_2dof(X(5:6))';
    TIPm(i,:) = fwdkin_2dof(X(1:2))';
    TAUhist(i,:) = transpose( Jm'*Fh );
    Fhist(i,:) = Fh';
```

```matlab
        i = i + 1;
    end

    t = t + tstep;
    count = count + 1;
end
Zave
%%
figure(1); clf;
plot(T(1:length(Ehist)),Ehist(:,1:2)); title('Joint position
    error');
legend('1','2');
xlabel('time (sec)'); ylabel('joint error (rad)');
%%
figure(2); clf;
plot(T(1:length(Ehist)),Ehist(:,3:4)); title('Joint rate
    error');
legend('1','2');
%%
fh = figure(3); clf;
plot(T,Fhist(:,1),'b-','LineWidth',2); hold on;
plot(T,Fhist(:,2),'r-','LineWidth',2);
%title('Operator force');
lh = legend('F_x teleop','F_y teleop');
xlabel('time (sec)','FontSize',14); ylabel('force (N)','
    FontSize',14);
set(lh, 'FontSize', 13);
set(lh, 'Position', [0.8 0.77 0.15 0.13]);
set(gca,'fontsize',14)
set(fh, 'Position', [100 100 800 400]);
axis([0 10 -10 10]);
%%
figure(4); clf;
plot(T,Xhist(:,1),'b-','LineWidth',2); hold on;
plot(T,Xhist(:,2),'g-','LineWidth',2);
plot(T,Xhist(:,5),'r--','LineWidth',2);
plot(T,Xhist(:,6),'k--','LineWidth',2);
legend('m1','m2','s1','s2');
xlabel('time (sec)'); ylabel('joint angle (rad)');
%%
figure(5); clf;
plot(T(1:end),TIPm(:,1),'b-','LineWidth',2); hold on;
plot(T(1:end),TIPm(:,2),'g-','LineWidth',2);
plot(T(1:end),TIPs(:,1),'r--');
plot(T(1:end),TIPs(:,1),'k--');
legend('x_m','y_m','x_s','y_s');
axis equal;
```

```matlab
%%
R = [];
for t=0:0.1:10
    R(end+1,:) = xdes(t);
end
%%
figure(5); clf;
plot(TIPm(:,1),TIPm(:,2),'b-','LineWidth',2); hold on;
plot(TIPs(:,1),TIPs(:,2),'g-','LineWidth',2);
plot(R(:,1),R(:,2),'k-.');
axis equal;
legend('master','slave','xdes');
xlabel('x'); ylabel('y');
%%
figure(6); clf;
plot(T,TIPm(:,1),'b-','LineWidth',2); hold on;
plot(T,TIPm(:,2),'g-','LineWidth',2);
plot(T,TIPs(:,1),'b--','LineWidth',2);
plot(T,TIPs(:,2),'g--','LineWidth',2);
plot(0:0.1:10,R(:,1),'k-.');
plot(0:0.1:10,R(:,2),'k-');
axis equal;
legend('master','slave','xdes');
xlabel('x'); ylabel('y');
%%
fh = figure(7); clf;
plot(0:0.1:10,R(:,1),'k.'); hold on;
plot(0:0.1:10,R(:,2),'g.');
plot(T,TIPm(:,1),'b-','LineWidth',2);
plot(T,TIPm(:,2),'r-','LineWidth',2);
xlabel('time (sec)','FontSize',14);
ylabel('position (m)','FontSize',14);
lh = legend('x desired','y desired','x teleop','y teleop','
    Location','Best');
set(lh, 'FontSize', 13);
set(lh, 'Position', [0.14 0.5 0.17 0.19]);
set(gca,'fontsize',14)
set(fh, 'Position', [100 100 800 400]);
%%
figure(8); clf;
plot(T,Xhist(:,9),'b-'); hold on;
plot(T,Xhist(:,10),'k--');
plot(T,Xhist(:,11),'r-');
xlabel('time (sec)');
ylabel('estimated stiffness (N/m)');
legend('K11est','K12est','K22est');
%%
```

```matlab
figure(9); clf;
plot(T,Xhist(:,12),'b-'); hold on;
plot(T,Xhist(:,14),'r-');
xlabel('time (sec)');
ylabel('b (N)');
legend('x','y');
%%
bsdot = diff(Bsarr)/tstep;
bmdot = diff(Bmarr)/tstep;
bsdotmax = zeros([2 2]);
bmdotmax = zeros([2 2]);
for i = 1:length(bsdot)
    for j = 1:2
        for k = 1:2
            if( abs(bsdot(i,j,k)) > bsdotmax(j,k) )
                bsdotmax(j,k) = abs(bsdot(i,j,k));
            end
            if( abs(bmdot(i,j,k)) > bmdotmax(j,k) )
                bmdotmax(j,k) = abs(bmdot(i,j,k));
            end
        end
    end
end
bsdotmax
bmdotmax
%%
fh = figure(10); clf;
T2 = 0:tstep:(Tend-2*tstep);
plot(T2,bmdot(:,1,1),'r-','LineWidth',2); hold on;
plot(T2,bmdot(:,2,2),'b--','LineWidth',2);
lh = legend('1,1','2,2','Location','NorthWest');
set(lh, 'FontSize', 13);
set(gca,'fontsize',14)
set(fh, 'Position', [100 100 800 400]);
xlabel('time (sec)');
ylabel('Bdot master');
%%
fh = figure(11); clf;
T2 = 0:tstep:(Tend-2*tstep);
plot(T2,bsdot(:,1,1),'r-','LineWidth',2); hold on;
plot(T2,bsdot(:,2,2),'b--','LineWidth',2);
lh = legend('1,1','2,2','Location','NorthWest');
set(lh, 'FontSize', 13);
set(gca,'fontsize',14)
set(fh, 'Position', [100 100 800 400]);
xlabel('time (sec)');
ylabel('Bdot slave');
```

D.3 Phantom Omni supporting functions

The following C++ code makes use of the Eigen library [99].

D.3.1 Phantom Omni System Parameters

Header file (omni.h):

```
/* **********************************************************
    These files implement the kinematics and dynamics
    of the Sensable Phantom Omni
    **********************************************************
        */

#ifndef OMNI_H
#define OMNI_H

#include <cmath>
#include <eigen3/Eigen/Core>
#include <eigen3/Eigen/Dense>


// Parameters
#define O_M1 0.035
#define O_M2 0.060
#define O_M3 0.040
#define O_I0ZZ 1e-4
#define O_I1XX 4e-7
#define O_I1YY 5.2e-5
#define O_I1ZZ 5.2e-5
#define O_I2XX 8e-7
#define O_I2YY 9e-5
#define O_I2ZZ 9e-5

// Kinematic parameters verified from analysis of Phantom's
    FK results
#define O_L1 0.13335
#define O_L2 0.13335
#define O_L3 0.02335
#define O_L4 0.16835

// Inertia matrix
int omni_M( Eigen::Vector3d q, Eigen::Matrix3d &M, double
```

```cpp
   mpay=0);

// Centripetal and Coriolis matrix
int omni_C( Eigen::Vector3d q, Eigen::Vector3d qdot, Eigen::
   Matrix3d &C, double mpay=0);

// Gravity and spring vector (joint space, like all the
   other dynamics)
int omni_g( Eigen::Vector3d q,  Eigen::Vector3d &g);

// Forward kinematics
int omni_FK( Eigen::Vector3d q, Eigen::Vector3d &x);

// Jacobian
int omni_J( Eigen::Vector3d q, Eigen::Matrix3d &J);

#endif // OMNI_H
```

Source code (omni.cpp):

```cpp
#include "omni.h"

// Inertia matrix
int omni_M( Eigen::Vector3d q, Eigen::Matrix3d &M, double
   mpay)
{
    M(0,0) = O_I0ZZ + 0.5*(O_I1XX + O_I1YY + O_I2XX + O_I2YY
       ) + 1/8*O_M1*O_L1*O_L1 + 0.5*O_M2*O_L1*O_L1 + 1/8*
       O_M2*O_L2*O_L2 + 0.5*(O_M3+mpay)*O_L1*O_L1 + 0.5*(
       O_M3+mpay)*O_L2*O_L2 + (−0.5*O_I1XX+0.5*O_I1YY + O_L1
       *O_L1*(O_M1/8+O_M2/2+(O_M3+mpay)/2))*cos(2*q(1));
    M(0,1) = 0;
    M(0,2) = 0;
    M(1,0) = 0;
    M(1,1) = O_I1ZZ + O_L1*O_L1*(O_M1/4+O_M2+(O_M3+mpay));
    M(1,2) = O_L1*O_L2*(−0.5*O_M2−(O_M3+mpay))*sin(q(1)−q(2)
       );
    M(2,0) = 0;
    M(2,1) = M(1,2);
    M(2,2) = O_I2ZZ + O_L2*O_L2*(O_M2/4+(O_M3+mpay));

    return 0;
}


// Centripetal and Coriolis matrix
int omni_C( Eigen::Vector3d q, Eigen::Vector3d qdot, Eigen::
```

```cpp
        Matrix3d &C, double mpay)
{
    C(0,0) = 0;
    C(0,1) = qdot(0)*((O_I1XX-O_I1YY + O_L1*O_L1*(-O_M1/4-
        O_M2-(O_M3+mpay)))*sin(2*q(1)) + O_L1*O_L2*(-O_M2-2*(
        O_M3+mpay))*sin(q(1))*sin(q(2)));
    C(0,2) = qdot(0)*(O_L1*O_L2*(O_M2+2*(O_M3+mpay))*cos(q
        (1))*cos(q(2)) + (-O_I2XX + O_I2YY + O_L2*O_L2*(O_M2
        /4+O_M3)*sin(2*q(2))));
    C(1,0) = -0.5*C(0,1);
    C(1,1) = 0;
    C(1,2) = qdot(2)*(0.5*O_M2*O_L1*O_L2*cos(q(1)-q(2)) +
        O_M3*O_L1*O_L2*cos(q(1)-q(2)));
    C(2,0) = -0.5*C(0,2);
    C(2,1) = qdot(1)*(O_L1*O_L2*(-O_M2/2-(O_M3+mpay))*cos(q
        (1)-q(2)));
    C(2,2) = 0;

    return 0;
}


// Gravity and spring terms (not used)
int omni_g( Eigen::Vector3d q,   Eigen::Vector3d &g)
{
    g(0) = 0;
    g(1) = ((q(1)<M_PI/4)?0.067*(q(1)-M_PI/2):0) +
        9.8*0.13335*0.1*cos(q(1));
    g(2) = 9.8*0.13335*0.07*sin(q(2));

    return 0;
}


// Forward kinematics, consistent with manufacturer's model
int omni_FK( Eigen::Vector3d q, Eigen::Vector3d &x)
{
    double num = O_L1*cos(q(1)) + O_L2*sin(q(2));
    x(0) = sin(-q(0))*num;
    x(1) = O_L1*sin(q(1)) - O_L2*cos(q(2)) - O_L3;
    x(2) = cos(-q(0))*num - O_L4;

    return 0;
}


// Jacobian matrix, also consistent with manufacturer's
```

```
    model
int omni_J( Eigen::Vector3d q, Eigen::Matrix3d &J)
{
    double R = O_L1*cos(q(1)) + O_L2*sin(q(2));
    J(0,0) = -R*cos(q(0));
    J(0,1) = sin(q(0))*sin(q(1))*O_L1; // Sansanayuth et al.
        say O_L2, but that's not consistent with FK model,
        even as printed in their paper.
    J(0,2) = -sin(q(0))*O_L2*cos(q(2));
    J(1,0) = 0;
    J(1,1) = O_L1*cos(q(1));
    J(1,2) = O_L2*sin(q(2));
    J(2,0) = -R*sin(q(0));
    J(2,1) = -O_L1*cos(q(0))*sin(q(1));
    J(2,2) = O_L2*cos(q(0))*cos(q(2));

    return 0;
}
```

D.3.2   Equations of Motion

```
// Equations of motion (for system state x, populates xdot
   with derivative)
bool rhsfast( double t, int n, double x[], double xdot[] )
{
    assert(STATESIZE == n);

    Eigen::Vector3d q, qdot, qbldot, g, Fe, r;
    Eigen::Matrix3d M, C, J;
    Eigen::JacobiSVD<Eigen::Matrix3d> svdsolver;

    q(0) = x[0]; q(1) = x[1]; q(2) = x[2];
    qdot(0) = x[3]; qdot(1) = x[4]; qdot(2) = x[5];

    // Enforce joint limits on first two joints
    if( (-0.97>=q(0)) && (0>qdot(0)) )
        qdot(0) = 0.0;
    else if ( (1.00<=q(0)) && (0<qdot(0)) )
        qdot(0) = 0.0;
    if( (0.03>=q(1)) && (0>qdot(1)) )
        qdot(1) = 0.0;
    else if ( (1.79<=q(1)) && (0<qdot(1)) )
        qdot(1) = 0.0;

    omni_M( q, M, mpay );
```

```cpp
    omni_C ( q , qdot , C, mpay ) ;
    omni_g ( q , g ) ;
    omni_J ( q , J ) ;

    omni_FK ( q , r ) ;

    Fe = Kec*( x e q u i l i b − r ) ; // spring with linear region
        and then saturation

    qdbldot = M. colPivHouseholderQr ( ) . solve ( −C*qdot + Fsc +
        J . transpose ( )*Fe − SLAVEDAMP*qdot ) ; // gravity
        ignored

    xdot [ 0 ] = qdot ( 0 ) ;
    xdot [ 1 ] = qdot ( 1 ) ;
    xdot [ 2 ] = qdot ( 2 ) ;
    xdot [ 3 ] = qdbldot ( 0 ) ;
    xdot [ 4 ] = qdbldot ( 1 ) ;
    xdot [ 5 ] = qdbldot ( 2 ) ;

    //std :: cout << std :: endl ;

    return true ;
}
```

Bibliography

[1] W. Ferrell. Delayed force feedback. *Human Factors*, 8(5):449–454, 1966.

[2] T. Sheridan. Space teleoperation through time delay: review and prognosis. *IEEE Transactions on Robotics and Automation*, 9:592–606, 1993.

[3] P. Hokayem and M. Spong. Bilateral teleoperation: An historical survey. *Automatica*, 42:2035–2057, 2006.

[4] J. Zhu, X. He, and W. Gueaieb. Trends in the Control Schemes for Bilateral Teleoperation with Time Delay. In *Autonomous and Intelligent Systems*, pages 146–155. Springer, 2011.

[5] R. Held, A. Efstathiou, and M. Greene. Adaptation to displaced and delayed visual feedback from the hand. *Journal of Experimental Psychology*, 72:887–891, 1966.

[6] W. Ferrell. Remote manipulation with transmission delay. *IEEE Transactions on Human Factors in Electronics*, 6:24–32, 1965.

[7] M. Noyes. Superposition of graphics on low bit rate video as an aid in teleoperation. Master's thesis, Dept of Mechanical Engineering, Massachusetts Institute of Technology, 1982.

[8] F. Buzan and T. Sheridan. A model-based predictive operator aid for telemanipulators with time delay. In *Proc. IEEE International Conference on Systems, Man and Cybernetics*, volume 1, pages 138–143, 1989.

[9] M. Massimino. *Sensory substitution for force feedback in space teleoperation*. PhD thesis, Dept of Mechanical Engineering, Massachusetts Institute of Technology, 1992.

[10] P. Arcara and C. Melchiorri. Control schemes for teleoperation with time delay: a comparative study. *Robotics and Autonomous Systems*, 38:49–64, 2002.

[11] J. Lee and S. Payandeh. Stability of internet-based teleoperation systems using bayesian predictions. In *Proc. IEEE World Haptics Conference*, pages 499–504, 2011.

[12] J. Huang and F. Lewis. Neural-network predictive control for nonlinear dynamic systems with time-delay. *IEEE Transactions on Neural Networks*, 14:377–389, 2003.

[13] A. Smith and K. Hashtrudi-Zaad. Neural network-based teleoperation using Smith predictors. In *Proc. IEEE International Conference on Mechatronics & Automation*, pages 1654–1659, 2005.

[14] H. Cho and J. Park. Sliding-mode-based impedance controller for bilateral tele-operation under varying time-delay. In *Proc. IEEE International Conference on Robotics and Automation*, pages 1025–1030, 2001.

[15] H. Cho and J. Park. Stable bilateral teleoperation under a time delay using a robust impedance control. *Mechatronics*, 15:611–625, 2005.

[16] L. García-Valdovinos, V. Parra-Vega, and M. Arteaga. Observer-based sliding mode impedance control of bilateral teleoperation under constant unknown time delay. *Robotics and Autonomous Systems*, 55:609–617, 2007.

[17] Y. Yang, C. Hua, and X. Guan. Finite-time synchronization control for bilateral teleoperation under communication delays. *Robotics and Computer-integrated Manufacturing*, 31:61–69, 2015.

[18] R. Ortega and M. Spong. Adaptive motion control of rigid robots: a tutorial. In *Proc. IEEE Conference on Decision and Control*, pages 1575–1584, 1988.

[19] M. Spong, S. Hutchinson, and M. Vidyasagar. Multivariable control. In *Robot modeling and control*, chapter 8, pages 289–318. Wiley, 2006.

[20] H. Khalil. Passivity. In *Nonlinear Systems*, chapter 6, pages 227–259. Prentice, 3 edition, 2002.

[21] Emmanuel Nuño, Luis Basañez, and Romeo Ortega. Passivity-based control for bilateral teleoperation: a tutorial. *Automatica*, 47:485–495, 2011.

[22] D. Sun, F. Naghdy, and H. Du. Application of wave-variable control to bilateral teleoperation systems: a survey. *Annual Reviews in Control*, 38:12–31, 2014.

[23] R. Anderson and M. Spong. Bilateral control of teleoperators with time delay. *IEEE Transactions on Automatic Control*, 34:494–501, 1989.

[24] T. Imaida, Y. Yokokhoji, T. Doi, M. Oda, and T. Yoshikawa. Ground-space bilateral teleoperation of ETS-VII robot arm by direct bilateral coupling under 7-s time delay condition. *IEEE Transactions on Robotics and Automation*, 20, 2004.

[25] G. Niemeyer and J. Slotine. Stable adaptive teleoperation. *IEEE Journal of Oceanic Engineering*, 16:152–162, 1991.

[26] R. Anderson and M. Spong. Bilateral control of teleoperators with time delay. In *IEEE Conf. on Decision and Control*, volume 1, pages 167–173, 1988.

[27] G. Niemeyer and J. Slotine. Towards force-reflecting teleoperation over the internet. In *Proc. IEEE International Conference on Robotics and Automation*, pages 1909–1915, 1998.

[28] N. Hogan. Impedance control: an approach to manipulation. In *American Control Conference*, pages 304–313, 1984.

[29] S. Hirche, M. Ferre, J. Barrio, C. Melchiorri, and M. Buss. Bilateral control architectures for telerobotics. In *Advances in telerobotics*, chapter 10, pages 163–176. 2007.

[30] M. Boukhnifer and A. Ferreira. Wave-based passive control for transparent micro-teleoperation system. *Robotics and Autonomous Systems*, 54:601–615, 2006.

[31] N. Chopra, P. Berestesky, and M. Spong. Bilateral teleoperation over unreliable communication networks. *IEEE Transactions on Control Systems Technology*, 16(2):304–313, 2008.

[32] Y. Yokokohji, T. Tsujioka, and T. Yoshikawa. Bilateral Control with Time-Varying Delay including Communication Blackou. In *Proc. Symp. On Haptic Interfaces For Virtual Envir. & Teleoperator Systs.*, pages 285–292, 2002.

[33] N. Chopra, M. Spong, R. Ortega, and N. Barabanov. On tracking performance in bilateral teleoperation. *IEEE Transactions on Robotics*, 22(4):861–866, 2006.

[34] N. Chopra, M. Spong, and R. Lozano. Adaptive coordination control of bilateral teleoperators with time delay. In *Proc. IEEE Conference on Decision and Control*, pages 4540–4547, 2004.

[35] D. Tian, D. Yashiro, and K. Ohnishi. Frequency-domain analysis of wave variable based teleoperation and its equivalent implementation. In *Proc. International Symposium on Access Spaces*, pages 41–46. IEEE, 2011.

[36] G. Niemeyer and J. Slotine. Telemanipulation with time delays. *International Journal of Robotics Research*, 23:873–890, 2004.

[37] N. Tanner and G. Niemeyer. Improving perception in time-delayed telerobotics. *International Journal of Robotics Research*, 24(8):631–644, 2005.

[38] T. Kanno and Y. Yokokhoji. Multilateral teleoperation control over time-delayed computer networks using wave variables. In *Proc. IEEE Haptics Symposium*, pages 125–131, 2012.

[39] M. Mendoza, I. Bonilla, E. González-Galván, and F. Reyes. Impedance control in a wave-based teleoperator for rehabilitation motor therapies assisted by robots. *Computer methods and programs in biomedicine*, 123:54–67, 2016.

[40] D. Sun, F. Naghdy, and H. Du. A novel approach for stability and transparency control of nonlinear bilateral teleoperation system with time delays. *Control Engineering Practice*, 47:15–27, 2016.

[41] C. Carignan and P. Olsson. Cooperative control of virtual objects over the internet using force-reflecting master arms. In *Proc. IEEE International Conference on Robotics and Automation*, pages 1221–1226, 2004.

[42] N. Diolaiti, G. Niemeyer, and N. Tanner. Wave haptics: buliding stiff controllers from the natural motor dynamics. *International Journal of Robotics Research*, 26:5–21, 2007.

[43] C. Cho, J. Song, and M. Kim. Stable haptic display of slowly updated virtual environment with multirate wave transform. *IEEE/ASME Trans. on Mechatronics*, 13(5):566–575, 2008.

[44] N. Yasrebi and D. Constantinescu. Passive multirate wave communications for haptic interaction in slow virtual environments. *IEEE/ASME Trans. on Mechatronics*, 18(1):328–336, 2013.

[45] N. Chopra and M. Spong. Passivity-based control of multi-agent systems. In S. Kawamura and M. Svinin, editors, *Advances in robot control, from everyday physics to human-like movements*, pages 107–134. Springer-Verlag, 2006.

[46] N. Chopra, M. Spong, and R. Lozano. Synchronization of bilateral teleoperators with time delay. *Automatica*, 44:2142–2148, 2008.

[47] E. Nuño, R. Ortega, and L. Basañez. An adaptive controller for nonlinear teleoperators. *Automatica*, 46:155–159, 2010.

[48] D. Lee and M. Spong. Passive bilateral teleoperation with constant time delay. *IEEE Transactions on Robotics*, 22(2):269–280, 2006.

[49] K. Hashtrudi-Zaad and S. Salcudean. Transparency in time-delayed systems and the effect of local foce feedback. *IEEE Transactions on Robotics and Automation*, 18:108–114, 2002.

[50] U. Tumerdem and K. Ohnishi. Robust four channel teleoperation under time delay by damping injection. In *Proc. IEEE International Conference on Mechatronics*, 2009.

[51] X. Liu and M. Tavakoli. Adaptive control for linearly and nonlinearly parameterized dynamic uncertainties in bilateral teleoperation systems. In *IEEE International Conference on Robotics and Automation*, pages 1329–1334, 2011.

[52] M. Oda, K. Kibe, and F. Yamagate. ETS-VII, Space robot in-orbit experiment satellite. In *Proc. IEEE International Conference on Robotics and Automation*, pages 739–744, 1996.

[53] M. Oda and T. Doi. Teleoperation system of ETS-VII robot experiment satellite. In *Proc. IEEE International Conference on Intelligent Robots and Systems*, pages 1644–1650, 1997.

[54] E. Rodríguez-Seda, D. Lee, and M. Spong. Experimental comparison study of control architectures for bilateral teleoperators. *IEEE Transactions on Robotics*, 25:1304–1318, 2009.

[55] P. Dario, B. Hannaford, and A. Menciassi. Smart surgical tools and augmenting devices. *IEEE Transactions on Robotics and Automation*, 19:782–792, 2003.

[56] S. Butner and M. Ghodoussi. Transforming a surgical robot for human telesurgery. *IEEE Transactions on Robotics and Automation*, 19:818–824, 2003.

[57] C. Lawn and B. Hannaford. Performance testing of passive communication and control in teleoperation with time delay. *Proc. IEEE International Conference on Robotics and Automation*, 34:776–783, 1993.

[58] G. Niemeyer and J. Slotine. Designing force reflecting teleoperators with large time delays to appear as virtual tools. In *Proc. IEEE International Conference on Robotics and Automation*, volume 3, pages 2212–2218, 1997.

[59] S. Hirche and M. Buss. Human-oriented control for haptic teleoperation. *Proceedings of the IEEE*, 100:623–647, Mar 2012.

[60] M. Mason. Compliance and force control for computer controlled manipulators. *IEEE Transactions on Systems, Man, and Cybernetics*, 11(6):418–432, 1981.

[61] J. Craig and M. Raibert. A systematic method of hybrid position/force control of a manipulator. In *IEEE Computer Society International Conference on Computers, Software, and Applications*, pages 446–451, 1979.

[62] O. Khatib. A unified approach for motion and force control of robot manipulators: the operational space formulation. *IEEE Journal of Robotics and Automation*, RA-3(1):43–53, 1987.

[63] J. Salisbury. Active stiffness control of a manipulator in Cartesian coordinates. In *IEEE Conference on Decision and Control*, 1980.

[64] H. Wang and Y. Xie. Task-space framework for bilarateral teleoperation with time delays. *ASME Journal of Dynamic Systems, Measurement, and Control*, 134(5), 2012.

[65] N. Chopra, M. Spong, R. Ortega, and N. Barabanov. On position tracking in bilateral teleoperation. In *Proc. American Control Conference*, pages 5244–5249, 2004.

[66] E. Rodríguez-Seda and M. Spong. A time-varying wave impedance approach for transparency compensation in bilateral teleoperation. In *IEEE/RSJ International Conf. on Intelligent Robots and Systems*, pages 4609–4615, 2009.

[67] N. Tanner and G. Niemeyer. Online tuning of wave impedance in telerobotics. In *IEEE Conf. on Robotics, Automation and Mechatronics*, pages 7–12, 2004.

[68] E. Rodríguez-Seda. Passive Transparency Compensation for Bilateral Teleoperators with Communication Delays. *Journal of Robotics*, 2015.

[69] N. Chopra and M. Spong. Adaptive synchronization of bilateral teleoperators with time delay. In *Advances in telerobotics*, chapter 15, pages 257–270.

[70] M Alise, R. Roberts, D. Repperger, C. Moore, and S. Tosunoglu. On extending the wave variable method to multiple-DOF teleoperation systems. *IEEE/ASME Trans. on Mechatronics*, 14(1):55–63, 2009.

[71] G. Niemeyer and J. Slotine. Using wave variables for system analysis and robot control. In *Proc. IEEE International Conference on Robotics and Automation*, pages 1619–1625, 1997.

[72] H. Ross and D. Murray, editors. *E. H. Weber on the tactile senses*. Taylor & Francis, 1996.

[73] S. Biggs and M. Srinivasan. Haptic Interfaces. In K. Stanney, editor, *Handbook of virtual environments: design, implementation, and applications*, chapter 5, pages 93–115. 2002.

[74] H. Tan, M. Srinivasan, B. Eberman, and B. Cheng. Human factors for the design of force-reflecting haptic interfaces. In C. Radcliffe, editor, *Dynamic Systems and Control*, number G0909A-1994, pages 353–359. 1994.

[75] D. Lawrence. Stability and Transparency in Bilateral Teleoperation. *IEEE Transactions on Robotics and Automation*, 9:624–637, 1993.

[76] G. Beauregard, Srinivasan M., and N. Durlach. The manual resolution of viscosity and mass. *Proc. ASME Dynamic Systems and Control Division*, 57-2:657–662, 1995.

[77] M. Spong, S. Hutchinson, and M. Vidyasagar. Dynamics. In *Robot modeling and control*, chapter 7, pages 239–287. Wiley, 2006.

[78] G. Niemeyer and J. Slotine. Telemanipulation with time delays. *International Journal of Robotics Research*, 23(9):873–890, 2004.

[79] E. Vance. *Adaptive control of free-floating and free-flying robotic manipulators*. PhD thesis, Dept of Aerospace Engineering, University of Maryland, College Park, 1998.

[80] D. O'Leary. *Scientific computing with case studies.* SIAM, 2009.

[81] C. Meyer. Eigenvalues and eigenvectors. In *Matrix analysis and applied linear algebra*, chapter 7, pages 489–660. SIAM, 2001.

[82] Using SVD to generalise Sylvester's law of inertia to non-square matrices. *Jack's personal blog on mathematics and sometimes other things too*, `https://jaxwebster.wordpress.com/2012/01/14/a-bit-about-sylvesters-law-of-inertia/`.

[83] K. Kreutz-Delgado, M. Long, and H. Seraji. Kinematic Analysis of 7-DOF Manipulators. In *Proc. IEEE International Conference on Robotics and Automation*, pages 824–830, 1990.

[84] T. Yoshikawa. Manipulability of robotic mechanisms. *International Journal of Robotics Research*, 4:3–9, 1985.

[85] M. Togai. An application of the singular value decomposition to manipulability and sensitivity of industrial robots. *SIAM Journal on Algebraic Discrete Methods*, 7(2):315–320, 1986.

[86] N. Tanner and G. Niemeyer. Practical limitations of wave variable controllers in teleoperation. In *IEEE Conf. on Robotics, Automation and Mechatronics*, pages 25–30, 2004.

[87] N. Yasrebi and D. Constantinescu. Passive wave variable control of haptic interaction with an unknown virtual environment. In *IEEE International Conference on Robotics and Automation*, pages 919–924, 2011.

[88] N. Hogan. Controlling impedance at the man/machine interface. In *Proc. IEEE International Conference on Robotics and Automation*, volume 3, pages 1626–1631, 1989.

[89] M. Dyck, A. Jazayeri, and M. Tavakoli. Is the human operator in a teleoperation system passive? In *Proc. IEEE World Haptics Conference*, 2013.

[90] G. Niemeyer. *Using wave variables in time delayed force reflecting teleoperation.* PhD thesis, Dept. of Aeronautics and Astronautics, Massachusetts Institute of Technology, 1996.

[91] J. McIntyre and J. Slotine. Does the brain make waves to improve stability? *Brain Research Bulletin*, 75:717–722, 2008.

[92] A. Jazayeri and M. Tavakoli. Bilateral teleoperation system stability with non-passive and strictly passive operator or environment. *Control Engineering Practice*, 40:45–60, 2015.

[93] T. Matiakis, S. Hirche, and M. Buss. Independent-of-delay stability of nonlinear networked control systems by scattering transformation. In *American Control Conference*, 2006.

[94] P. Neilson. Speed of response or bandwidth of voluntary system controlling elbow position of intact man. *Medical and Biological Engineering*, 10:450–459, 1972.

[95] S. Hirche. *Haptic telepresence in packet switched communication networks*. PhD thesis, Technische Universität München, 2005.

[96] M. Cavusoglu and D. Feygin. Kinematics and dynamics of PHANToM model 1.5 haptic interface. Technical Report UCB/ERL M01/15, EECS Department, University of California, Berkeley, 2001.

[97] D. Erickson, M. Weber, and I. Sharf. Contact stiffness and damping estimation for robotic systems. *International Journal of Robotics Research*, 22(1):41–57, 2003.

[98] E. Naerum, J. Cornellà, and O. Elle. Contact force estimation for backdrivable robotic manipulators with coupled friction. In *Proc. IEEE International Conference on Intelligent Robots and Systems*, pages 3021–3027, 2008.

[99] Gaël Guennebaud, Benoît Jacob, et al. Eigen v3. `http://eigen.tuxfamily.org`, 2010.